Model Supported Analysis of Water Management in Alkaline Membrane Direct Methanol Fuel Cells

Von der Fakultät für Maschinenbau
der Technischen Universität Carolo-Wilhelmina zu Braunschweig

zur Erlangung der Würde

einer Doktor-Ingenieurin (Dr.-Ing.)

genehmigte Dissertation

von:	Dipl.-Ing. Christine Weinzierl
aus (Geburtsort):	Freyung

eingereicht am:	20.10.2016
mündliche Prüfung am:	17.02.2017

Gutachter:	Prof. Dr.-Ing. Ulrike Krewer
	Prof. Dr.-Ing. Kai Sundmacher

2017

Abstract

Fuel cells reach high electric efficiencies also in low and medium sized power systems and, thus, are a promising alternative for decentralised, mobile and portable power supply. Full establishment is mainly hindered by high material cost which can be reduced by usage of non noble metals like nickel as catalyst instead of expensive platinum, as possible in alkaline fuel cells (AFCs). Direct methanol fuel cells of the alkaline type (ADMFCs) require anion exchange membranes (AEMs) as solid electrolyte since liquid alkaline solutions react with carbon dioxide forming carbonate salts and reducing cell performance. This new kind of fuel cell is not sufficiently analysed yet and it is not identified whether its low performance is caused by low ionic conductivity, slow reaction kinetics, process engineering issues like water management or any other effect. In present literature, research focusses on increasing ADMFC performance by improving catalyst or membrane material.

In this doctoral thesis, water management in ADMFCs with AEM electrolyte is analysed to identify possible limitations as well as requirements for stable operation. In a first step, extreme case scenarios are modelled to analyse two challenges: Water supply to cathode and stable water level at anode. Water diffusion through membrane is identified as the key process for effective water management and is therefore quantified experimentally in a second step revealing that water supply to cathode is not limiting present performance of ADMFCs. Parameters corresponding to a detailed model of water diffusion are estimated from experimental results using a complex three dimensional model of the diffusion test cell used for experiments. The last step includes the detailed model of water and methanol transport through membrane into the model of an ADMFC in order to analyse anodic water level stabilisation by adjusting cathodic conditions. This three step analysis provides a guideline for design of new membrane material as well as for fuel cell design and reveals options for stable operation of ADMFC systems.

Kurzfassung

Brennstoffzellen (BZ) erreichen auch in kleinen oder mittelgroßen Anlagen hohe elektrische Wirkungsgrade und sind daher eine vielversprechende Alternative für die dezentrale, mobile oder portable Stromversorgung. Dennoch konnten sich BZ auf dem Markt bislang nicht durchsetzen, u.a. aufgrund hoher Materialkosten, welche sich durch den Einsatz unedler Metalle wie Nickel statt Platin als Katalysator deutlich reduzieren lassen. Dies ist in alkalischen BZ möglich. Alkalische BZ, die mit Methanol betrieben werden, (ADMFCs) benötigen eine anionenleitende Membran als Elektrolyten, da flüssige alkalische Lösungen mit CO_2 reagieren wodurch Karbonate gebildet werden und die Leistung der Zelle sinkt. Diese neue Brennstoffzellenart wurde bislang unzureichend analysiert und es wurde noch nicht geklärt, wodurch die derzeit niedrige Leistung der ADMFC beschränkt wird. In der Literatur werden hauptsächlich neue Katalysatoren oder Membranen untersucht, um die Leistung der ADMFC zu verbessern.

Diese Doktorarbeit befasst sich mit der Analyse des Wassermanagements in ADMFCs mit einem Membranelektrolyten, um mögliche Grenzen sowie die Anforderungen an einen stabilen Betrieb zu identifizieren. Dafür werden zunächst mehrere Extremfälle modelliert um zwei Herausforderungen zu untersuchen: die Wasserversorgung der Kathode und ein stabiler Wasserhaushalt an der Anode. Als Kernprozess für ein erfolgreiches Wassermanagement wird die Wasserdiffusion durch die Membran experimentell bestimmt. Die Ergebnisse lassen auf eine ausreichende Wasserversorgung der Kathode für die derzeitige Leistung von ADMFCs schließen. Mit Hilfe eines komplexen 3D-Modells der Messzelle und Ablgeich mit den experimentellen Ergebnissen werden Parameter für eine detaillierte Modellierung der Wasserdiffusion abgeschätzt. Schließlich wird das detaillierte Diffusionsmodell in ein ADMFC-Modell integriert, um die Stabilisierung des Wasserhaushaltes an der Anode durch Justierung der Zuflussbedingungen an der Kathode zu untersuchen. Diese mehrschrittige Analyse gibt Aufschluss über die Anforderungen an neue Membranmaterialien sowie an das Brennstoffzellendesign und zeigt Optionen für den stabilen Betrieb von ADMFC-Systemen auf.

Acknowledgement

I want to use this opportunity to thank some people who supported my scientific work and without whom the present thesis would not exist in its form.

I sincerely thank my dissertation advisor Prof. Ulrike Krewer for the confidence she placed in me and her continuous support and guidance in all issues relating my doctoral studies as well as my personal development. Her open door policy even in stressful periods contributed to an excellent working atmosphere in her group and I absolutely appreciated her critical questioning as well as the motivating discussions with her which inspired me and improved the quality of my work.

Many thanks to my colleagues, especially Prashant Khadke, Maik Kraus, Daniel Schröder and Youngseung Na, for many interesting and inspiring scientific and non-scientific discussions and for the support in experimental questions. It was a pleasure to meet you and it was a lot of fun to work with you. I hope we will stay in contact.

I want to thank Prof. Kai Sundmacher for accepting to be second examiner of my thesis as well as for supporting our research group during the time at MPI Magdeburg. The assistance from and discussions with members of his research group was appreciated very much and promoted our research. I want to especially thank Bianka Stein and Markus Ikert for their support in the lab and for answering the innumerable questions of a lab newbie. I don't want to miss to also thank the mechanical and electrical workshops at MPI who provided their know how to supported me in designing my experimental setups. Thanks also to all the people of the technical and organisation staff at MPI who created excellent working conditions at MPI.

After our move to TU Braunschweig I also got a lot of support at our institute. Many thanks to the technical staff at InES especially to Nina Böge and Wilfried Janßen for their support in the lab and to Horst Müller and Ina Schunke for the their readiness to help in administrative issues and questions relating TU Braunschweig.

Thank's also to my students Mareike Carstens, Florian Klitsch and Ganesh Swaminathan for their assistance in carrying out some of the experiments.

Furthermore, I want to thank Prof. Dario Dekel for providing a second membrane for my measurements which allowed me to compare and rate the experimental results . Many thanks to Dr. Jürgen Fuhrmann from Weierstrass Institute in Berlin and to Bolaji James Adesokan from DTU in Denmark for the valuable discussions about boundary layer determination and Comsol simulations. Due to their support I was able to determine the boundary layer thickness in my setup.

I take this opportunity to also thank Prof. Richard Hanke-Rauschenbach who introduced me to fundamental research. Although he did not support me during my time as PhD student, he though me a lot regarding methods and strategies in research which I needed for my studies during the past years.

Warm thanks to Christian Kunde and Astrid Bensmann for the interesting and helpful discussions during lunch time about Matlab, modelling problems and all other topics about which nobody else was willing or capable of discussing with me.

Last but not least, I want to thank my family for being patient and not being annoyed about the permanent stress aura surrounding me in the past years.

Christine Weinzierl Braunschweig, 19.10.2016

Contents

List of Symbols and Abbreviations

Symbols that are solely used locally may not be found in this list but are explained at the point they are used.

Latin Symbols

A^{M}	Area of membrane (m^2)
A	Peak area in chromatogramm ($\mu\mathrm{V\,s}^{-1}$)
$\mathcal{A}$	Amplitude of cosine oscillations
$\overline{A}$	Mean peak area in chromatogramm ($\mu\mathrm{V\,s}^{-1}$)
A_β,B_β,C_β,D_β	Wagner coefficients of component β for vapour pressure
a	Number of angle discretisation
$a_{\mathrm{i,1\text{-}4}}$	Coefficients for membrane gas equilibrium
$B^{\mathrm{DL}}_{\alpha/\beta}$	Substitution term
b_κ	Coefficient for diffusion layer thickness
c_β	Concentration of component β ($\mathrm{mol\,l}^{-1}$)
c^*_β	Concentration of pure substance β ($\mathrm{mol\,l}^{-1}$)
D^{M}_β	Diffusion coefficient of component β through membrane ($\mathrm{m}^2\,\mathrm{s}^{-1}$)
d	Thickness (m)
F	Faraday constant ($\mathrm{As\,mol}^{-1}$)
F^{d}_α	Driving force for diffusion of component α through membrane
$F(\vec{z})$	General function in Appendix A.3
$F_{\mathrm{in/out}}$	Volume flow rate at inlet/outlet ($\mathrm{m}^3\,\mathrm{s}^{-1}$)
f^{M}	Membrane wetness
I	Current (A)
$I^{\mathrm{a\text{-}f}}$	Substitution term ($\mathrm{mol\,m}^{-5}$)
i	Current density ($\mathrm{A\,m}^{-2}$)
$j_{k,\beta}$	Diffusive molar flux ($\mathrm{mol\,m}^{-2}\mathrm{s}^{-1}$)
$\tilde{j}_{k,\beta}$	Diffusive mass flux ($\mathrm{kg\,m}^{-2}\mathrm{s}^{-1}$)
l	Number of discretisation elements in diffusion layer
M_β	Molar mass of component β ($\mathrm{kg\,mol}^{-1}$)

m	Number of radius discretisation
n	Number of discretisation elements through membrane
n_β	Amount of substance of component β (mol)
$\vec{n}$	Surface normal vector
$\dot{n}_\beta$	Molar flow of component β ($\mathrm{mol\,s^{-1}}$)
$\dot{n}_{\mathrm{Me}}^{\mathrm{new}}$	Molar flow of neat methanol to the loop ($\mathrm{mol\,s^{-1}}$)
p	Pressure (Pa)
$p_{\beta,1\text{-}3}^{\mathrm{cc}}$	Coefficients of calibration curve of component β
$p_{1\text{-}3}$	Coefficients for membrane gas equilibrium
$p_\beta^{\mathrm{o}}(T)$	Vapour pressure of β at temperature T (Pa)
R	Universal gas constant ($\mathrm{J\,mol^{-1}K^{-1}}$)
RH	Relative humidity (%)
R^{MW}	Radius of membrane window (m)
r	Radius (m)
s	Distance (m)
T	Temperature (K)
t	Time (s)
V	Volume ($\mathrm{m^3}$)
v_k	Velocity in direction k ($\mathrm{m\,s^{-1}}$)
v_β	Diffusion volume of component β
w_β	Mass fraction of component β
X_β	Mole fraction of component β in liquid phase
x	Universal variable for derivations
$\vec{x}$	Vector of cylindrical coordinates
y	Universal variable for derivations
y_β	Mole fraction of component β in gas phase
z	Spatial coordinate (m)
$\vec{z}$	Vector of cartesian coordinates

Greek Symbols

η_{Me}	Methanol efficiency
κ	Water drag coefficient
λ	Excess ratio of reactant
ξ	Water accumulation
ρ	Density ($\mathrm{kg\,m^{-3}}$)
$\tilde{\rho}_{\mathrm{dry}}^{\mathrm{M}}$	Area density of dry membrane ($\mathrm{kg\,m^{-2}}$)

σ	Uncertainty
σ_β	Molar sources and sinks of component β ($\mathrm{mol\,s^{-1}}$)
$\tilde{\sigma}_\beta$	Mass sources and sinks of component β ($\mathrm{kg\,m^{-3}s^{-1}}$)
φ	Angle coordinate
ψ	Phase shift of cosine oscillation
ζ_α	Substitution term

Superscripts

A	At anode
ACL	At anode catalyst layer
ad	Additional
bulk	In bulk flow
CL	At catalyst layer
C	At cathode
CCL	At cathode catalyst layer
cc	Calibration curve
co	Cross-over
crit	Critical value
DG	Dial gauge
DL	In diffusion layer
diff	Diffusion
drag	Electro-osmotic water drag
eq	Equilibrium
G	In gas chamber
g	Vapour
L	In liquid chamber
l	liquid
Lo	In loop
loc	At any location
max	Maximum value
M	In membrane
Mg	Membrane at gas side
Ml	Membrane at liquid side
norec	Without methanol recycling
PB	At phase boundary
RH	Humidity sensor

rec	With methanol recycling
SL	In sample loop
ST	Shim stock
Sys	System
wet	Wet

Subscripts

α	Component at anode
β	General component
γ	Component at cathode
ζ	Liquid component
0	At start of simulation
CO_2	Carbon dioxide
dry	Dry gas or membrane
end	At end of simulation
gas	Of gas phase
h	Volume element number in φ direction
i	Volume element number in z direction
in	At inlet
j	Volume element number in r direction
k	Direction
lim	Limit
liq	Of liquid phase
max	Maximum value
Me	Methanol
Me^g	Methanol vapour
N_2	Nitrogen
N	Norm value
O_2	Oxygen
out	At outlet
s	Stable water level
VE	Volume element
W	Water
W^g	Water vapour

Abbreviations

AEM	Anion exchange membrane
ADMFC	Alkaline direct methanol fuel cell
AFC	Alkaline fuel cell
DMFC	Direc methanol fuel cell
MEA	Membrane electrode assembly
PEEK	Polyetheretherketon
PTFE	Polytetrafluoroethylene

CHAPTER 1

Introduction and Motivation

It is generally accepted that fuel cells have great potential to support our journey towards 100 % renewable energies. Their ability to convert chemically stored energy directly into electrical energy via electrochemical reactions enables high electric efficiencies even for small systems which qualifies fuel cells for decentralised, mobile and portable power supply. Highest power is achieved using hydrogen as a fuel. However, methanol and other alcohols are especially suitable for portable application due to easier storage and higher energy density of alcohols compared to hydrogen. Since electrochemical reactions do not emit noise, a fuel cell itself is a very silent device which is desirable for all applications. Nevertheless, fuel cells are not yet fully established on the market yet mainly due to the high cost e.g. for platinum (Pt) which is required as catalyst in acidic low temperature fuel cells. Since non-Pt catalysts show higher activity and stability in alkaline media compared to acidic media, alkaline fuel cells (AFC) could reduce fuel cell cost and play a progressively increasing role in present fuel cell research.

1.1 Origins of Alkaline Fuel Cells

Alkaline fuel cells are not a new technology. There have been patents by James H. Reid for a kind of AFC in 1903 already [1–3]. A more practicable approach was adopted by Francis T. Bacon starting in 1939 who used nickel electrodes and potassium hydroxide (KOH) as electrolyte. He found a way to prevent corrosion of cathode electrode by doping the nickel electrodes with lithium and successfully extended his fuel cell to a fuel cell system with 40 cells which was used as power supply for devices like a fork lift in 1959 [4]. This fuel cell system was the kick off for industrial research on AFCs. A summary of industrial research projects on AFC in the past is given by [5]. The most popular project applying this technology is the Apollo project of the NASA who equipped rockets with three alkaline hydrogen-oxygen fuel cell stacks from 1966 onwards [6]. However, these fuel cells used potassium hydroxide as liquid electrolyte which caused technical difficulties

that inhibited commercialisation of AFCs. Besides corrosion and leakage problems, hydroxide ions (OH^-) in alkaline solutions react with carbon dioxide (CO_2) which is present in ambient air and which is produced if alcohols such as methanol (CH_3OH) are used as fuel. This carbonation of alkaline solutions not only decreases pH value and conductivity of the electrolyte but also causes precipitation of carbonate salts due to the low solubility of potassium carbonate (K_2CO_3).

$$CO_2 + 2\,OH^- \longrightarrow CO_3^{2-} + H_2O \tag{1.1}$$

$$2\,K^+ + CO_3^{2-} \longrightarrow K_2CO_3\downarrow \tag{1.2}$$

Precipitated salt can block pores or coat catalyst particles which decreases the electrochemically active area of the catalyst and, thus, reduces fuel cell performance and life time.

In the late 1950s, Willard T. Grubb invented a fuel cell with an ion conducting membrane as sole electrolyte and platinum electrodes and operated it with hydrogen and oxygen [7]. The advantages of this kind of fuel cell are low operation temperature and pressure as well as a decrease of volume and prevention of electrolyte leakage. In the following years, several scientists worked on proton conducting polymer membranes for use as solid electrolyte in acidic fuel cells. The most famous electrolyte membrane, *Nafion*, was developed in the 1970s by Walter G. Groth [8] and became standard for proton exchange membrane fuel cells (PEMFCs). With this membrane electrolyte, fuel cell research focussed on PEMFCs and the interest in alkaline fuel cells progressively diminished. Public as well as industrial research has been done mainly on hydrogen fuelled PEMFC but also alcohols such as methanol or ethanol were used as fuels. The continuous improvement of fuel cell technology allowed for successful prototyping of several applications such as fuel cell cars. However, serial mass production failed to appear mainly due to low life time of fuel cells at high cost e.g. for the required platinum catalyst. The invention of anion exchange membranes (AEM) as solid electrolyte for alkaline fuel cells at the beginning of this millennium [9, 10] rekindled the interest in AFCs which allow usage of cheap base metals such as nickel as catalyst. Usage of AEMs as sole electrolyte prevents precipitation of carbonate salts and allows for realisation of alkaline direct methanol fuel cells (ADMFCs).

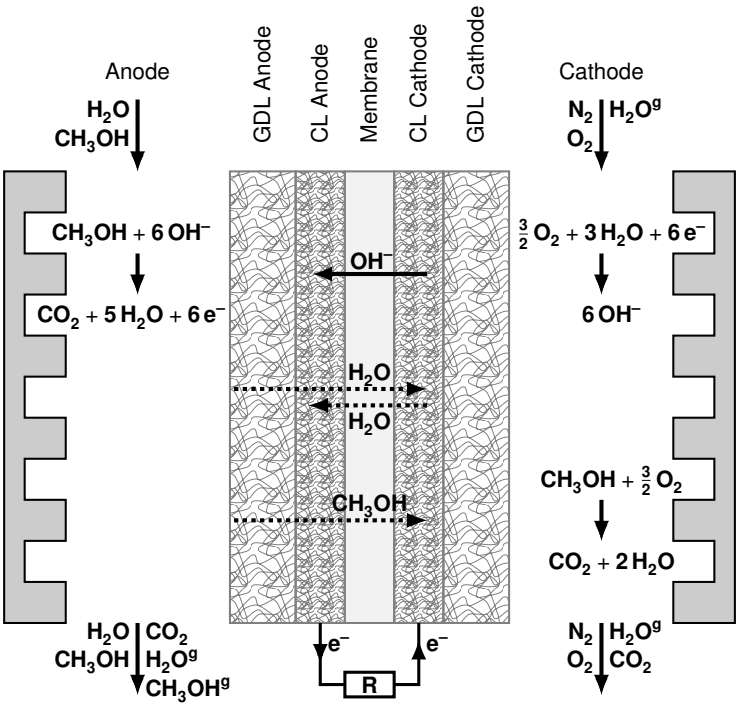

Figure 1.1: Schematic of an ADMFC including anode and cathode fluid channels, gas diffusion layers (GDLs), catalyst layers (CLs) and a solid electrolyte membrane [11].

1.2 Structure and Principle of an ADMFC

The electrochemical reactions taking place in a fuel cell enable direct conversion of chemical energy into electrical energy. The working principle is similar for all fuel cell types and explained for the alkaline direct methanol fuel cell with AEM as electrolyte in this section.

Fuel cells of the alkaline type are based on an electrolyte that conducts OH^- ions, e.g. an anion exchange membrane. The function of the membrane is to separate fuel and oxidant, to allow ion exchange and to inhibit electron conduction. The membrane is sandwiched between two electrodes, anode and cathode, that consist of a catalyst layer (CL) and a gas diffusion layer (GDL) as displayed in Fig. 1.1. Since the reactions in a fuel cell are electrochemical reactions, they can only take place at a location where three phases meet in which ions, electrons and neutral reactants can exist. Therefore, the catalyst layer consists of a porous structure of electronically conductive material and an ionomer as solid electrolyte. The reactants in the mobile phase can diffuse through the pores to the three phase boundary. The function of the GDL is the protection of the catalyst layer from erosion due to convective flux, the distribution of reactants over

the effective area as well as electron conduction. The flow channels are bordered by flow field plates which are also electronically conductive.

Either pure oxygen or air is supplied to the cathode of an ADMFC and reduced in the electrochemical reduction reaction (Eq. (1.3)) consuming water and electrons and producing OH^-. The ions are conducted by ionomer and membrane from cathode to anode. At anode, OH^- is consumed by the electrochemical oxidation of methanol (Eq. (1.4)) which is fed to the anode of an ADMFC. Moreover, the anodic reaction produces water and carbon dioxide and releases electrons. The overall reaction taking place in ADMFCs (Eq. (1.5)) is equivalent to the standard oxidation of methanol with a net production of two water molecules per molecule of methanol.

$$\tfrac{3}{2}\,O_2 + 3\,H_2O + 6\,e^- \longrightarrow 6\,OH^- \tag{1.3}$$

$$CH_3OH + 6\,OH^- \longrightarrow CO_2 + 5\,H_2O + 6\,e^- \tag{1.4}$$

$$CH_3OH + \tfrac{3}{2}\,O_2 \longrightarrow CO_2 + 2\,H_2O \tag{1.5}$$

In order to use the electric power provided by the fuel cell, anode and cathode need to be connected via an electric circuit through which electrons can flow from anode to cathode.

Although the membrane is supposed to inhibit mass transport between the electrodes, mass transport through membrane still takes place in ADMFCs. Both, methanol and water have a high concentration at anode but a low concentration at cathode and, thus, diffuse through the membrane along the concentration gradient. The quantity of diffusion depends on the respective diffusivity of the membrane. Water diffusion can result in evaporation at cathode according to phase equilibrium. Methanol diffusion is called methanol cross-over and has two big disadvantages. First, it diminishes cell performance since methanol is oxidised at cathode in a chemical reaction according to Eq. (1.5) consuming oxygen and causing a mixed potential [12]. Second, it decreases fuel efficiency due to the additional loss of methanol. Another transport process that takes place in the membrane is the electro-osmotic drag of water. Because of the dipole character of water, OH^- ions form hydrogen bonds with surrounding water molecules. Hence, ions that are conducted from cathode to anode drag the bonded water in the same direction which is from gas side to liquid side intensifying the need of water management.

1.3 State of the Art

Alkaline fuel cells with AEMs as electrolyte are in the early stages of development and focus of research is still on new material. Since no similarly high performance equivalent to *Nafion* is found for alkaline fuel cells so far, there is an ongoing research on new or modified membrane material [13, 14]. Main challenges of membrane improvement are ionic conductivity and long term stability in OH^- form [15]. Some research is done on special membranes for alkaline direct alcohol fuel cells with reduced alcohol cross-over through membrane [16–18]. Other studies show that carbonation also takes place when using an alkaline membrane electrolyte which can cause a gradient of pH value across the membrane [19]. However, Varcoe et al. [15] stated that bicarbonate (HCO_3^-) severely decreases cell performance due to lower conductivity while CO_3^{2-} has only slightly negative effect on fuel cell performance and stability is even higher in CO_3^{2-} form. They therefore suggested to use membranes in carbonate form and to use catalysts that prevent forming of intermediates such as HCO_3^-. Main advantage of alkaline fuel cells is the usage of cheap base metals as catalyst. Consequently, studies on new catalyst materials for AFCs are also strongly represented in literature e.g. [20–22]. Studies on new materials primarily focus on achieving better fuel cell performance with cheap materials by improving stability, ion conductivity or fuel reactivity. Further studies investigate the effect of operation conditions and material parameters on cell performance. For example, a study of Yu and Scott on ADMFCs [23] reveals that an increase of operation temperature or of methanol flow rate results in better performance while the effect of rising methanol concentration indicates that best cell performance can be achieved with a methanol concentration between $1\,\mathrm{mol\,l^{-1}}$ and $4\,\mathrm{mol\,l^{-1}}$. Poynton et al. [24] observed an increase in cell performance with a decrease of membrane thickness and concluded that water transport through membrane is a limiting process for AFC performance at least for thick membranes. However, process engineering issues like mass transport through the membrane or water management are inadequately represented in literature so far. Few studies on experimental investigation of water uptake as well as determination of transport parameters such as electro-osmotic drag coefficient and diffusion coefficients can be found in literature [25–27]. Cathode flooding in an alkaline direct ethanol fuel cell (ADEFC) was studied by Li et al. [28] who operated their cell with KOH mixed to ethanol solution in addition to the AEM and a dry air or oxygen feed to cathode. They observed an increase of liquid formation at cathode with current densities rising from low to medium values while an

increase from 200 mA cm^{-2} to 300 mA cm^{-2} reduces liquid formation at the same gas flow rate. Unfortunately, only anode temperature was controlled to 60 °C while gas temperature at cathode was not measured and, as a result, it is not impossible that liquid water formation was caused by condensation. However, the same group detected improved cell performance of an ADEFC if a micro porous layer which is hydrophobic due to PTFE loading is included at cathode of the cell [29]. They concluded that hydrophobicity reduces liquid water formation and, thus, allows for better oxygen transport. The same conclusion has been drawn by Kim et al. [30] after detecting that hydrophobic ionomer and PTFE loading in the cathode catalyst layer is beneficial to performance of passive ADMFC electrodes. Furthermore, Khalidi et al.[31] demonstrated that AFCs with non-circulating liquid electrolyte show best performance with stable water level of the liquid electrolyte. Control of water level can be achieved by adjusting humidity and flow rate of the hydrogen fuel in order to remove produced water. Zhang et al. [32] examined the importance of water diffusion from anode to cathode by experimental determination of water transport processes in a hydrogen fuelled AEMFC without liquid electrolyte and also discovered that inlet conditions have significant influence on cell performance. With help of a simple model, they were able to improve cell performance by optimizing inlet conditions.

The same topics that are found in experimental studies are also covered by modelling studies which aim to understand limitations, to identify dependencies on parameters and to optimise fuel cell operation. Several models include alkaline solutions as sole electrolyte or in addition to an AEM. However, some results of these models are also interesting for AFCs without liquid electrolyte and are therefore mentioned here. A study of performance of hydrogen fuelled AFCs for different concentrations of liquid electrolyte reveals that an optimal KOH concentration around 3 mol l^{-1} results in the best cell performance and that diffusive transport of dissolved oxygen is the limiting process [33]. The limitation by dissolved oxygen in H_2 fuelled AFCs has also been identified by Kimble and White [34] who concluded that this limitation results from a higher concentration of KOH at cathode during operation with high current densities. This model has further been used for a sensitivity analysis and optimization [35] revealing that optimal thickness of cathode catalyst layer is about 223 µm and they recommend to increase the three phase boundary to enable higher oxygen dissolution rates. This can be achieved by using a membrane electrode assembly with solid electrolyte which comprises a porous electrode structure of solid catalyst and ionomer providing a larger three phase boundary. A model of an ADEFC was used to

analyse the effect of concentration changes or geometry parameters of anode gas diffusion layer on the fuel cell performance [36]. Furthermore, the model is used to calculate voltage losses in an ADEFC which reveals high activation losses at both electrodes and a limitation by mass transport at anode. A similar study has been done on an ADMFC [37] and both models are using liquid electrolyte in addition to an AEM. Verhaert et al. [38] used modelling to analyse water management in a hydrogen fuelled AFC with a circulating liquid electrolyte. They unveiled that operation temperature as well as air excess ratio influence water level of the electrolyte solution. The latter is suggested as control parameter and also variation of humidity and temperature of inlet gas is recommended to maintain water content in the electrolyte. Models that describe fuel cells with solely an AEM as electrolyte are still scarce in literature and done by two research groups so far: The group of Prof. K. Jiao and our research group led by Prof. U. Krewer. The group of Prof. Jiao analysed the performance of hydrogen fuelled AEMFCs for different inlet conditions and other parameter changes [39, 40]. Among other results, they observed that humidification of cathode as well as of anode significantly improves cell performance and that liquid water formation at anode only occurs for anode inlet humidities above 80 %. An analysis of the water management in the anode of a hydrogen fuelled AEMFC [41] reveals that full humidification at anode and cathode leads to significant liquid water formation and to water diffusions that are lower than electro-osmotic drag of water. High porosities as well as high contact angles of gas diffusion layers and catalyst layers reduce water formation and with it also water diffusion. The effect of a micro porous layer (MPL) on performance of a passive ADMFC as well as on transport processes in this fuel cell was also analysed by modelling [42]. An MPL at cathode slightly increases performance and decreases water transport from anode to cathode which also effects water management at anode. This effect is increased with hydrophobicity of the MPL while hydrophobicity of cathodic catalyst layer increases water transport. An MPL at anode has a negative effect on fuel cell performance but reduces methanol cross-over. This effect decreases with increasing methanol concentration but increases with hydrophobicity of anode MPL. However, they only determined water content in GDL, MPL, CL and membrane while the impact on the methanol solution in the reservoir as well as potential limitations due to insufficient water supply to cathode were solely analysed by our research group [11, 43]. This analysis is part of the present thesis.

1.4 Purpose and Motivation

ADMFCs which are highly attractive as power supply for portable applications continuously produce CO_2 at anode during operation. It is therefore not advisable to operate ADMFCs with liquid electrolyte due to carbonation problems explained above. Hence, the liquid electrolyte needs to be replaced by a solid alkaline electrolyte membrane. But AEMFCs do not show the same performance as AFCs with liquid electrolyte so far [44, 45] and the reason for that is not yet clear. Khadke and Krewer observed that oxygen transport in the cathode catalyst layer is not limiting [46] as predicted for liquid electrolyte AFCs [33]. Among other possibilities, deficient water management is a potential reason for the low performance. Water is consumed at cathode which is fed with air or oxygen. A cycling liquid electrolyte provides a water reservoir between the two electrodes of an AFC. This reduces water management to maintaining water content of the liquid electrolyte which can be conducted outside of the fuel cell. Replacing the liquid electrolyte by a solid electrolyte membrane removes this water buffer and increases the importance of water management. Although methanol fuel cells contain sufficient water, this water is available at anode and needs to be transported through the membrane to be available for cathode reaction. Hence, insufficient water supply is a potential reason for decreased reaction rate of reduction reaction Eq. (1.3) and, thus, for performance drop. Furthermore, water is produced and is not taken up and removed from fuel cell by the flowing electrolyte but results in methanol dilution, which decreases reaction rate at anode, and also results in water accumulation in case of recycling methanol solution. This leads to two challenges regarding water management in ADMFCs: Water supply to the cathode and stabilisation of water level at the anode. These challenges are additionally influenced by further processes and conditions in ADMFCs: Electro-osmotic drag of water transports water from cathode to anode and, thus, intensifies both challenges depending on the current produced by the fuel cell. As opposed to this, methanol cross-over mitigates the challenge of water supply since methanol crossing over to cathode is oxidised producing water (Eq. (1.5)). This effect is independent of current. Furthermore, water in membrane and gas phase at cathode strive towards an equilibrium which inhibits complete dehumidification of the gas. Hence, depending on relative humidity of the gas and water content of the membrane, water is absorbed or evaporated at the membrane-gas interface. Only absorbed water is available for water drag or oxygen reduction. Last but

not least, water diffusion takes place from anode to cathode which is favourable for both challenges.

Evidently, water management in ADMFCs is a complex network of many processes that needs to be considered for long term operation of ADMFCs. The key process to cope with the challenges is the water diffusion through the membrane. However, a detailed analysis of water management in ADMFCs is missing in literature. Therefore, this thesis first analyses different extreme case scenarios (Chapter 2) in order to determine limitations by water management and demands for autonomous operation of the ADMFC. Furthermore, the influence of parameters is studied to identify which parameters can be used to improve water management and water level stability. Since water diffusion is a key process of water management, diffusion fluxes are determined experimentally (Chapter 3) and compared with the simulation results of a complex model of the diffusion experiment to obtain diffusion coefficients for a detailed transport model approach (Chapter 4). The determined parameters are included in an enhanced transport model to analyse the identified option of changing cathode conditions to stabilise water level at anode in more detail (Chapter 5).

CHAPTER 2

Extreme Case Scenarios

The working principle of an ADMFC indicates two challenges regarding water management: water supply to cathode and water level stabilisation at anode. As a first step, model based analysis of water management is used to reveal limitations as well as the importance of and requirements for mastering these challenges. Therefore, the following general mathematical model is derived to describe and analyse transport processes and water management in an ADMFC. In order to study different aspects of water management, the general model is then modified forming five extreme case scenarios. The first two scenarios aim at analysis of water supply to cathode and, thus, solely describe the fuel cell while scenarios 3 to 5 include an anodic loop for liquid recycling to study water level stabilisation at anode. The content of this chapter has already been published [11, 43]. This includes equations, pictures as well as conclusions drawn from results and the explanatory text is only slightly modified to unify the two publications.

2.1 General Mathematical Model

The general model considers three chambers – anode, cathode and the anodic loop for recycling of methanol solution – which are partly interacting as shown in Fig. 2.1. The outlet of the anodic loop is connected to anode inlet while anode outlet is connected to the inlet of the loop. The membrane which couples anode and cathode is not modelled in detail, but it is implemented as a semipermeable wall that allows transport of certain species. In order to focus on the important processes, the model is kept as simple as possible by including the following assumptions: Pressure and temperature in all chambers are assumed to be constant at $p = 1\,\mathrm{bar}$ and $T = 50\,^{\circ}\mathrm{C}$, respectively. Therefore, it is not necessary to include an energy balance. Furthermore, dynamic charge balances are not considered since the model is not used to study the performance but to analyse procedural

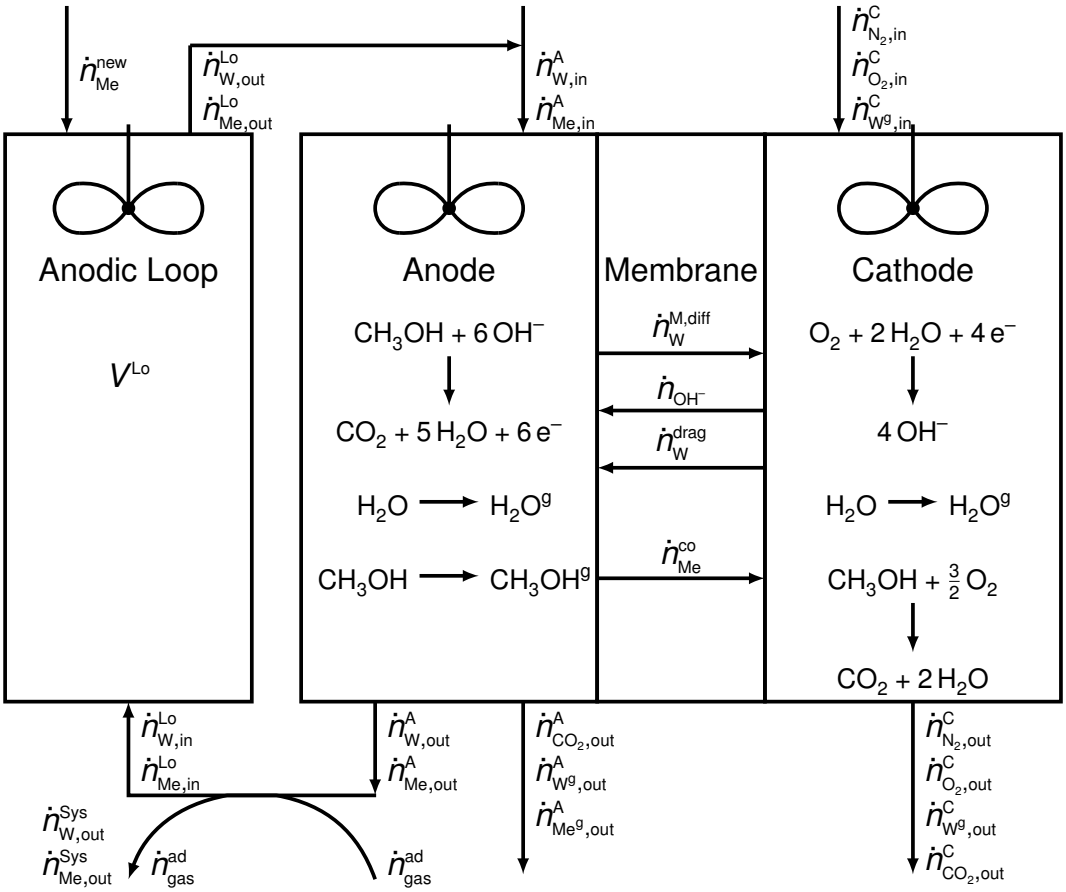

Figure 2.1: Sketch of the general ADMFC model including fuel cell and anodic loop. The chambers are well mixed (no local gradients) and reactions only occur at anode and cathode.

requirements regarding water management. Hence, differential equations of this model arise from mass balances of the components β with the space direction k.

$$\frac{\partial \rho_\beta}{\partial t} = -\frac{\partial}{\partial z_k}\left(\rho_\beta v_k + \tilde{j}_{k,\beta}\right) + \tilde{\sigma}_\beta \tag{2.1}$$

Transport limitations within the chambers, e.g. by diffusion through gas diffusion layer and catalyst layer, are disregarded. Therefore, no local gradients appear in anode, cathode and anodic loop and the chambers are modelled as continuous stirred tank reactors (CSTRs). Volumes of anode and cathode chambers are constant. Methanol (Me) diffusing through the membrane to cathode is immediately oxidised and liquid water is immediately consumed or evaporated at cathode ($c^{C}_{\beta,\mathrm{liq}} = 0$). Evaporation may saturate cathodic gas with water but oversaturation is not possible ($RH^{C} \leq 100\,\%$). Moreover, the anodic loop is solely a storage and mixing unit for methanol solution in which no reactions or phase transitions

take place and no other source or sink terms appear. Thus, the mass balances for components α at anode (A), γ at cathode (C) and ζ in the anodic loop (Lo) reduce to:

$$V^{\mathrm{A}}\frac{dc_\alpha^{\mathrm{A}}}{dt} = \dot{n}_{\alpha,\mathrm{in}}^{\mathrm{A}} - \dot{n}_{\alpha,\mathrm{out}}^{\mathrm{A}} + \dot{n}_{\alpha}^{\mathrm{A,diff}} + \sigma_\alpha^{\mathrm{A}} \tag{2.2}$$

$$V^{\mathrm{C}}\frac{dc_\gamma^{\mathrm{C}}}{dt} = \dot{n}_{\gamma,\mathrm{in}}^{\mathrm{C}} - \dot{n}_{\gamma,\mathrm{out}}^{\mathrm{C}} + \dot{n}_{\gamma}^{\mathrm{C,diff}} + \sigma_\gamma^{\mathrm{C}} \tag{2.3}$$

$$\frac{dn_\zeta^{\mathrm{Lo}}}{dt} = \dot{n}_{\zeta,\mathrm{in}}^{\mathrm{Lo}} - \dot{n}_{\zeta,\mathrm{out}}^{\mathrm{Lo}} + \dot{n}_{\zeta}^{\mathrm{new}} \tag{2.4}$$

Electro-osmotic drag of water from cathode to anode solely depends on current density i and is independent of any concentration:

$$\dot{n}_{\mathrm{W}}^{\mathrm{drag}} = \kappa\frac{A^{\mathrm{M}}i}{F} \tag{2.5}$$

with water drag coefficient κ, membrane area A^{M} and Faraday constant F. This transport process is included in the sources and sinks terms, $\sigma_\beta^{\mathrm{A}}$ and $\sigma_\beta^{\mathrm{C}}$, which also include rates of electrochemical reactions, evaporation at anode to achieve equilibrium between gas and liquid phase and methanol oxidation that result from methanol cross-over $\dot{n}_{\mathrm{Me}}^{\mathrm{C,diff}}$. Evaporation at cathode is not a source or sink since solely gas phase is considered at cathode and all water that is gained at cathode is assumed to be evaporated immediately. Since the models in this thesis are not used to analyse dynamics or cell performance, reaction kinetics are disregarded and rates of electrochemical reactions are described by Faraday's law. Due to the assumption of CSTR, sources and sinks in the chambers are equal to those that actually occur at catalyst layers: $\sigma_\beta^{\mathrm{A}} = \sigma_\beta^{\mathrm{ACL}}$ and $\sigma_\beta^{\mathrm{C}} = \sigma_\beta^{\mathrm{CCL}}$. They are defined as:

$$\begin{aligned}
\sigma_\beta^{\mathrm{loc}} &= \pm\text{reaction} \pm \text{evaporation} && \pm \text{drag} \pm \text{cross-over} \\
\sigma_{\mathrm{Me}}^{\mathrm{ACL}} &= -\frac{A^{\mathrm{M}}i}{6F} && - \frac{y_{\mathrm{Me^g}}^{\mathrm{A}}}{1-y_{\mathrm{Me^g}}^{\mathrm{A}}-y_{\mathrm{W^g}}^{\mathrm{A}}}\frac{A^{\mathrm{M}}i}{6F} + 0 && + 0 && (2.6)\\
\sigma_{\mathrm{W}}^{\mathrm{ACL}} &= +\frac{5A^{\mathrm{M}}i}{6F} && - \frac{y_{\mathrm{W^g}}^{\mathrm{A}}}{1-y_{\mathrm{Me^g}}^{\mathrm{A}}-y_{\mathrm{W^g}}^{\mathrm{A}}}\frac{A^{\mathrm{M}}i}{6F} + \dot{n}_{\mathrm{W}}^{\mathrm{drag}} && + 0 && (2.7)\\
\sigma_{\mathrm{CO_2}}^{\mathrm{ACL}} &= +\frac{A^{\mathrm{M}}i}{6F} && + 0 && + 0 && + 0 && (2.8)\\
\sigma_{\mathrm{Me^g}}^{\mathrm{ACL}} &= +0 && + \frac{y_{\mathrm{Me^g}}^{\mathrm{A}}}{1-y_{\mathrm{Me^g}}^{\mathrm{A}}-y_{\mathrm{W^g}}^{\mathrm{A}}}\frac{A^{\mathrm{M}}i}{6F} + 0 && + 0 && (2.9)\\
\sigma_{\mathrm{W^g}}^{\mathrm{ACL}} &= +0 && + \frac{y_{\mathrm{W^g}}^{\mathrm{A}}}{1-y_{\mathrm{Me^g}}^{\mathrm{A}}-y_{\mathrm{W^g}}^{\mathrm{A}}}\frac{A^{\mathrm{M}}i}{6F} + 0 && + 0 && (2.10)\\
\sigma_{\mathrm{Me}}^{\mathrm{CCL}} &= +0 && + 0 && + 0 && - \dot{n}_{\mathrm{Me}}^{\mathrm{C,diff}} && (2.11)
\end{aligned}$$

$$\sigma_{\mathrm{O_2}}^{\mathrm{CCL}} = -\frac{A^{\mathrm{M}} i}{4F} + 0 + 0 \quad - \frac{3}{2}\dot{n}_{\mathrm{Me}}^{\mathrm{C,diff}} \tag{2.12}$$

$$\sigma_{\mathrm{W}}^{\mathrm{CCL}} = -\frac{A^{\mathrm{M}} i}{2F} + 0 - \dot{n}_{\mathrm{W}}^{\mathrm{drag}} + 2\dot{n}_{\mathrm{Me}}^{\mathrm{C,diff}} \tag{2.13}$$

$$\sigma_{\mathrm{CO_2}}^{\mathrm{CCL}} = +0 \quad + 0 + 0 \quad + \dot{n}_{\mathrm{Me}}^{\mathrm{C,diff}} \tag{2.14}$$

$$\sigma_{\mathrm{N_2}}^{\mathrm{CCL}} = +0 \quad + 0 + 0 \quad + 0 \tag{2.15}$$

Equilibrium molar fractions of water $y_{\mathrm{W^g}}^{\mathrm{A}}$ and methanol $y_{\mathrm{Me^g}}^{\mathrm{A}}$ in gas phase at anode are calculated by Eq. (2.36) using laws of Raoult and Dalton. Molar inlet and outlet fluxes of anode and cathode ($\mathrm{loc} \in \{\mathrm{A,C}\}$) are defined by:

$$\dot{n}_{\beta,\mathrm{in}}^{\mathrm{loc}} = c_{\beta,\mathrm{in}}^{\mathrm{loc}} F_{\mathrm{in}}^{\mathrm{loc}} \tag{2.16}$$

$$\dot{n}_{\beta,\mathrm{out}}^{\mathrm{loc}} = c_{\beta}^{\mathrm{loc}} F_{\mathrm{out}}^{\mathrm{loc}} \tag{2.17}$$

Inlet volume flow rates are defined by excess ratios of methanol and oxygen, respectively:

$$F_{\mathrm{in}}^{\mathrm{A}} = \frac{\lambda^{\mathrm{A}}}{c_{\mathrm{Me,in}}^{\mathrm{A}}} \frac{A^{\mathrm{M}} i}{6F} \tag{2.18}$$

$$F_{\mathrm{in}}^{\mathrm{C}} = \frac{\lambda^{\mathrm{C}}}{c_{\mathrm{O_2,in}}^{\mathrm{C}}} \frac{A^{\mathrm{M}} i}{4F} \tag{2.19}$$

Cathode is fed with air including humidification to a specific molar fraction $y_{\mathrm{W,in}}^{\mathrm{C}}$. The resulting concentrations at cathodic inlet are calculated by:

$$c_{\mathrm{O_2,in}}^{\mathrm{C}} = 0.21(1 - y_{\mathrm{W,in}}^{\mathrm{C}}) c_{\mathrm{gas,in}}^{\mathrm{C}} \tag{2.20}$$

$$c_{\mathrm{W,in}}^{\mathrm{C}} = y_{\mathrm{W,in}}^{\mathrm{C}} c_{\mathrm{gas,in}}^{\mathrm{C}} \tag{2.21}$$

Considering that total volumes of anode and cathode chamber are constant, volume flow rates leaving anode and cathode can be calculated by:

$$F_{\mathrm{out}}^{\mathrm{A}} = F_{\mathrm{in}}^{\mathrm{A}} + \frac{\dot{n}_{\mathrm{W}}^{\mathrm{A,diff}}}{c_{\mathrm{W}}^{*}} + \frac{\dot{n}_{\mathrm{Me}}^{\mathrm{A,diff}}}{c_{\mathrm{Me}}^{*}} + \sum_{\alpha} \frac{\sigma_{\alpha}^{\mathrm{A}}}{c_{\alpha}^{*\mathrm{A}}} \tag{2.22}$$

$$F_{\mathrm{out}}^{\mathrm{C}} = \frac{c_{\mathrm{gas,in}}^{\mathrm{C}}}{c_{\mathrm{gas}}^{\mathrm{C}}} F_{\mathrm{in}}^{\mathrm{C}} + \sum_{\gamma} \frac{\dot{n}_{\gamma}^{\mathrm{C,diff}} + \sigma_{\gamma}^{\mathrm{C}}}{c_{\mathrm{gas}}^{\mathrm{C}}} \tag{2.23}$$

Derivation of these flow rates is given in Appendix A.1. Concentrations marked with an asterisk, c^{*}, are concentrations of pure components.

Since this chapter aims at identification of general demands on and options for water management, a detailed description of diffusive fluxes is not required and

Fick's law of diffusion is used to describe methanol and water diffusion through membrane as in most experimental studies in literature:

$$\dot{n}_{\beta}^{\mathrm{M,diff}} = -D_{\beta}^{\mathrm{M}} A^{\mathrm{M}} \frac{c_{\beta,\mathrm{liq}}^{\mathrm{C}} - c_{\beta,\mathrm{liq}}^{\mathrm{A}}}{d^{\mathrm{M}}} \tag{2.24}$$

$$\dot{n}_{\beta}^{\mathrm{A,diff}} = -\dot{n}_{\beta}^{\mathrm{M,diff}} \tag{2.25}$$

$$\dot{n}_{\beta}^{\mathrm{C,diff}} = \dot{n}_{\beta}^{\mathrm{M,diff}} \tag{2.26}$$

Due to gas production at anode, anode chamber is filled with gas and liquid. The phases are assumed to be in equilibrium at each point of time. Calculation of diffusive fluxes through membrane requires concentrations in liquid phase $c_{\beta,\mathrm{liq}}^{\mathrm{A}}$ which are solely based on the volume filled with liquid instead of the whole volume of the anode chamber:

$$c_{\alpha,\mathrm{liq}}^{\mathrm{A}} = \frac{c_{\alpha}^{\mathrm{A}} V^{\mathrm{A}}}{V_{\mathrm{liq}}^{\mathrm{A}}} \tag{2.27}$$

$$V_{\mathrm{gas}}^{\mathrm{A}} = \frac{\left(c_{\mathrm{CO_2}}^{\mathrm{A}} + c_{\mathrm{Me^g}}^{\mathrm{A}} + c_{\mathrm{W^g}}^{\mathrm{A}}\right)}{c_{\mathrm{gas}}^{\mathrm{A}}} V^{\mathrm{A}} \tag{2.28}$$

$$V_{\mathrm{liq}}^{\mathrm{A}} = V^{\mathrm{A}} - V_{\mathrm{gas}}^{\mathrm{A}} \tag{2.29}$$

In case the modelled scenario contains an anodic loop, it is assumed that a complete separation of gas and liquid is possible at anodic outlet. Deducting additional losses, liquid components $\zeta \in \{\mathrm{W,Me}\}$ of the flow leaving the anode are recycled and fed to the loop while gaseous components leave the system. Molar flows leaving the anodic loop are equal to those fed to the anode:

$$\dot{n}_{\zeta,\mathrm{in}}^{\mathrm{Lo}} = \dot{n}_{\zeta,\mathrm{out}}^{\mathrm{A}} - \dot{n}_{\zeta,\mathrm{out}}^{\mathrm{Sys}} = c_{\zeta}^{\mathrm{A}} F_{\mathrm{out}}^{\mathrm{A}} - \dot{n}_{\zeta,\mathrm{out}}^{\mathrm{Sys}} \tag{2.30}$$

$$\dot{n}_{\zeta,\mathrm{out}}^{\mathrm{Lo}} = \dot{n}_{\zeta,\mathrm{in}}^{\mathrm{A}} = c_{\zeta}^{\mathrm{Lo}} F_{\mathrm{in}}^{\mathrm{A}} \tag{2.31}$$

Neat methanol is fed to the anodic loop to compensate methanol consumption at anode. In order to keep the amount of methanol in the loop constant, a feed forward control for methanol is implemented which considers methanol consumption by reaction, cross-over and evaporation at anode:

$$\dot{n}_{\mathrm{Me}}^{\mathrm{new}} = -\sigma_{\mathrm{Me}}^{\mathrm{A}} - \dot{n}_{\mathrm{Me}}^{\mathrm{A,diff}} \tag{2.32}$$

Table 2.1: General equations valid for all models.

$$c_{\mathrm{gas}}^{\mathrm{loc}} = \frac{p^{\mathrm{loc}}}{RT^{\mathrm{loc}}} \tag{2.35}$$

$$y_{\alpha}^{\mathrm{loc}} = X_{\alpha}^{\mathrm{loc}} \frac{p_{\alpha}^{\mathrm{o}}(T^{\mathrm{loc}})}{p^{\mathrm{loc}}} \tag{2.36}$$

$$X_{\zeta}^{\mathrm{loc}} = \frac{c_{\zeta}^{\mathrm{loc}}}{c_{\mathrm{W}}^{\mathrm{loc}} + c_{\mathrm{Me}}^{\mathrm{loc}}} \tag{2.37}$$

$$y_{\mathrm{W}}^{\mathrm{loc}} = \frac{c_{\mathrm{W}}^{\mathrm{loc}}}{c_{\mathrm{gas}}^{\mathrm{loc}}} = RH^{\mathrm{loc}} \frac{p_{\mathrm{W}}^{\mathrm{o}}(T^{\mathrm{loc}})}{p^{\mathrm{loc}}} \tag{2.38}$$

$$p_{\beta}^{\mathrm{o}}(T) = p_{\beta}^{\mathrm{crit}} \exp\left[\frac{T_{\beta}^{\mathrm{crit}}}{T}\left(A_{\beta}\left(1-\frac{T}{T_{\beta}^{\mathrm{crit}}}\right) + B_{\beta}\left(1-\frac{T}{T_{\beta}^{\mathrm{crit}}}\right)^{1.5} + C_{\beta}\left(1-\frac{T}{T_{\beta}^{\mathrm{crit}}}\right)^{3} \cdots \right.\right.$$
$$\left.\left. \cdots + D_{\beta}\left(1-\frac{T}{T_{\beta}^{\mathrm{crit}}}\right)^{6}\right)\right] \tag{2.39}$$

$$D_{\alpha\beta}^{\mathrm{DL}} = \frac{0.00143\ \mathrm{cm^2\,s^{-1}} \left(\frac{T}{\mathrm{K}}\right)^{1.75} \left(\frac{\mathrm{g\,mol^{-1}}}{M_{\beta}} + \frac{\mathrm{g\,mol^{-1}}}{M_{\alpha}}\right)^{0.5}}{\left(\frac{p}{\mathrm{bar}}\sqrt{2}\left(\sqrt[3]{\Delta v_{\beta}} + \sqrt[3]{\Delta v_{\alpha}}\right)^2\right)} \tag{2.40}$$

Total volume of and concentrations in the anodic loop may change with operating conditions and time. They are calculated by:

$$V^{\mathrm{Lo}} = \frac{n_{\mathrm{Me}}^{\mathrm{Lo}}}{c_{\mathrm{Me}}^{*}} + \frac{n_{\mathrm{W}}^{\mathrm{Lo}}}{c_{\mathrm{W}}^{*}} \tag{2.33}$$

$$c_{\zeta}^{\mathrm{Lo}} = \frac{n_{\zeta}^{\mathrm{Lo}}}{V^{\mathrm{Lo}}} \tag{2.34}$$

Some general equations, which are listed in Table 2.1, are valid for all models presented in this thesis. It is assumed that all gases behave as ideal gases (Eq. (2.35)) and equilibrium between gas and liquid phase is described using the laws of Raoult and Dalton (Eq. (2.36)). Definition of mole fractions in liquid phase, X_{ζ}^{loc}, and of water in gas phase, $y_{\mathrm{W}}^{\mathrm{loc}}$ (Eq. (2.38)), are also generally valid. Vapour pressures are calculated by Wagner equation (Eq. (2.39)) and diffusion coefficients in gas phases are estimated by Fuller method (Eq. (2.40)) as given in [47]. The coefficients for the Wagner equation, A_{β} to D_{β}, are given in Table 2.2.

Natural constants as well as data on chemical media are also generally valid, independent of the model and its assumptions. Parameters of this kind which are used in this thesis are listed in Table 2.2.

Table 2.2: Constants and data on chemical media.

Constants:					
F	=	$96\,485\,\mathrm{As\,mol^{-1}}$	R	=	$8.31\,\mathrm{J\,mol^{-1}K^{-1}}$
p_N	=	$1.013\cdot10^5\mathrm{Pa}$	T_N	=	$273.15\,\mathrm{K}$
Molar masses and pure substance concentrations:					
M_Me	=	$32.04\,\mathrm{g\,mol^{-1}}$	M_{O_2}	=	$32\,\mathrm{g\,mol^{-1}}$
M_W	=	$18.02\,\mathrm{g\,mol^{-1}}$	M_{CO_2}	=	$44.01\,\mathrm{g\,mol^{-1}}$
M_air	=	$28.97\,\mathrm{g\,mol^{-1}}$	M_{N_2}	=	$28.01\,\mathrm{g\,mol^{-1}}$
M_He	=	$4\,\mathrm{g\,mol^{-1}}$			
c^*_Me	=	$24.66\,\mathrm{mol\,l^{-1}}$	c^*_W	=	$55.4\,\mathrm{mol\,l^{-1}}$
Data for vapour pressure calculation [47]:					
$T^\mathrm{crit}_\mathrm{Me}$	=	$512.5\,\mathrm{K}$	$T^\mathrm{crit}_\mathrm{W}$	=	$647.1\,\mathrm{K}$
$p^\mathrm{crit}_\mathrm{Me}$	=	$80.8\cdot10^5\mathrm{Pa}$	$p^\mathrm{crit}_\mathrm{W}$	=	$220.6\cdot10^5\mathrm{Pa}$
A_Me	=	-8.54582	A_W	=	-7.71374
B_Me	=	0.67266	B_W	=	1.31467
C_Me	=	-2.54743	C_W	=	-2.51444
D_Me	=	-2.71874	D_W	=	-1.72542
Data for binary diffusion coefficient calculation [47]:					
Δv_Me	=	31.25	Δv_{O_2}	=	16.3
Δv_W	=	13.1	Δv_{CO_2}	=	26.9
Δv_air	=	19.7	Δv_{N_2}	=	18.5
Δv_He	=	2.67			

Parameters and initial conditions used for simulation of all scenarios in this chapter unless specified differently are listed in Table 2.3. Compared to other literature values [14], the used value for methanol diffusion coefficient [48] is relatively low. A higher value would increase all effects of methanol cross-over but the qualitative statements remain same.

The general mathematical model derived above is modified in the following to describe five different scenarios for the analysis of water management in ADMFCs. All scenarios are simulated with *Matlab* using *ode15s* if integration is needed. A structure diagram of all scenarios is displayed in Fig. 2.2. The following section

Table 2.3: Parameters used for simulation of all scenarios.

Geometry and material parameters:					
V^{A}	=	$12.5\,\mathrm{ml}$	V^{C}	=	$12.5\,\mathrm{ml}$
d^{M}	=	$30\,\mu\mathrm{m}$	A^{M}	=	$25\,\mathrm{cm}^2$
κ	=	4	$D^{\mathrm{M}}_{\mathrm{Me}}$	=	$1.23\cdot10^{-7}\mathrm{cm}^2\,\mathrm{s}^{-1}$
Initial conditions:					
$c^{\mathrm{A}}_{\mathrm{Me},0}$	=	$1\,\mathrm{mol\,l}^{-1}$	$c^{\mathrm{A}}_{\mathrm{W},0}$	=	$53.15\,\mathrm{mol\,l}^{-1}$
$c^{\mathrm{A}}_{\mathrm{Me^g},0}$	=	$0\,\mathrm{mol\,l}^{-1}$	$c^{\mathrm{A}}_{\mathrm{W^g},0}$	=	$0\,\mathrm{mol\,l}^{-1}$
$c^{\mathrm{A}}_{\mathrm{CO_2},0}$	=	$0\,\mathrm{mol\,l}^{-1}$			
$c^{\mathrm{C}}_{\mathrm{O_2},0}$	=	$7.92\cdot10^{-3}\mathrm{mol\,l}^{-1}$	$c^{\mathrm{C}}_{\mathrm{N_2},0}$	=	$29.8\cdot10^{-3}\mathrm{mol\,l}^{-1}$
$c^{\mathrm{C}}_{\mathrm{W^g},0}$	=	$0\,\mathrm{mol\,l}^{-1}$	$c^{\mathrm{C}}_{\mathrm{CO_2},0}$	=	$0\,\mathrm{mol\,l}^{-1}$
$n^{\mathrm{Lo}}_{\mathrm{Me},0}$	=	$0.5\,\mathrm{mol}$	$n^{\mathrm{Lo}}_{\mathrm{W},0}$	=	$26.58\,\mathrm{mol}$
Inlet data:					
$T^{\mathrm{C}}_{\mathrm{in}}$	=	$20\,^\circ\mathrm{C}$	$p^{\mathrm{C}}_{\mathrm{in}}$	=	$1.013\,\mathrm{bar}$
λ^{C}	=	10	$c^{\mathrm{A}}_{\mathrm{CO_2,in}}$	=	$0\,\mathrm{mol\,l}^{-1}$
$c^{\mathrm{A}}_{\mathrm{Me^g,in}}$	=	$0\,\mathrm{mol\,l}^{-1}$	$c^{\mathrm{A}}_{\mathrm{W^g,in}}$	=	$0\,\mathrm{mol\,l}^{-1}$
Operating conditions:					
p	=	$1.013\,\mathrm{bar}$	T	=	$50\,^\circ\mathrm{C}$

presents the first three scenarios which study requirements for sufficient water supply to cathode.

2.2 Water Supply to Cathode

The following scenarios are created for the analysis of cathodic water supply. In order to keep the models as simple as possible, the first two scenarios do not include an anodic loop but only describe a single fuel cell fed with a methanol solution of $1\,\mathrm{mol\,l}^{-1}$. The molar flows entering the anode are time-independent and all flows leaving the anode are leaving the system at the same time in these scenarios. The first scenario is used to identify inlet conditions that lead to sufficient water supply to cathode. Therefore, water is only supplied by humidifying cathodic inlet gas. In the second scenario, water is supplied by mass transport

Figure 2.2: Structure diagram of all scenarios modelled and analysed in this chapter.

through membrane to analyse requirements on water diffusion for sufficient water supply. The third scenario, which is an extension of Scenario 2 including an anodic loop, describes the loop behaviour without water level control. It shows the importance of considering the second challenge.

2.2.1 Scenario 1 - Supply by Cathodic Inlet

In order to study the option of water supply by humidified inlet gas, this theoretical scenario is generated which assumes that membrane blocks all mass transport between anode and cathode except for OH^- conduction. Hence, anode and cathode are decoupled and it is sufficient to solely model cathode chamber. Since the scenarios aim at analysis of water management in steady state, explicit calculation without numerical integration is possible for this greatly reduced model. However, numerical integration would lead to the same results. The modification of the mathematical model to generate this scenario is followed by the discussion of the results.

2.2.1.1 Mathematical Modelling

As already mentioned, molar flows through membrane are assumed to be zero which is implemented by setting the corresponding coefficients equal to zero: $\kappa = 0$, $D_\beta^{\mathrm{M}} = 0$ for $\beta \in \{\mathrm{W,Me}\}$. Furthermore, it is assumed that the gas entering the cathode is saturated with water $RH_{\mathrm{in}}^{\mathrm{C}} = 100\,\%$. Considering these assumptions, the molar balance, Eq. (2.3), for cathodic water in steady state can be reduced to:

$$0 = c_{\mathrm{Wg,in}}^{\mathrm{C}} F_{\mathrm{in}}^{\mathrm{C}} - c_{\mathrm{Wg}}^{\mathrm{C}} F_{\mathrm{out}}^{\mathrm{C}} + \sigma_{\mathrm{Wg}}^{\mathrm{C}} \tag{2.41}$$

and Eq. (2.12) - Eq. (2.14) can be modified as follows:

$$\sigma_{\mathrm{O_2}}^{\mathrm{C}} = -\frac{A^{\mathrm{M}} i}{4F} \tag{2.42}$$

$$\sigma_{\mathrm{Wg}}^{\mathrm{C}} = -\frac{A^{\mathrm{M}} i}{2F} \tag{2.43}$$

$$\sigma_{\mathrm{CO_2}}^{\mathrm{C}} = 0 \tag{2.44}$$

Table 2.4: Additional parameters and inlet conditions used for calculations of Scenario 1.

d^{DL}	=	$300\,\mu\mathrm{m}$	$D_{\mathrm{W}}^{\mathrm{DL}}$	=	$0.15\,\mathrm{cm}^2\,\mathrm{s}\text{-}1$
i	=	$400\,\mathrm{mA\,cm}^{-2}$	$RH_{\mathrm{in}}^{\mathrm{C}}$	=	$100\,\%$

The volume flow leaving cathode is calculated by including Eqs. (2.19), (2.20) and (2.42) to (2.44) into Eq. (2.23) for $\dot{n}_{\mathrm{W^g}}^{\mathrm{diff}} = 0$:

$$F_{\mathrm{out}}^{\mathrm{C}} = \frac{1}{c_{\mathrm{gas}}} \left(\frac{\lambda^{\mathrm{C}}}{0.21(1 - y_{\mathrm{W^g,in}}^{\mathrm{C}})} \frac{A^{\mathrm{M}} i}{4F} - \frac{3A^{\mathrm{M}} i}{4F} \right) \tag{2.45}$$

With this equation and Eqs. (2.19) and (2.21), Eq. (2.41) can be solved for the air excess ratio λ^{C} required to supply sufficient water:

$$\lambda^{\mathrm{C}} = \frac{2 - 3\frac{c_{\mathrm{W^g}}^{\mathrm{C}}}{c_{\mathrm{gas}}}}{y_{\mathrm{W^g,in}}^{\mathrm{C}} - \frac{c_{\mathrm{W^g}}^{\mathrm{C}}}{c_{\mathrm{gas}}}} 0.21 \left(1 - y_{\mathrm{W^g,in}}^{\mathrm{C}}\right) \tag{2.46}$$

The corresponding volume flow rate of air at cathodic inlet is calculated by Eq. (2.19). In cases that consider a gas diffusion layer between cathode channel and catalyst layer, diffusive flux of water through GDL needs to be equal to water consumption by reaction:

$$A^{\mathrm{M}} D_{\mathrm{W^g}}^{\mathrm{DL}} \frac{c_{\mathrm{W^g}}^{\mathrm{C}} - c_{\mathrm{W^g}}^{\mathrm{CM}}}{d^{\mathrm{DL}}} = \frac{A^{\mathrm{M}} i}{2F} \tag{2.47}$$

Assuming total water consumption at membrane gas interface ($c_{\mathrm{W^g}}^{\mathrm{CM}} = 0$), the minimal required water concentration in the cathode chamber $c_{\mathrm{W^g}}^{\mathrm{C}}$ can be calculated by:

$$c_{\mathrm{W^g}}^{\mathrm{C}} = \frac{i}{2F} \frac{d^{\mathrm{DL}}}{D_{\mathrm{W^g}}^{\mathrm{DL}}} \tag{2.48}$$

Additional parameters and inlet conditions needed for calculations of this scenario are listed in Table 2.4.

2.2.1.2 Results and Discussion

This scenario solely describes the cathode of an alkaline anion exchange membrane fuel cell. Therefore, the results discussed in this section can be applied to all alkaline fuel cells fed with air at cathode.

Figure 2.3a shows the minimum air excess ratio required to supply sufficient water to the cathode as a function of inlet temperature calculated by Eq. (2.46) for $RH_{\mathrm{in}}^{\mathrm{C}} = 100\,\%$. The inlet gas contains more water with increasing inlet temperature and, thus, lower air excess ratio is required. The limiting curve that assumes total water consumption ($c_{\mathrm{W}}^{\mathrm{C}} = 0$) is independent of current density. Below the curve, water supply is insufficient, above the curve some water remains in the cathodic gas. Further limitations due to mass transport from chamber through GDL to reaction region and dehumidification kinetics inhibit total dehumidification and intensify the requirements especially for low inlet temperatures. Mass transport through GDL is proportional to current density (Eq. (2.47)). Thus, if transport of water vapour through GDL is considered, higher current density necessitates higher water diffusion. As a consequence, higher water vapour concentration at cathode needs to be realised by higher air excess ratios to supply sufficient water to cathode. This is indicated by the curves in Fig. 2.3a which include water vapour transport through a GDL of 300 µm thickness at a current density of $i = 200\,\mathrm{mA\,cm^{-2}}$ and $i = 400\,\mathrm{mA\,cm^{-2}}$ respectively. The remaining water concentration in the cathode chamber $c_{\mathrm{W}}^{\mathrm{C}}$ is then calculated by Eq. (2.48). The results show that full humidification at a temperature above 45 °C is required to supply sufficient water for air excess ratios below 5 if mass transport through membrane does not occur.

Figure 2.3b reveals the influence of pressure and relative humidity. All three curves in this figure assume total water consumption at cathode. Reference conditions include a constant pressures at cathode of $p^{\mathrm{C}} = p_{\mathrm{in}}^{\mathrm{C}} = p = 1.013\,\mathrm{bar}$ and relative humidity at cathodic inlet is $RH_{\mathrm{in}}^{\mathrm{C}} = 100\,\%$. These conditions are identical to the conditions of the blue curve in Fig. 2.3a. A pressure increase, e.g. to $p = 2.026\,\mathrm{bar}$, lowers the molar fraction of water in the inlet gas and, thus, necessitates higher values of air excess ratio in order to supply sufficient water. The same impact is observed if relative humidity of air at cathodic inlet is lowered, e.g. to $RH_{\mathrm{in}}^{\mathrm{C}} = 60\,\%$ which also decreases water content of the inlet gas.

Since it is assumed that water vapour in the cathodic gas is totally consumed, the required air excess ratios in Fig. 2.3b are not influenced by current produced by the fuel cell (Eq. (2.46)). However, the corresponding volume flow rates which are calculated by Eq. (2.19) for the same conditions are proportional to current

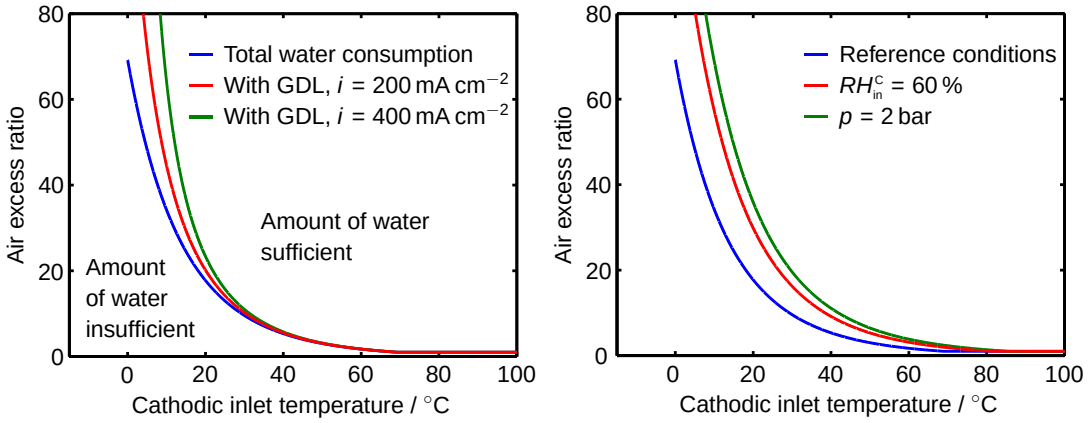

(a) (b)

Figure 2.3: Required air excess ratio for sufficient water supply as a function of inlet temperature: (a) for total water consumption and considering diffusion through GDL for two current densities; (b) For total water consumption at reference conditions ($p = 1\,\mathrm{bar}$ and $RH_{\mathrm{in}}^{\mathrm{C}} = 100\,\%$) and for $RH_{\mathrm{in}}^{\mathrm{C}} = 60\,\%$ as well as for $p = 2\,\mathrm{bar}$

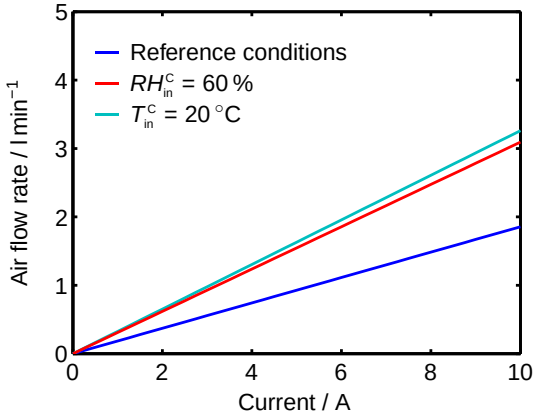

Figure 2.4: Required inlet volume flow rate of air for sufficient water supply by cathodic inlet gas as a function of current for total water consumption at reference conditions ($T_{\mathrm{in}}^{\mathrm{C}} = 30\,^{\circ}\mathrm{C}$, $RH_{\mathrm{in}}^{\mathrm{C}} = 100\,\%$ and $p = 1.013\,\mathrm{bar}$) and for $RH_{\mathrm{in}}^{\mathrm{C}} = 60\,\%$ as well as for $T_{\mathrm{in}}^{\mathrm{C}} = 20\,^{\circ}\mathrm{C}$.

as shown in Fig. 2.4. A volume flow rate of approximately $F_{\mathrm{N,in}}^{\mathrm{C}} = 1.9\,\mathrm{l\,min^{-1}}$ is required to supply sufficient water to produce a current of $I = 10\,\mathrm{A}$ at reference conditions which corresponds to an air excess ratio of $\lambda^{\mathrm{C}} = 18$. Reference conditions include $T_{\mathrm{in}}^{\mathrm{C}} = 30\,^{\circ}\mathrm{C}$ and $RH_{\mathrm{in}}^{\mathrm{C}} = 60\,\%$. If relative humidity is fixed, pressure has no influence on water vapour concentration (cf. Eqs. (2.21), (2.35) and (2.38)). As a result, volume flow rate of air required to supply the same molar flux of water does not change with pressure. However, a decrease of inlet

temperature to $T_{\mathrm{in}}^{\mathrm{C}} = 20\,^{\circ}\mathrm{C}$ results in lower water content of the inlet gas and leads to a higher required volume flow rate e.g. $F_{\mathrm{N,in}}^{\mathrm{C}} = 3.3\,\mathrm{l\,min^{-1}}$ for $I = 10\,\mathrm{A}$. A decrease in relative humidity of the cathodic inlet gas has a similar effect on air flow rate as a decrease in temperature. Hence, for low inlet temperatures or humidities, unreasonably high volume flow rates at cathodic inlet are required for high currents, while cathodic water supply seems feasible for low currents, albeit efficiency decreases due to oversized gas pump.

In conclusion, sufficient water supply to cathode of an AEMFC is only possible if inlet air is humidified to a high level and either inlet temperature or volume flow rate is at a high level as well. In that case, ambient air has to be treated before it can be used as cathodic inlet gas which requires additional components such as humidifier and heater. As a consequence, the fuel cell system is significantly complicated by new components which are also detrimental to system efficiency. Hence, this scenario reveals that water supply by cathodic inlet is insufficient and mass transport through membrane is essential for cathodic water supply in alkaline anion exchange membrane fuel cells.

2.2.2 Scenario 2 - Supply by Membrane Diffusion

Scenario 1 identifies cathodic inlet gas to be unsuitable as sole water supply to AFC cathodes. Therefore, Scenario 2 is generated to analyse requirements on water diffusion through membrane for sufficient water supply to cathode. The general model is slightly modified in the following to describe this new scenario.

2.2.2.1 Mathematical Modelling

As already mentioned, this scenario does not include an anodic loop and anode is fed with 1 M methanol solution. However, this scenario allows water and methanol transport through membrane which couples anode and cathode and requires modelling of both chambers. Water is supplied to cathode by oxidation of methanol diffusing through membrane as well as directly by water diffusion from anode to cathode. It is assumed that water diffusion exactly satisfies cathodic water demand and the corresponding diffusion coefficient according to Fick's law of diffusion, Eq. (2.24), can be derived from Eq. (2.3) for water in steady state:

$$\dot{n}_{\mathrm{W}}^{\mathrm{diff}} = c_{\mathrm{W}}^{\mathrm{C}} F_{\mathrm{out}}^{\mathrm{C}} - \dot{n}_{\mathrm{W,in}}^{\mathrm{C}} - \sigma_{\mathrm{W}}^{\mathrm{C}} \tag{2.49}$$

$$D_{\mathrm{W}}^{\mathrm{M}} = \left(c_{\mathrm{W}}^{\mathrm{C}} F_{\mathrm{out}}^{\mathrm{C}} - \dot{n}_{\mathrm{W,in}}^{\mathrm{C}} - \sigma_{\mathrm{W}}^{\mathrm{C}}\right) \frac{d^{\mathrm{M}}}{A^{\mathrm{M}} c_{\mathrm{W}}^{\mathrm{A}}} \tag{2.50}$$

Table 2.5: Additional parameters used for simulation of Scenario 2.

λ^{A}	=	4	RH^{C}	=	100 %
$c^{\mathrm{A}}_{\mathrm{W,in}}$	=	$53.15\,\mathrm{mol\,l^{-1}}$	$RH^{\mathrm{C}}_{\mathrm{in}}$	=	60 %
$c^{\mathrm{A}}_{\mathrm{Me,in}}$	=	$1\,\mathrm{mol\,l^{-1}}$			

Instead of humidifying cathodic inlet gas, ambient air is used with a relative humidity of $RH^{\mathrm{C}}_{\mathrm{in}} = 60\,\%$ at a temperature of $T^{\mathrm{C}}_{\mathrm{in}} = 20\,^{\circ}\mathrm{C}$. As such, gas in the cathode chamber does not supply water for the electrochemical reaction. On the contrary, it is assumed that the gas is either further humidified by evaporating some of the available water, which is therefore lost for reaction, or the water content of the gas does not change at all. Water is additionally removed from cathode by electro-osmotic drag of water which is included in the sources and sinks term $\sigma^{\mathrm{C}}_{\mathrm{W}}$.

Without liquid recycling, all methanol fed to anode is lost and methanol efficiency is inversely proportional to methanol excess ratio:

$$\eta_{\mathrm{norec}} = \frac{1}{\lambda^{\mathrm{A}}} \tag{2.51}$$

Assuming that methanol solution leaving anode can be recycled and is not lost, methanol efficiency is calculated by:

$$\eta_{\mathrm{rec}} = \frac{\frac{I}{6F}}{-\sigma^{\mathrm{A}}_{\mathrm{Me}} - \dot{n}^{\mathrm{A,diff}}_{\mathrm{Me}}} \tag{2.52}$$

Additional parameters needed to simulate the model of this scenario are listed in Table 2.5.

2.2.2.2 Results and Discussion

Reference conditions for the analysis of Scenario 2 include water drag, methanol cross-over and evaporation at cathode to $RH^{\mathrm{C}} = 100\,\%$ with $\lambda^{\mathrm{C}} = 10$. In order to analyse the effect of these three processes, the other analysed cases switch off or reduce one of the processes. Figure 2.5 displays the required diffusion coefficient of water calculated by Eq. (2.50). In all cases, the required water diffusion coefficient increases with current density since a higher current leads to increased water consumption. Thus, regarding water transport through membrane, cathodic wa-

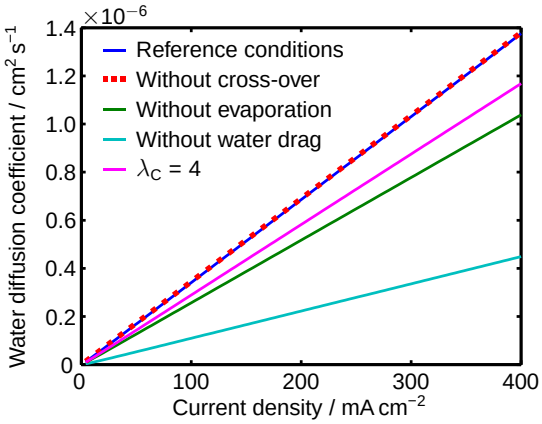

Figure 2.5: Required water diffusion coefficient in Scenario 2 with reference conditions including methanol cross-over, water drag and evaporation with $\lambda^{\mathrm{C}} = 10$.

ter supply is mainly a challenge for high current densities. A significant decrease of required water diffusion can be observed in cases that switch off electro-osmotic water drag or evaporation or reduce the latter because less water is removed from cathode in theses cases. On the contrary, insignificantly higher water diffusion is required in the case without methanol cross-over for the used methanol diffusion coefficient (Table 2.3) and methanol concentration of $c^{\mathrm{A}}_{\mathrm{Me,in}} = 1\,\mathrm{mol\,l^{-1}}$ at anodic inlet. In cases in which evaporation occurs, the required water diffusion coefficient decreases with decreasing air excess ratio because less water leaves the system at cathode. Thus, the influence of evaporation is reduced in case of a smaller air excess ratio. The case without evaporation is per se independent of air excess ratio.

Mass transport through GDL and CL which is disregarded in this scenario would of course influence these results. At cathode, a diffusive transport of water from CL to cathode chamber would lead to lower evaporation rates and, thus, the required diffusion coefficient lies in between the cases of no evaporation and full evaporation. At anode, water is in excess and is produced by reaction. Therefore, diffusive transport through GDL would lead to a lower methanol concentration in the CL and methanol cross-over would decrease accordingly. However, this has insignificant effect on the required water diffusion coefficient.

The value of the diffusion coefficient for real materials is no function of current density. Therefore, the simulated values of diffusion coefficient give an information on the minimum diffusion coefficient which is required in order to allow operation up to the given current. In the investigated range of current density, the required water diffusion coefficients seem feasible to achieve since experimen-

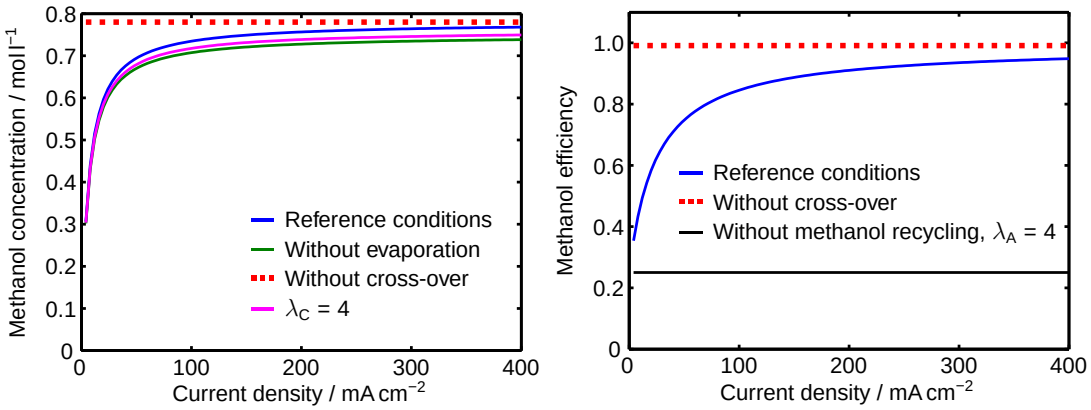

(a) (b)

Figure 2.6: Results of Scenario 2 with reference conditions including methanol cross-over, water drag and evaporation with $\lambda^C = 10$: (a) methanol concentration in liquid phase at anode, (b) methanol efficiency.

tally determined values of water diffusion coefficients in literature are in the same order of magnitude [25]. Hence, it may be expected that water diffusion through an anion exchange membrane is sufficient to supply sufficient water for cathode reaction if membrane is about 30 µm. Nevertheless, there will be a discrepancy between the required and the actual diffusion coefficient of water. If the actual diffusion coefficient is higher than the required one, water is accumulated at the cathode and the assumption $c_W^C = 0$ is no longer valid. Consequently, the concentration gradient decreases and water diffusion is diminished. Nevertheless, it is possible that some pores of catalyst layer or gas diffusion layer at the cathode get blocked by liquid water which would lead to a decrease in cell performance. If the actual diffusion coefficient is indeed below the required one, water transport through membrane is not sufficient for cathodic water supply. Either the lacking water has to be taken from the gas or the current density has to be reduced until the water diffusion is sufficient.

The resulting methanol concentrations in the liquid phase at anode as a function of current density are displayed in Fig. 2.6a. This concentration is below the methanol concentration at the inlet since methanol is consumed while water is produced by electrochemical reaction. Due to the definitions of inlet flows by constant excess ratios, the only process in the fuel cell which is independent of current density is methanol cross-over. Hence, if methanol cross-over is disregarded, all processes are proportional to current density and, thus, all terms of the molar balances (Eqs. (2.2) and (2.3)) in steady state with Eqs. (2.16) and (2.17) are proportional to current density which can be cancelled. This results in a

system of algebraic equations that is independent of current density and can be solved for steady state concentrations of components. Consequently, methanol concentration does not change with current density in the case without methanol cross-over as shown in Fig. 2.6a. Since methanol concentration is independent of current density, methanol efficiency is also independent of current density and is nearly 100 % as shown in Fig. 2.6b. The slight efficiency loss is caused by methanol evaporation at anode.

If methanol cross-over occurs, sources and sinks at cathode as well as water diffusion and outlet volume flows contain terms that are not proportional to current density and concentrations are no longer independent of current density. The higher the current density, the smaller is the influence of terms independent of current density. As a consequence, the influence of methanol loss by cross-over is substantial at low current densities and causes small methanol concentrations and low efficiencies. At high current densities, methanol loss caused by cross-over is small compared to the other processes and methanol concentration converges to the value of the case without cross-over. In the three cases in Fig. 2.6a that include cross-over, methanol concentration differs slightly since the required water diffusion is smaller in case of lower air excess ratio $\lambda^{\mathrm{c}} = 4$ or without evaporation and methanol dilution is more intense. However, the difference is small and the corresponding change in efficiency is insignificant. For calculation of efficiencies in reference conditions and in the case without methanol cross-over, it is assumed that all methanol at anodic exit can be recycled. The third case in Fig. 2.6b shows methanol efficiency if exiting methanol solution is disposed of as waste. It is obvious that high fuel efficiencies can only be achieved by recycling the methanol at anodic outlet. Since methanol concentration for all cases shown in Fig. 2.6a is below the inlet concentration, recycling of methanol solution requires treatment to keep the methanol concentration constant and to avoid methanol dilution.

2.2.3 Scenario 3 - Impact of Methanol Recycling

The results of Scenario 2 indicate that water can potentially be supplied to cathode by mass transport through membrane for 1 M methanol solution at anode. They further reveal that reasonable methanol efficiencies can only be achieved if methanol solution is recycled which influences concentrations at anode and, thus, affects mass transport through membrane. This scenario is modelled in order to reveal the impact of methanol recycling by an anodic loop on the water supply

by mass transport through membrane and to understand the behaviour of water level in an anodic loop without active stabilisation.

2.2.3.1 Mathematical Modelling

In order to create a scenario with methanol recycling that also fulfils the demands for sufficient water supply, Scenario 2 is modified by including an anodic loop. Therefore, Eqs. (2.4) and (2.30) to (2.34) including the related assumptions are added to the model of Scenario 2. The anode is fed with liquid coming from the loop as shown in Fig. 2.1. Since the concentrations in the loop may change, either anodic inlet volume flow rate or methanol excess ratio cannot be fixed. For this scenario, it is decided to fix the volume flow rate from loop to anode to a value such that initial methanol excess ratio is $\lambda_0^{\mathrm{A}} = 10$. This relatively high initial value for λ^{A} is chosen in order to reduce the concentration differences between anode chamber and anodic loop by small residence times in the anode chamber. The resulting inlet volume flow rate is calculated by Eq. (2.18).

In the present scenario, no additional gas is added to the anodic outlet, i.e. $\dot{n}_{\mathrm{dry}}^{\mathrm{ad}} = 0$, and water level is not actively controlled. As a consequence, volume of the anodic loop is changing during operation and is described by Eq. (2.33). Since the amount of methanol in the anodic loop is kept constant by feed forward control, a change in loop volume results in a change of concentrations which are calculated by Eq. (2.34).

Since methanol concentration is not constant in this scenario, the temporary methanol efficiency as calculated in Scenario 2 (Eq. (2.52)) changes with time. Therefore, an average value of methanol efficiency over operation time is used for analysis of this scenario. This average efficiency is defined as the ratio between the amount of methanol used to provide current during operation and the amount of methanol consumed during operation. The latter is equivalent to the amount of methanol inside the system at start of simulation deducting methanol at end of simulation in addition to the methanol fed to anodic loop during operation. The efficiency is thus calculated by:

$$\eta_{\mathrm{Me}} = \frac{\frac{iA}{6F} t_{\mathrm{end}}}{c_{\mathrm{Me},0}^{\mathrm{A}} V^{\mathrm{A}} - c_{\mathrm{Me,end}}^{\mathrm{A}} V^{\mathrm{A}} + n_{\mathrm{Me},0}^{\mathrm{Lo}} - n_{\mathrm{Me,end}}^{\mathrm{Lo}} + \int_0^{t_{\mathrm{end}}} \dot{n}_{\mathrm{Me}}^{\mathrm{new}} dt} \tag{2.53}$$

Table 2.6: Additional parameters for simulation of Scenario 3.

λ_0^{A}	$= 10$	$RH_{\mathrm{in}}^{\mathrm{C}}$	$= 60\,\%$
V_0^{Lo}	$= 0.5\,\mathrm{l}$	RH^{C}	$= 100\,\%$

The change of water level ξ_{W} is defined as the ratio between water accumulation in the loop and the amount of water which initially is inside anode and anodic loop:

$$\xi_{\mathrm{W}} = \frac{\dot{n}_{\mathrm{W,in}}^{\mathrm{Lo}} - \dot{n}_{\mathrm{W,out}}^{\mathrm{Lo}}}{c_{\mathrm{W},0}^{\mathrm{A}} V^{\mathrm{A}} + n_{\mathrm{W},0}^{\mathrm{Lo}}} \tag{2.54}$$

Additional parameters and initial conditions needed to simulate Scenario 3 are listed in Table 2.6.

2.2.3.2 Results and Discussion

In this scenario, anodic water level can change during operation. If water level sinks, the system runs out of water and methanol concentration rises. If water level rises, methanol gets diluted and, due to the constant volume flow to anode, fuel cell runs out of methanol after some time. Simulation is stopped if one of the concentrations becomes zero or if a maximum operation time $t_{\mathrm{max}} = 5000\,\mathrm{h}$ is reached.

This scenario is analysed for five cases with different operation conditions. The first case considers reference conditions which include methanol cross-over and water evaporation at cathode to $RH^{\mathrm{C}} = 100\,\%$ with an air excess ratio of $\lambda^{\mathrm{C}} = 10$. In order to investigate the effect of methanol cross-over on the water level in the anodic loop, this process is excluded in one of the other analysed cases. The impact of water evaporation at cathode on the water level at anode is analysed by three other cases. One assumes that no evaporation at cathode takes place at all. The other two cases consider reduced evaporation by reducing air excess ratio to $\lambda^{\mathrm{C}} = 4$ or assuming lower achieved relative humidity of $RH^{\mathrm{C}} = 60\,\%$, respectively. Since water diffusion is assumed to exactly satisfy cathodic water demand, water diffusion rises with increasing current density and electro-osmotic drag of water does not have an influence on anodic water level because the water dragged from cathode to anode is assumed to be transported back by diffusion.

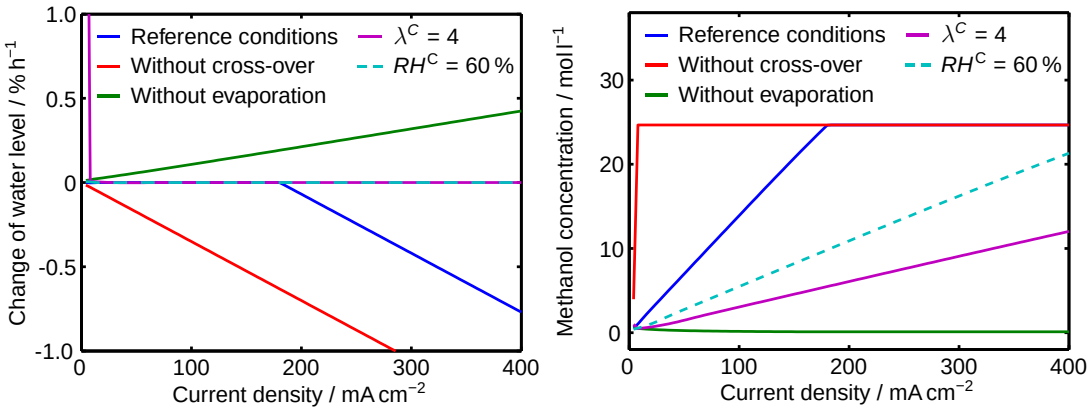

(a) (b)

Figure 2.7: Simulation results of Scenario 3 for the case with reference conditions (methanol cross-over and evaporation at cathode to $RH^{\mathrm{C}} = 100\%$ occur with $\lambda^{\mathrm{C}} = 10$), and for four other cases that differ from the reference condition in one of the mentioned conditions: (a) change of anodic water level at the end of simulation, (b) anodic methanol concentration at the end of simulation.

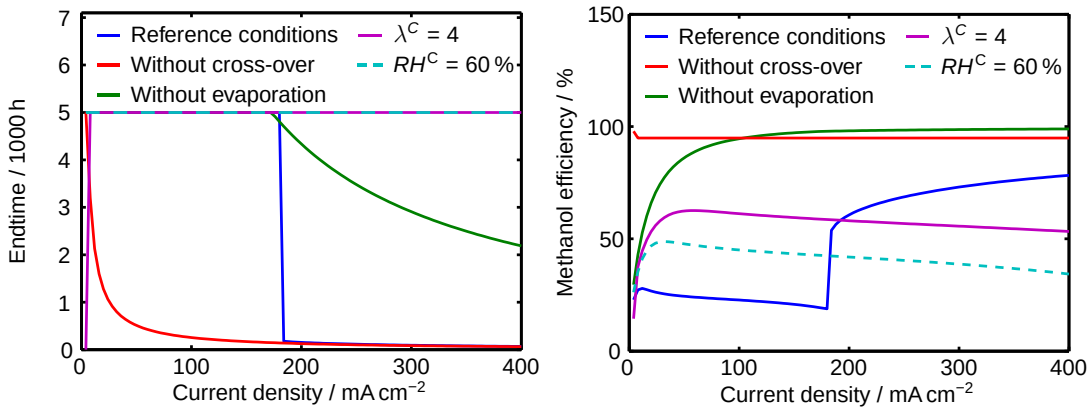

(a) (b)

Figure 2.8: Simulation results of Scenario 3 for the case with reference conditions (methanol cross-over and evaporation at cathode to $RH^{\mathrm{C}} = 100\%$ occur with $\lambda^{\mathrm{C}} = 10$), and for four other cases that differ from the reference condition in one of the mentioned conditions: (a) simulated operation time of fuel cell system, maximum operation time is set to 5000 h and (b) methanol efficiency for whole operation until end of simulation.

Figure 2.7a shows the change in water level at the end of operation time. It reveals that water can be either accumulated or depleted in the loop – positive or negative change of water level – depending on operation conditions. Without methanol cross-over, water depletion in the anodic loop occurs for all current densities during whole operation time as indicated by the red line. The depletion increases with increasing current density due to a rise in water consumption at cathode. E.g. at a current density of approximately $i \approx 280\,\mathrm{mA\,cm^{-2}}$ the loop looses 1 % of the initial amount of water each hour of operation. As a consequence, methanol concentration rises until pure methanol remains with $c^{\mathrm{A}}_{\mathrm{Me,liq}} = 24.66\,\mathrm{mol\,l^{-1}}$ (Fig. 2.7b) and simulation is stopped (Fig. 2.8a) because no water is left at anode $c^{\mathrm{A}}_{\mathrm{W,liq}} = 0$. This is only a theoretical consideration since nearly pure methanol solutions would require infinite diffusion coefficient of water which obviously is not possible in reality. Hence, fuel cell performance would drop distinctly before pure methanol is reached because of insufficient water supply to cathode. However, this scenario is supposed to demonstrate the consequences of uncontrolled anodic water level and is therefore carried to the unachievable extreme. The resulting methanol efficiency (Fig. 2.8b) is reduced due to high methanol evaporation at anode caused by high methanol concentration. This efficiency loss of $\approx 5\,\%$ is an average value over operation time. Since methanol concentration increases with time, the temporary methanol efficiency (cf. Eq. (2.52)) is quite high at initial conditions and is below 50 % at end of simulation.

Reference conditions include methanol cross-over which leads to a stabilising effect for small current densities (Fig. 2.7a) which is explained as follows. As in the case without methanol cross-over, water production at anode is smaller than water transport through membrane and methanol concentration rises during operation (Fig. 2.9a). As a consequence, methanol cross-over is increased which results in higher water production at cathode and lower required water diffusion which slows down water depletion. Figure 2.9a shows that methanol concentration stabilises for small current densities while simulation is stopped for a current density of $200\,\mathrm{mA\,cm^{-2}}$ when concentration of pure methanol is reached. Increasing current density causes an increase in steady state methanol concentration until only pure methanol is remaining which happens at $180\,\mathrm{mA\,cm^{-2}}$ (Fig. 2.7b). Since methanol cross-over cannot increase further, further increase of current density leads to water depletion during whole operation and simulation is stopped before 5000 h of operation time are reached. However, the stabilising effect causes a methanol efficiency below 30 % for reference conditions (Fig. 2.8b).

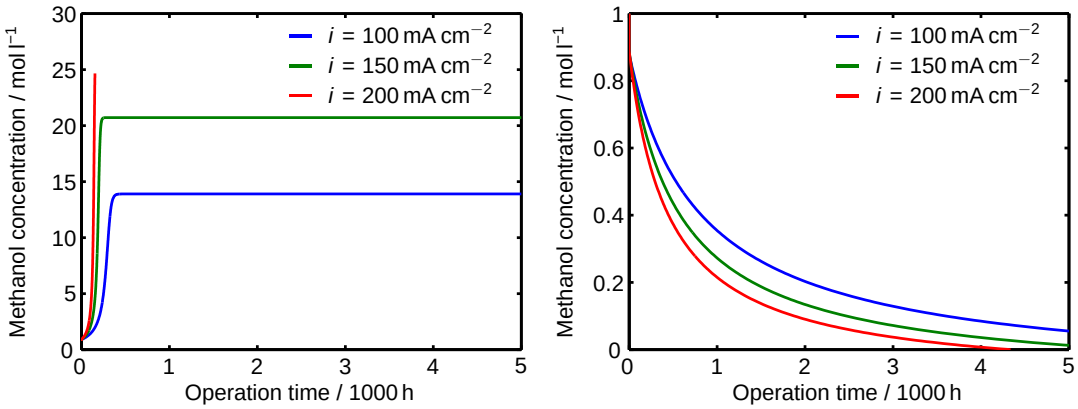

Figure 2.9: Temporal change of methanol concentration for three different current densities, $i = 100\,\mathrm{mA\,cm^{-2}}$, $i = 150\,\mathrm{mA\,cm^{-2}}$ and $i = 200\,\mathrm{mA\,cm^{-2}}$: (a) at reference conditions, (b) without evaporation at cathode.

Due to the lower operation time for current densities above $180\,\mathrm{mA\,cm^{-2}}$, the duration of operation with high methanol concentration is reduced and methanol efficiency is increased significantly.

For the cases of reduced evaporation rates, i.e. evaporation to $RH^{\mathrm{C}} = 60\,\%$ and $\lambda_{\mathrm{C}} = 4$, water consumption and, accordingly, water diffusion are smaller and the stabilising effect is extended to higher current densities. The simulation is not stopped before the maximum operation time (Fig. 2.8a) since final methanol concentration is smaller than concentration of pure methanol (Fig. 2.7b) for the investigated range of current density. As such, an important feature to stabilise water level for higher current densities without active control is to decrease cathodic water evaporation. However, in case without water evaporation at cathode, the anodic loop accumulates water for all current densities (Fig. 2.7a). The system does not reach steady state (Fig. 2.9b) and for high current densities, simulation is stopped when $c^{\mathrm{A}}_{\mathrm{Me,liq}} = 0$. For small current densities, the system can still be operated longer than the set maximum operation time but Fig. 2.9b proves that no steady state is reached. Due to the low methanol concentration, methanol losses are small and the average methanol efficiency for current densities above $100\,\mathrm{mA\,cm^{-2}}$ is above 95 % (Fig. 2.8b). In contrast, methanol efficiencies below 60 % are achieved in the cases that lead to high methanol concentrations. The high volume flow rate $F^{\mathrm{A}}_{\mathrm{in}}$ caused by $\lambda^{\mathrm{A}}_{0} = 10$ delays substance starvation since concentration of a substance needs to drop to a small value in the whole loop to cause total consumption in the anode chamber. Hence, maximum operation time

decreases with decreasing volume flow rate from loop to anode if concentrations are not maintained stable during operation.

It can be concluded from Scenario 3 that stabilisation of water level is essential for operation of ADMFCs with respect to operation time and methanol efficiency, if methanol solution is recycled. It should also be mentioned that high methanol concentration and high methanol cross-over are strongly detrimental to electrochemical performance and, thus, maintaining a low methanol concentration is also essential for high fuel cell performance.

2.3 Water Level Stabilisation at Anode

The first three scenarios show that the challenge of water supply to cathode can be mastered if membrane allows sufficient water transport. However, if methanol solution is recycled, stable water level in the anodic loop is also a challenging topic. Scenario 3 reveals the necessity to master this challenge in order to achieve high methanol efficiencies at long term operation. Therefore, the next two scenarios are created to study two options of water level stabilisation. Scenario 4 is used to analyse requirements on water diffusion through membrane and cathodic conditions to stabilise water level by adjusting cathodic inlet conditions. Scenario 5 presents active stabilisation by water removal from anodic loop.

2.3.1 Scenario 4 - Adjustment of Cathodic Inlet Conditions

This scenario is designed to determine the required diffusion coefficient of water through membrane and the corresponding conditions at cathode that lead to stable water level in the anodic loop. Therefore, the general model including an anodic loop is modified and analysed in the following.

2.3.1.1 Mathematical Modelling

The model of this scenario is similar to the model of Scenario 3. However, in this model, water diffusion coefficient is not fixed to fulfil cathodic water demands but to stabilise anodic water level without active water removal from anode: $\dot{n}^{\mathrm{Sys}}_{\mathrm{W,out}} = 0$. Water level in the anodic loop is stable if the molar flow of water entering the loop $\dot{n}^{\mathrm{Lo}}_{\mathrm{W,in}}$ is equal to the molar flow leaving the loop $\dot{n}^{\mathrm{Lo}}_{\mathrm{W,out}}$. Since

these flows are coupled to the convective flows entering and leaving the anode (Eqs. (2.30) and (2.31)), this constraint can be applied for the anode:

$$\dot{n}^{\mathrm{A}}_{\mathrm{W,out}} - \dot{n}^{\mathrm{A}}_{\mathrm{W,in}} = 0 \tag{2.55}$$

In order to achieve this in steady state, the amount of water received at anode needs to be equal to the amount removed from anode. Water is gained by electrochemical oxidation of methanol and by electro-osmotic water drag. Water removal at anode takes place by evaporation and by diffusion through the membrane to the cathode. Hence, the mass balance Eq. (2.2) for water at anode in steady state in combination with Eq. (2.55) leads to:

$$0 = -\dot{n}^{\mathrm{diff}}_{\mathrm{W}} + \sigma^{\mathrm{A}}_{\mathrm{W}} \tag{2.56}$$

Assuming that no liquid water is formed at cathode ($c^{\mathrm{C}}_{\mathrm{W,liq}} = 0$), combination of Eq. (2.56) with the definition of the diffusive flux Eq. (2.24) and the sources and sink term of water at anode Eq. (2.7) results in an equation for the diffusion coefficient of water through membrane required to stabilise anodic water level:

$$D^{\mathrm{M}}_{\mathrm{W}} = \left(\frac{5i}{6F} - \frac{y^{\mathrm{A}}_{\mathrm{W}}}{1 - y^{\mathrm{A}}_{\mathrm{Me}} - y^{\mathrm{A}}_{\mathrm{W}}} \frac{i}{6F} + \kappa \frac{i}{F} \right) \frac{d^{\mathrm{M}}}{c^{\mathrm{A}}_{\mathrm{W,liq}}} \tag{2.57}$$

The water diffusing through the membrane is partly transported back due to electro-osmotic water drag and partly consumed by the electrochemical reduction reaction Eq. (1.3). The remaining water at cathode gained by water diffusion and methanol oxidation needs to leave cathode in order to prevent water accumulation and flooding. It is assumed that this water evaporates, humidifying cathodic gas to a certain relative humidity. Molar flux of water in gas phase can generally be expressed by:

$$\dot{n}_{\mathrm{W^g}} = y_{\mathrm{W}} \dot{n}_{\mathrm{gas}} = \frac{y_{\mathrm{W}}}{1 - y_{\mathrm{W}}} \dot{n}_{\mathrm{dry}} \tag{2.58}$$

With the molar flux of dry gas $\dot{n}_{\mathrm{dry}}$ which is defined as:

$$\dot{n}^{\mathrm{C}}_{\mathrm{dry,in}} = \frac{\lambda^{\mathrm{C}}}{0.21} \frac{A^{\mathrm{M}} i}{4F} \tag{2.59}$$

$$\dot{n}^{\mathrm{C}}_{\mathrm{dry,out}} = \dot{n}^{\mathrm{C}}_{\mathrm{dry,in}} + \sigma^{\mathrm{C}}_{\mathrm{O_2}} + \sigma^{\mathrm{C}}_{\mathrm{CO_2}} + \sigma^{\mathrm{C}}_{\mathrm{N_2}} \tag{2.60}$$

at inlet and outlet of cathode, respectively. Combining the mass balance for water at cathode Eq. (2.3) in steady state:

$$0 = \dot{n}^{\mathrm{C}}_{\mathrm{W,in}} - \dot{n}^{\mathrm{C}}_{\mathrm{W,out}} + \dot{n}^{\mathrm{diff}}_{\mathrm{W}} + \sigma^{\mathrm{C}}_{\mathrm{W^g}} \tag{2.61}$$

with Eqs. (2.56) and (2.58) results in:

$$0 = \frac{y^{\mathrm{C}}_{\mathrm{W,in}}}{1 - y^{\mathrm{C}}_{\mathrm{W,in}}} \dot{n}^{\mathrm{C}}_{\mathrm{dry,in}} - \frac{y^{\mathrm{C}}_{\mathrm{W}}}{1 - y^{\mathrm{C}}_{\mathrm{W}}} \dot{n}^{\mathrm{C}}_{\mathrm{dry,out}} + \sigma^{\mathrm{A}}_{\mathrm{W}} + \sigma^{\mathrm{C}}_{\mathrm{W^g}} \tag{2.62}$$

Considering Eqs. (2.7), (2.13), (2.59) and (2.60) and rearranging leads to:

$$y^{\mathrm{C}}_{\mathrm{W}} = \frac{\frac{A^{\mathrm{M}} i}{3F}\left(2 - \frac{y^{\mathrm{A}}_{\mathrm{W^g}}}{1-y^{\mathrm{A}}_{\mathrm{Me^g}}-y^{\mathrm{A}}_{\mathrm{W^g}}} + \frac{y^{\mathrm{C}}_{\mathrm{W,in}}}{1-y^{\mathrm{C}}_{\mathrm{W,in}}} \frac{\lambda^{\mathrm{C}}}{0.21} \frac{3}{2}\right) + 4\dot{n}^{\mathrm{M,diff}}_{\mathrm{Me}}}{\frac{A^{\mathrm{M}} i}{6F}\left(1 - \frac{2y^{\mathrm{A}}_{\mathrm{W^g}}}{1-y^{\mathrm{A}}_{\mathrm{Me^g}}-y^{\mathrm{A}}_{\mathrm{W^g}}} + \frac{3\lambda^{\mathrm{C}}}{0.21} \frac{1}{1-y^{\mathrm{C}}_{\mathrm{W,in}}}\right) + 3\dot{n}^{\mathrm{M,diff}}_{\mathrm{Me}}} \tag{2.63}$$

Including Eq. (2.38), the resulting relative humidity at cathode in steady state can be calculated by:

$$RH^{\mathrm{C}} = \frac{\frac{A^{\mathrm{M}} i}{3F}\left(2 - \frac{y^{\mathrm{A}}_{\mathrm{W}}}{1-y^{\mathrm{A}}_{\mathrm{W}}-y^{\mathrm{A}}_{\mathrm{Me}}} + \frac{3}{2}\frac{\lambda^{\mathrm{C}}}{0.21} \frac{y^{\mathrm{C}}_{\mathrm{W,in}}}{1-y^{\mathrm{C}}_{\mathrm{W,in}}}\right) + 4\dot{n}^{\mathrm{M,diff}}_{\mathrm{Me}}}{\frac{A^{\mathrm{M}} i}{6F}\left(1 - \frac{2y^{\mathrm{A}}_{\mathrm{W}}}{1-y^{\mathrm{A}}_{\mathrm{W}}-y^{\mathrm{A}}_{\mathrm{Me}}} + \frac{3\lambda^{\mathrm{C}}}{0.21} \frac{1}{1-y^{\mathrm{C}}_{\mathrm{W,in}}}\right) + 3\dot{n}^{\mathrm{M,diff}}_{\mathrm{Me}}} \frac{p}{p^{\mathrm{O}}_{\mathrm{W}}} \tag{2.64}$$

2.3.1.2 Results and Discussion

Water is produced during operation of an ADMFC. In order to keep the water level in the fuel cell (system) constant, water needs to be removed from the fuel cell. Scenario 4 analyses the possibility to remove water at cathode side. This requires two processes: sufficient water diffusion through membrane to stabilise water level at anode and subsequent evaporation of excess water at cathode to remove the water via cathodic outlet. The required conditions for the two processes are analysed separately.

Since membrane thickness and steady state conditions at anode ($y^{\mathrm{A}}_{\mathrm{W}}$, $y^{\mathrm{A}}_{\mathrm{Me}}$ and $c^{\mathrm{A}}_{\mathrm{W,liq}}$) are assumed to be constant in this scenario, the required diffusion coefficient for stable water level is solely depending on water drag coefficient and current density (Eq. (2.57)). Its dependency on current density is displayed in Fig. 2.10 (blue curve) for two cases: including electro-osmotic water drag (Fig. 2.10a) and neglecting water drag (Fig. 2.10b). It is compared to the corresponding diffusion coefficients of Scenario 2 and 3 (red and green curves in Fig. 2.10) at equal conditions for the cases of full evaporation to $RH^{\mathrm{C}} = 100\,\%$ and no evaporation at

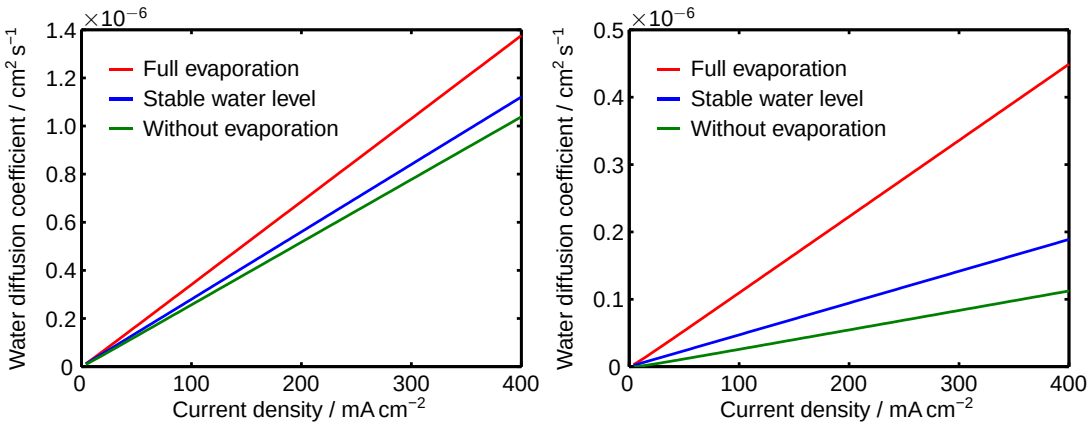

Figure 2.10: Diffusion coefficients of Scenario 4 (blue lines) required for stable water level compared to diffusion coefficients of Scenario 2 (red and green lines) required for sufficient water supply: (a) with electro-osmotic water drag, (b) Without electro-osmotic water drag.

cathode. Diffusion coefficients below the blue curves lead to water accumulation while diffusion coefficients above lead to water depletion.

In case that no water drag occurs, the water diffusion needed for water level stabilisation is expectedly smaller than in the case with water drag. However, in both cases, the diffusion coefficient required to stabilise anodic water level lies in between the cases of sufficient water supply to cathode without and with full evaporation for an air excess ratio of $\lambda^{\mathrm{C}} = 10$ calculated in Scenario 2. This implies that the water diffusion which is required for stable water level also supplies sufficient water for the electrochemical reaction at cathode but not for full evaporation to 100 % relative humidity for all current densities. It further implies that no liquid water is formed at cathode for an air excess ratio of $\lambda^{\mathrm{C}} = 10$ since relative humidity stays below $RH^{\mathrm{C}} \leq 100\%$ for all current densities.

Assuming that water diffusion through membrane removes sufficient water from anode to stabilise anodic water level, excess water at cathode needs to be evaporated to remove it from fuel cell via cathode outlet. The corresponding relative humidity at cathode depends on methanol cross-over, air excess ratio and on operation conditions in the fuel cell and at cathodic inlet (Eq. (2.64)). Relative humidity at cathodic inlet and in the anode chamber as well as all pressures and temperatures are assumed to be constant in this scenario. Hence, relative humidity at cathode required to remove sufficient water from fuel cell solely changes with current density and air excess ratio. Figure 2.11 displays the relative humidity in the cathode chamber, which is equivalent to humidity at cathodic outlet,

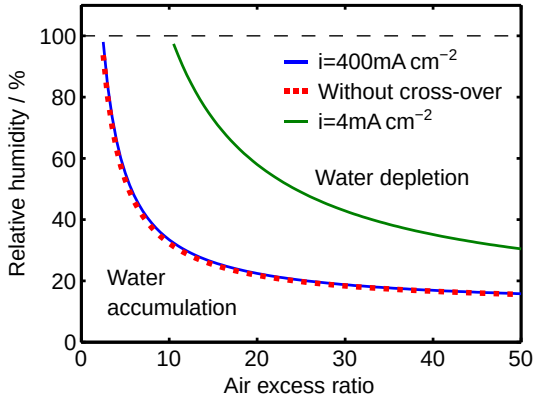

Figure 2.11: Relative humidity at cathode needed for water level stabilisation in the anodic loop in Scenario 4 as a function of air excess ratio for current densities of $i = 4\,\mathrm{mA\,cm^{-2}}$ and $i = 400\,\mathrm{mA\,cm^{-2}}$ and without methanol cross-over.

as a function of air excess ratio. These curves can be used to identify change in water level in real ADMFC-systems in which water diffusion does not exactly stabilise anodic water level. Relative humidities above the curves lead to water depletion while humidities below the curves result in water accumulation. The figure displays three cases: without methanol cross-over, with cross-over for a current density of $i = 4\,\mathrm{mA\,cm^{-2}}$ and with cross-over for $i = 400\,\mathrm{mA\,cm^{-2}}$. At low current densities, methanol cross-over and the resulting water production at cathode significantly increases the amount of water that needs to be removed by cathodic gas flow. Since gas flow rate is linearly increasing with current density, relative humidity needs to be high for low current densities to also remove water produced by direct methanol oxidation at cathode. At high current densities, the effect of methanol cross-over is insignificant and the curve of relative humidity converges to the case of no methanol cross-over which is independent of current density (cf. Eq. (2.64)).

Furthermore, the relative humidity needed to remove excess water from the fuel cell decreases with increasing excess ratio due to the increased gas flow rate and lies below the maximum relative humidity of $RH^{\mathrm{c}} = 100\%$ for most air excess ratios. However, for small λ^{c}, the corresponding relative humidity is above 100% which would cause formation of liquid water at cathode. Therefore, the minimum air excess ratio which is needed to remove sufficient water from the fuel cell is $\lambda^{\mathrm{c}} \geq 10$ for $i = 4\,\mathrm{mA\,cm^{-2}}$ and $\lambda^{\mathrm{c}} \geq 2.5$ for high current densities or without methanol cross-over.

In case of a smaller methanol excess ratio, e.g. $\lambda^{\mathrm{A}} = 4$, the methanol concentration at anode decreases. As a consequence, the influence of methanol crossover also decreases and the quantity of the curve for small current density of $i = 4\,\mathrm{mA\,cm^{-2}}$ in Fig. 2.11 decreases slightly. However, the tendencies and conclusions remain same. A change of methanol excess ratio has no influence on anodic water level and, thus, no influence on the required diffusion coefficient to stabilise water level.

The results of this scenario assume that water diffusion through membrane is sufficient to stabilise water level at anode. Since diffusion coefficients for real material do not change with current density, comparing the value for water diffusion coefficient of a given membrane material with the black curve shown in Fig. 2.10 yields a maximum current density i_{max} that allows water level stabilisation. For higher current densities, water will be accumulated in the anodic loop. Current densities below i_{max} might cause water depletion in the loop. However, diffusion also depends on the concentration gradient across the membrane which is diminished if water concentration at anode is decreased or concentration at cathode is increased. The latter happens if spare water at cathode is not evaporated but stays in the electrolyte membrane as liquid water. As a result, water diffusion through membrane will decrease and adjust itself to the required value. In this case, water level at anode is still stabilised if relative humidity at cathode adjusts according to Fig. 2.11. If the self adjusting effect fails, excess water needs to be removed from cathode to avoid flooding which leads to relative humidities above the curves in Fig. 2.11 and water recovery from cathodic exhaust gas is required as described for acidic DMFC systems [49].

Humidification of inlet gas decreases water evaporation and can help to diminish water loss for current densities below i_{max} but needs to be considered when adjusting air excess ratio and relative humidity according to Fig. 2.11. Optimal inlet gas humidification depends on fuel cell structure and used materials and cannot be generalised. Though, according to Fig. 2.11, $RH^{\mathrm{C}} \approx 30\,\%$ is required for $\lambda^{\mathrm{C}} \approx 10$ and, thus, inlet humidities above 70 % at cell temperature would definitely lead to water accumulation for this excess ratio. For current densities above i_{max}, humidification of cathodic inlet gas up to $RH^{\mathrm{C}} = 100\,\%$ at cell temperature might help for cathodic water supply. However, these conditions definitely lead to water accumulation at anode and require further water removal to stabilise anodic water level. It should further be mentioned that temperature also influences this method of water level stabilisation. In addition to the effect of temperature on water diffusion through the membrane, operation temperature

also influences water content in the gas phase. At low temperatures, evaporation is reduced and higher gas flow rates at cathode are needed to remove sufficient water which might be infeasible. In contrast, high temperatures would require lower gas flow rates which could result in oxygen starvation.

2.3.2 Scenario 5 - Active Water Removal

Scenario 4 reveals that water level stabilisation by sufficient water diffusion through membrane is limited to current densities below a maximum value $i_{\max}$which depends on the diffusion coefficient of water through membrane. Current densities above $i_{\max}$ lead to water accumulation in the anodic loop and water needs to be removed from anode in addition to water diffusion through membrane to cathode. Scenario 5 is modelled to analyse the possibility of removing water from recycled liquid leaving anode before it is fed to anodic loop.

2.3.2.1 Mathematical Modelling

The model of this scenario includes active water removal from the anodic loop by feeding additional gas $\dot{n}^{\mathrm{ad}}_{\mathrm{gas}}$ to the anodic outlet in order to evaporate excess water. Subsequently, liquid and gas are separated (see Fig. 2.1). Liquid is recycled while gas including additionally evaporated water $\dot{n}^{\mathrm{Sys}}_{\mathrm{W,out}}$ is removed from the system. For stable water level, the molar flow of recycled liquid water fed to anodic loop needs to be equal to molar flow of water leaving the loop which is equal to the flow fed to anode:

$$\dot{n}^{\mathrm{Lo}}_{\mathrm{W,in}} = \dot{n}^{\mathrm{Lo}}_{\mathrm{W,out}} = \dot{n}^{\mathrm{A}}_{\mathrm{W,in}} \tag{2.65}$$

Combining this equation with Eq. (2.30) results in:

$$\dot{n}^{\mathrm{Sys}}_{\mathrm{W,out}} = \dot{n}^{\mathrm{A}}_{\mathrm{W,out}} - \dot{n}^{\mathrm{A}}_{\mathrm{W,in}} \tag{2.66}$$

The molar flow that has to be removed from system can be calculated by including this equation in the mass balance of water at anode, Eq. (2.2), in steady state:

$$\dot{n}^{\mathrm{Sys}}_{\mathrm{W,out}} = \sigma^{\mathrm{A}}_{\mathrm{W}} - \dot{n}^{\mathrm{diff}}_{\mathrm{W}} \tag{2.67}$$

As in Scenario 3, water diffusion is assumed to satisfy cathodic water demand and is calculated by Eq. (2.49).

It is assumed that additional gas is fed to anodic outlet with $T_{\text{in}}^{\text{ad}} = 20\,^{\circ}\text{C}$ and $RH_{\text{in}}^{\text{ad}} = 60\,\%$ and that it is saturated with water at cell temperature $T = 50\,^{\circ}\text{C}$ when leaving the system. The amount of water that is evaporated by the additional gas is supposed to be equal to the amount that needs to be removed:

$$\dot{n}_{\text{W,out}}^{\text{Sys}} = \dot{n}_{\text{W}^{\text{g}},\text{out}}^{\text{ad}} - \dot{n}_{\text{W}^{\text{g}},\text{in}}^{\text{ad}} \tag{2.68}$$

Considering that the gas consists of dry gas and vapour of water and methanol:

$$\begin{aligned}\dot{n}_{\text{gas}} =& \dot{n}_{\text{dry}} + \dot{n}_{\text{W}^{\text{g}}} + \dot{n}_{\text{Me}^{\text{g}}} = \dot{n}_{\text{dry}} + y_{\text{W}}\dot{n}_{\text{gas}} + y_{\text{Me}}\dot{n}_{\text{gas}} \\ \dot{n}_{\text{gas}} =& \frac{\dot{n}_{\text{dry}}}{1 - y_{\text{W}} - y_{\text{Me}}}\end{aligned} \tag{2.69}$$

the dry part of the additional gas does not change:

$$\dot{n}_{\text{dry,in}}^{\text{ad}} = \dot{n}_{\text{dry,out}}^{\text{ad}} = \dot{n}_{\text{dry}}^{\text{ad}} \tag{2.70}$$

Considering that additional gas does not contain methanol vapour at inlet, Eq. (2.68) results in:

$$\begin{aligned}\dot{n}_{\text{W,out}}^{\text{Sys}} &= \left(\frac{y_{\text{W}}^{\text{ad}}}{1 - y_{\text{W}}^{\text{ad}} - y_{\text{Me}}^{\text{ad}}} - \frac{y_{\text{W,in}}^{\text{ad}}}{1 - y_{\text{W,in}}^{\text{ad}}}\right)\dot{n}_{\text{dry}}^{\text{ad}} \\ &= \left(\frac{y_{\text{W}}^{\text{ad}} - y_{\text{W,in}}^{\text{ad}} + y_{\text{W,in}}^{\text{ad}} y_{\text{Me}}^{\text{ad}}}{1 - y_{\text{W}}^{\text{ad}} - y_{\text{Me}}^{\text{ad}}}\right)\frac{\dot{n}_{\text{dry}}^{\text{ad}}}{1 - y_{\text{W,in}}^{\text{ad}}}\end{aligned} \tag{2.71}$$

Thus, the molar flow of gas that needs to be added to anode outlet in order to remove excess water is calculated by:

$$\dot{n}_{\text{gas}}^{\text{ad}} = \frac{1 - y_{\text{W}}^{\text{ad}} - y_{\text{Me}}^{\text{ad}}}{y_{\text{W}}^{\text{ad}} - y_{\text{W,in}}^{\text{ad}} + y_{\text{W,in}}^{\text{ad}} y_{\text{Me}}^{\text{ad}}}\dot{n}_{\text{W,out}}^{\text{Sys}} \tag{2.72}$$

The additional gas also causes evaporation of methanol which is leaving the system along with the evaporated water. This additional loss of methanol is calculated by:

$$\dot{n}_{\text{Me,out}}^{\text{Sys}} = \frac{y_{\text{Me}}^{\text{ad}}}{1 - y_{\text{W}}^{\text{ad}} - y_{\text{Me}}^{\text{ad}}}\dot{n}_{\text{dry}}^{\text{ad}} \tag{2.73}$$

The resulting methanol efficiency is calculated by:

$$\eta_{\text{Me}} = \frac{\frac{A^{\text{M}} i}{6F}}{\dot{n}_{\text{Me}}^{\text{diff}} - \sigma_{\text{Me}}^{\text{A}} + \dot{n}_{\text{Me,out}}^{\text{Sys}}} \tag{2.74}$$

Table 2.7: Additional parameters used for simulation of Scenario 5.

$RH_{\text{in}}^{\text{ad}}$	$= 60\,\%$	$T_{\text{in}}^{\text{ad}}$	$= 20\,^{\circ}\text{C}$
$p_{\text{in}}^{\text{ad}}$	$= 1\,\text{bar}$	RH^{ad}	$= 100\,\%$

Additional parameters needed to simulate this scenario are listed in Table 2.7.

2.3.2.2 Results and Discussion

In this scenario, it is again assumed that water diffusion satisfies cathodic water demand and, thus, depends on current density, water drag, evaporation and methanol cross-over. Due to this definition, water dragged from cathode to anode is assumed to be transported back by diffusion. Consequently, electro-osmotic water drag does not influence the anode and is neglected in this scenario. In reality, water diffusion is not adjusted to water consumption and, thus, water drag influences anodic water level. Hence, this scenario is rather hypothetical but clarifies the impact of active water level stabilisation on methanol efficiency.

Conditions that lead to water accumulation in Scenario 3 and, hence, need additional water removal from anodic loop are chosen as reference conditions for the analysis of this scenario. These conditions include that methanol cross-over occurs, but no evaporation takes place at cathode, and that water is removed from anodic loop as water vapour with $RH^{\text{ad}} = 100\,\%$. The scenario is further analysed for three other cases which differ from reference conditions in one of the mentioned conditions. One case assumes that cathodic air is humidified to $RH^{\text{C}} = 30\,\%$. As a consequence, water diffusion is increased to satisfy both reaction and evaporation. Another case implies that additional gas is only humidified to $RH^{\text{ad}} = 80\,\%$ and, thus, a higher flow rate of additional gas is needed. Finally, the influence of methanol cross-over on the results is analysed by a case that excludes methanol cross-over.

Water production at anode is proportional to current density. Consequently, additional water evaporation needs to increase with rising current density as shown in Fig. 2.12a. The linearly increasing curve has an offset for the case without methanol cross-over which is equal to the water production by methanol oxidation at cathode. In the case that cathodic gas is partly humidified, only little amount of water needs to be removed from anodic loop because water is

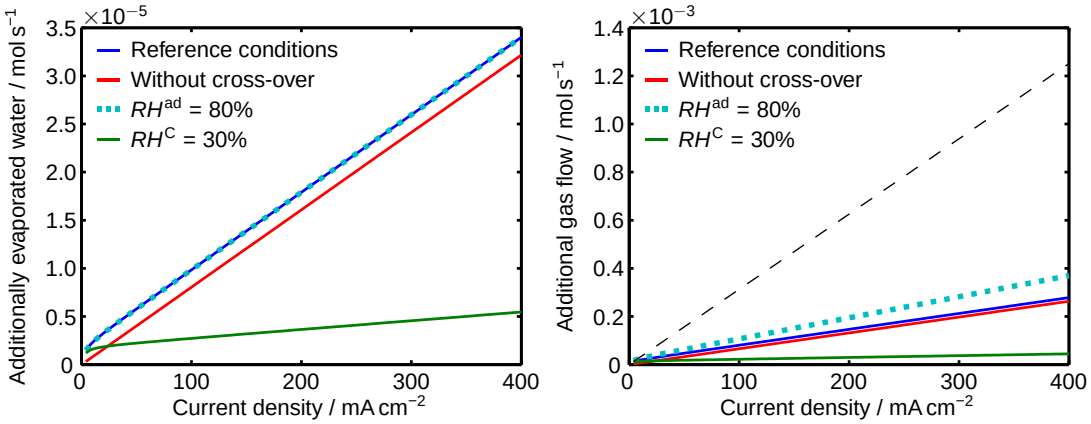

(a) (b)

Figure 2.12: Results of Scenario 5 for reference conditions (cross-over occurs, no evaporation at cathode and water is removed with $RH^{\mathrm{ad}} = 100\%$) and for three other cases that differ from reference conditions in one of the mentioned conditions: (a) amount of water that needs to be evaporated to stabilise water level, (b) required additional gas flow to evaporate sufficient water and, for comparison.

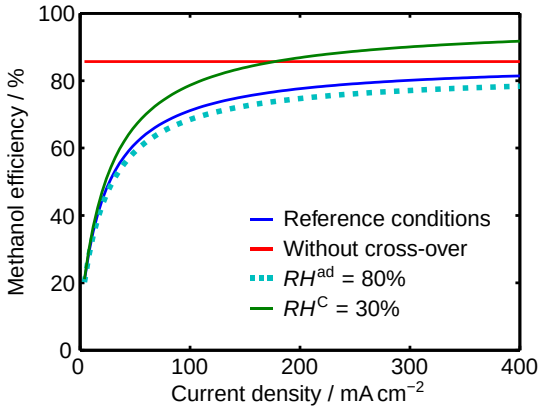

Figure 2.13: Methanol efficiency achieved in Scenario 5 for reference conditions (cross-over occurs, no evaporation at cathode and water is removed with $RH^{\mathrm{ad}} = 100\%$) and for three other cases that differ from reference conditions in one of the mentioned conditions.

already removed by diffusion. The achieved relative humidity in the additional gas flow has of course no impact on the required additional water evaporation.

Figure 2.12b displays the corresponding additional gas flow which is required to evaporate excess water as a function of current density as well as the cathodic air flow for $\lambda^{\mathrm{C}} = 10$ for comparison. $\dot{n}^{\mathrm{ad}}_{\mathrm{gas}}$ shows similar behaviour as the additional water evaporation. In case of water evaporation at cathode to $RH^{\mathrm{C}} = 30\,\%$, a much lower additional gas flow is needed than at reference conditions, since less

water needs to be removed. Reduction of achieved humidity to $RH^{\mathrm{ad}} = 80\,\%$ requires a higher additional gas flow because the same gas flow takes up less water. Furthermore, the gas flow also needs to be slightly lower if no methanol cross-over occurs since water diffusion is slightly higher in that case. However, in all cases, the required additional gas flow is much smaller than cathodic gas flow with $\lambda^{\mathrm{c}} = 10$ for all relevant current densities. Thus, cathodic gas flow is sufficient for water removal which can be realised by mixing part of cathodic outlet to anodic outlet. This is similar to a water transport through membrane with subsequent evaporation at the cathode as described in Scenario 4 (Fig. 2.11).

Nevertheless, there is a large difference between Scenario 4 and Scenario 5. Feeding additional gas to anodic outlet also leads to evaporation of methanol and, thus, decreases methanol efficiency. The additional efficiency losses caused by additional methanol evaporation may reach up to 20%. This is illustrated by Fig. 2.13 which displays the corresponding methanol efficiencies. In the case without methanol cross-over, methanol efficiency is not changing with current density because all terms in Eq. (2.74) are directly proportional to current density which can be cancelled causing methanol efficiency to be independent of current density. Comparing these efficiencies to the efficiency calculated in Scenario 2 (Fig. 2.6b) reveals that the additional efficiency loss in case of reference conditions is approximately 10 %. This efficiency loss is higher if lower relative humidities are achieved by additional evaporation due to a higher required additional gas flow. The efficiency in case of partial humidification at cathode indicates that the efficiency loss by evaporation is higher than losses by cross-over for current densities above $200\,\mathrm{mA\,cm^{-2}}$. However, efficiencies are acceptable especially compared to those obtained due to the stabilising effect in Scenario 3 (see Fig. 2.8b). In case that water level in the anodic loop is stabilised, methanol excess ratio can be decreased. This results in a lower methanol concentration at anode and a higher methanol efficiency.

2.4 Conclusions from Scenario Analysis

Five extreme case scenarios were derived from a general mathematical model in order to analyse the two big challenges regarding water management in ADMFCs: Sufficient water supply to cathode and water level stabilisation in an anodic loop. The analysis of these scenarios reveals that humidifying cathodic inlet gas is not sufficient for water supply to cathode and water transport through membrane is essential and desired for operation of any alkaline anion exchange membrane fuel

cell. The required water diffusion for sufficient water supply to cathode rises with increasing current density. However, current densities of $i \leq 400\,\mathrm{mA\,cm^{-2}}$ can be achieved with water diffusion coefficients below those reported in literature for an AEM. Therefore, cathodic water supply is mainly a challenge for high current densities and, thus, lack of water is not the reason for the low performance of present ADMFCs. For low current densities, low performance may rather be caused by flooding, especially if cathodic inlet is humidified.

Reasonable methanol efficiencies can only be achieved if methanol solution at anode is recycled by including an anodic loop which necessitates to master the second challenge. Stabilising water level of the anodic loop is essential to obtain high methanol efficiencies during long operation time in ADMFCs. Water diffusion coefficient and thickness of membrane define a maximum current density above which diffusion through membrane removes insufficient amount of water from anode. For current densities below maximum current density, water level can be stabilised by adjusting relative humidity and gas flow rate at cathode and, thus, controlling the amount of water removed from system. It should be mentioned that evaporation rates also depend on temperature and, thus, this method of water level stabilisation strongly depends on operation temperature and might not be applicable for much lower or very high temperatures. Current densities above the maximum current density require active water removal from anodic loop. Therefore, one scenario analyses the possibility to mix an additional gas flow to anodic outlet in order to evaporate and remove excess water from anode. Since methanol is also evaporating due to the additional gas flow, this way of water removal leads to an additional loss in methanol efficiency. Furthermore, active water removal from anode complicates the fuel cell system and reduces system efficiency even further. Therefore, water removal from anode should preferably be realised by diffusion through membrane as described by Scenario 4 and only extended by direct water removal from anode as described by Scenario 5 if necessary.

All scenarios identify diffusion through membrane as the key process for water management in ADMFCs which should be considered when developing new anion exchange membranes.

CHAPTER 3

Membrane Characterisation

Results of Chapter 2 reveal that water transport through membrane is essential for operation of alkaline anion exchange membrane fuel cells. However, results of diffusion experiments in literature are usually expressed by diffusion coefficients according to the most common version of Fick's law that uses concentration gradient as driving force [25]. This simplified version of Fick's law is not reasonable for a precise description of water diffusion through membrane in direct methanol fuel cells which have liquid phase at anode and gas phase at cathode and a concentration gradient across membrane would combine concentration of liquid water and water vapour. Hence, effect of concentration at cathode would be negligible while concentration at anode would be nearly constant and water diffusion would not change as well. This is not suitable for water management analysis. Therefore a different approach of diffusive transport is used in this thesis which considers the gradient of membrane wetness f^{M} as driving force:

$$\dot{n}_{\mathrm{W}}^{\mathrm{M,diff}} \sim \frac{1}{1+f^{\mathrm{M}}} \frac{\partial f^{\mathrm{M}}}{\partial z} \tag{3.1}$$

This approach is described in more details in Chapter 4. The required parameters for this approach are not available in literature and need to be determined from experimental results. Realisation and results of these experiments are described in this chapter after an introduction to anion exchange membranes and membrane characterisation techniques.

3.1 Membranes and Characterisation Techniques

Ion exchange membranes need some specific properties to be suitable as electrolyte in fuel cells. The main function of an electrolyte membrane is to enable ionic transport between the two electrodes. Thus, the most important requirement on membranes is a high ionic conductivity to decrease ohmic losses in the fuel cell. At the same time the membranes needs to be electronically isolating

to ensure that electric power is used by the connected electric device. Since membrane in a fuel cell can be wet or dry, membranes should be chemically and mechanically stable in wet as well as dry conditions and at elevated temperatures up to at least 100 °C to avoid membrane degradation during operation. Furthermore, membranes have either low pH value in acidic fuel cells or high pH value in alkaline fuel cells. Therefore, polymer membranes need to be stable at the pH value they are use at as well. Last but not least, membrane should block transport of the fuel, e.g. methanol, and of the oxidant, e.g. oxygen, to avoid cross-over effects that decrease fuel cell performance. These requirements hold for all kind of electrolyte membranes for fuel cell application. In case of alkaline anion exchange membranes, it is also required that the membranes enable water diffusion as revealed by scenario modelling in Chapter 2. Hence, an additional requirement on AEMs is to be highly selective regarding mass transport, especially if the AEM is used in a methanol fuel cell. Since no AEM created up to now shows all these properties, there is an ongoing research on membrane material and crafting techniques. A detailed overview on different material and synthesis of anion exchange membranes is given in [13, 50]. Both, homogeneous as well as heterogeneous membranes are investigated by different research groups and none of these membranes has been established or proved to be significantly better than all the others. However, all membranes have a polymer backbone equipped with functional groups that enable ionic transport. Quaternary ammonium groups have been proved to be suitable functional groups which are more stable than e.g. quaternary phosphonium groups [50]. The best known AEM which is commercially available is provided by *Tokuyama Corporation* which is a homogeneous membrane functionalized by quaternary ammonium groups. This also holds for another membrane which is manufactured by *CellEra* and shows good performance for hydrogen fuelled AEMFCs [51]. These two membranes are investigated in the experiments performed for this thesis.

3.1.1 Characterisation of Fuel Cell Membranes

In order to compare membranes for fuel cell application, some characterisation methods have been established which are usually carried out with new membranes to show their quality, e.g. [9, 52, 53]. The methods for electrochemical characterisation are described in the following.

Counter ions to the functional groups are often halide ions like CL^- or I^- for manufacturing because OH^- is easily carbonated when exposed to air. Before the

membranes are used in fuel cells or for electrochemical tests, the counter ions are exchanged by immersing the membrane in an alkaline solution, e.g. 1M KOH. The exchange of ions in combination with titration experiments is also used to determine the ion exchange capacity, IEC, which is defined as the amount of exchanged ions $n^{\mathrm{M}}_{\mathrm{ion}}$ based on the mass of the dry membrane $m^{\mathrm{M}}_{\mathrm{dry}}$:

$$IEC = \frac{n^{\mathrm{M}}_{\mathrm{ion}}}{m^{\mathrm{M}}_{\mathrm{dry}}} \tag{3.2}$$

The higher the IEC, the more ions are available for conduction and, thus, conductivity is higher. However, ionic conductivity is also influenced by other properties like ion mobility and is therefore determined in addition to IEC. Ionic conductivity of the membrane is defined as:

$$\sigma = \frac{d^{\mathrm{M}}}{R^{\mathrm{M}} A^{\mathrm{M}}} \tag{3.3}$$

where R^{M} is the ionic resistance of a membrane sample with thickness d^{M} and an area of ion conduction of A^{M}. Membrane resistance can be determined by impedance spectroscopy. Since R^{M} changes with membrane wetness, another important characterisation criterion is the affinity of the membrane to take up water as well as membrane swelling S^{M} which are determined by immersing a membrane sample into water, measuring weight or thickness of the wet membrane and dry the membrane subsequently in order to repeat measurements with the dry membrane. The definition of water uptake is used as definition of membrane wetness f^{M} in this thesis:

$$f^{\mathrm{M}} = \frac{m^{\mathrm{M}}_{\mathrm{wet}} - m^{\mathrm{M}}_{\mathrm{dry}}}{m^{\mathrm{M}}_{\mathrm{dry}}} \tag{3.4}$$

$$S^{\mathrm{M}} = \frac{d^{\mathrm{M}}_{\mathrm{wet}} - d^{\mathrm{M}}_{\mathrm{dry}}}{d^{\mathrm{M}}_{\mathrm{dry}}} \tag{3.5}$$

where $m^{\mathrm{M}}_{\mathrm{wet}}$ and $m^{\mathrm{M}}_{\mathrm{dry}}$ are weight of wet and dry membrane, respectively and $d^{\mathrm{M}}_{\mathrm{wet}}$ and $d^{\mathrm{M}}_{\mathrm{dry}}$ are membrane thickness of wet and dry membrane.

Last but not least, one criterion for membranes in methanol fuel cells is the permeability of methanol which is often represented by diffusion coefficient of methanol. Methanol permeability is measured by placing the membrane sample between two chambers, one filled with methanol solution and the other filled with water [53] or floated with gas [52]. The latter group used a gas chromatograph for quantification of diffusive flux. Since the standard membrane characterisa-

tion methods were developed for proton conducting membranes for which water transport is not as important as for AEMs, the water permeability is not part of the standard characterisation of electrolyte membranes and is not considered by most researchers who create new membranes.

3.1.2 Transport Phenomena in Electrolyte Membranes

The membrane in a fuel cell is supposed to block transport of reactants from anode to cathode. Therefore, it usually inhibits convective transport between the two electrodes and convection is limited to the flow channels and part of the gas diffusion layers. However, diffusion and migration take place due to a gradient in chemical potential $\tilde{\mu}_\beta$ which is defined as:

$$\tilde{\mu}_\beta = \mu_\beta^0 + RT\ln(a_\beta) + z_\beta F\Phi \tag{3.6}$$

$$\frac{\partial\tilde{\mu}_\beta}{\partial z} = \frac{RT}{a_\beta}\frac{\partial a_\beta}{\partial z} + z_\beta F\frac{\partial\Phi}{\partial z} \tag{3.7}$$

with gas constant R, Faraday constant F and the chemical potential μ_β^0 at standard conditions. a_β and z_β are the activity and the ionic charge of component β and Φ is the electric potential. The corresponding molar flux of component β is defined as:

$$j_\beta^{\mathrm{M}} = -M_{\beta,\mu}\left(\frac{RT}{a_\beta}\frac{\partial a_\beta}{\partial z} + z_\beta F\frac{\partial\Phi}{\partial z}\right) \tag{3.8}$$

with a mobility constant $M_{\beta,\mu}$ as transport coefficient.

The second term of Eq. (3.8) with the gradient of electric potential as driving force is called migration. This term is zero for uncharged species $z_\beta = 0$ because electric field has no influence on these species. However, due to the dipole character of water, water is indirectly influenced by the electric field because the water molecules are linked to charged species via hydrogen bridge bonds and, thus, are dragged along by transported ions from one electrode to the other. Hence, the migration term turns into water drag through membranes:

$$\dot{n}_{\mathrm{W}}^{\mathrm{drag}} = \kappa\frac{A^{\mathrm{M}}i}{F} \tag{3.9}$$

as defined in Eq. (2.5) in Chapter 2.

For charged species, the diffusive transport can usually be neglected. It can been shown that migration exceeds diffusion if potential difference across the membrane is higher than:

$$\Delta\Phi = \frac{RT}{z_\beta F} \tag{3.10}$$

which is about 26 mV at room temperature for $z_\beta = 1$ [54]. For uncharged species, diffusion is the main transport mechanism. The most common way of describing the activity of a species is by concentrations:

$$a_\beta = \frac{c_\beta}{c^0} \tag{3.11}$$

Often $1\,\mathrm{mol\,l^{-1}}$ is used as the constant standard concentration c^0. Inserting this definition of the activity into Eq. (3.8) for an uncharged species $z_\beta = 0$ results in:

$$j_\beta = -M_{\beta,\mu}\frac{RT}{c_\beta}\frac{\partial c_\beta}{\partial z} \tag{3.12}$$

which is equal to Fick's law of diffusion if the diffusion coefficient is defined as:

$$D_\beta = M_{\beta,\mu}\frac{RT}{c_\beta} \tag{3.13}$$

This definition already reveals that the diffusion coefficient is actually changing with concentration of component β. However, this dependency is often neglected if concentration changes are small. A more detailed description of transport processes can be found in literature, e.g. [54].

3.2 Error Estimation

Measured values are always containing errors which need to be estimated. These errors propagate on variables calculated from measured values. Errors of the results presented in this thesis are estimated by error propagation as described in literature [55]. For a variable y which depends on measured values x_i, the estimated error is a combination of individual uncertainties Δx_i weighted with

Table 3.1: Maximum errors of all measuring devices.

Device or variable	Symbol	Maximum error
Balance XS205	Δm	0.01 mg
Shim stock thickness	Δd^{ST}	2 µm
Dial gauge	Δd^{DG}	1 µm
Humidity sensor	ΔRH	$0.015(1 + RH)$
Temperature of humidity sensor	ΔT^{RH}	0.3 °C
Methanol concentration	Δc_{Me}	$0.03\,\mathrm{mol\,l^{-1}}$
Cori flow meter	$\Delta \dot{m}_{\mathrm{liq}}$	$0.1\,\mathrm{g\,h^{-1}}$
Gas mass flow controller	ΔF_{dry}	$0.008(F_{\mathrm{dry}}+1\,\mathrm{l_N\,min^{-1}})$
GC sample loop volume	ΔV^{SL}	2.5 µl
GC sample loop temperature	ΔT^{SL}	4 K
GC sample loop pressure	Δp^{SL}	9 mbar
Thermocouple	ΔT	1 K
Pressure sensor	Δp	0.01 bar

the corresponding sensitivity. Δy is calculated by the square root of the sum of squares of all individual errors:

$$\Delta y = \sqrt{\sum_{\mathrm{i}} \left(\frac{\partial y}{\partial x_{\mathrm{i}}} \Delta x_{\mathrm{i}} \right)^2} \tag{3.14}$$

Based on this general approach, errors for all results that are calculated from multiple measured values are estimated which are represented by error bars in the figures showing experimental results. Uncertainties of all measuring devices used for all experiments of this thesis are listed in Table 3.1.

Few anion exchange membranes that show good conductivity are commercially available yet. The best known alkaline membrane in literature is A201 from *Tokuyama* with a thickness of about 30 µm. Another promising membrane which is not represented in literature too much is produced by *CellEra* for alkaline fuel cell stacks. This membrane is called *CellEra's modified membrane* and abbreviated as CMM in this thesis. It has similar thickness as the A201. Both membranes are homogeneous membranes with a polymer backbone and quaternary

ammonium cations as functional groups and both are used for the following experiments. The membranes are characterised regarding processes that influence water management in order to provide data required to determine parameters for a detailed description of water transport through membrane. This includes measurements of membrane wetness and swelling as well as water and methanol diffusion through membrane.

3.3 Membrane Wetness and Thickness

Driving force for water diffusion through membrane is the gradient of membrane wetness. This gradient arises from equilibration of membrane wetness and surrounding media humidity. In ADMFCs and also in the diffusion setup used in this study, the membrane separates liquid and gas phase. Hence, equilibria between membrane and liquid water as well as between membrane and humidified gas are required for diffusion studies. These equilibria are determined by water uptake measurements from each phase. Furthermore, water uptake measurements from liquid phase are also used to determine thickness of the wet membrane.

3.3.1 Liquid Phase

Equilibrium between membrane wetness and liquid phase as well as thickness of the wet membrane are important parameters for modelling of water transport through membrane. Therefore, water uptake measurements from liquid phase were carried out to determine both parameters.

3.3.1.1 Setup and Procedure

Preparation of membrane samples is identical for measurements of both parameters. A hole puncher was used to get equally sized membrane samples of 20 mm diameter. The samples were dipped in ultrapure water which was purified by a *MILLI-Q Direct8* from *Merck Millipore*. With help of a heating plate, water temperature was adjusted to selected measurement temperature of 25 °C, 30 °C, 40 °C, 50 °C or 60 °C, respectively. After at least four hours, which was verified in preliminary tests to be sufficient time for full soaking of the membrane, the membrane sample was taken out of water and measurements for the wet membrane were carried out. Subsequently, the samples were dried in an oven at 60 °C for another four hours which again was verified in preliminary tests to be sufficient

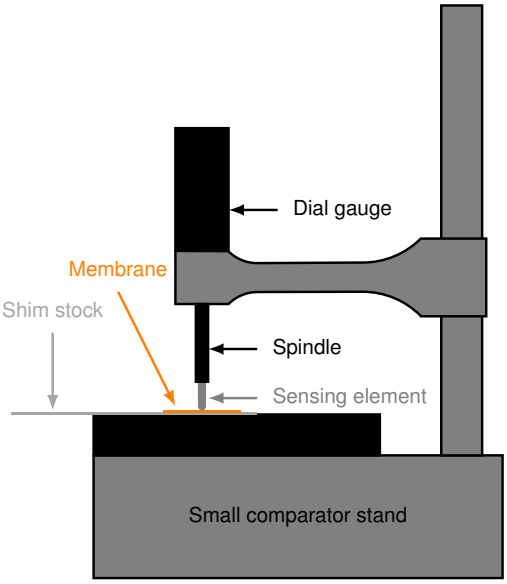

Figure 3.1: Setup for thickness measurements consists of a dial gauge clamped in a small comparator stand.

time for complete drying of the membrane and weight and thickness of the dry membrane were also measured.

Membrane Thickness was determined for several membrane samples. Four new membrane samples of A201 were prepared for each temperature and, additionally, one membrane sample that had been used for measurements at a lower temperature before was reused at the next higher temperature. For CMM, three new membrane samples were prepared for each temperature. Thickness in wet and dry conditions was measured for each membrane sample. In order to get precise measurements, a dial gauge *IP66* from *Mitutoyo* with a spindle fixed sensing element was clamped in a small comparator stand as shown in Fig. 3.1 and was reset to zero with a shim stock of 20 µm stainless steel between the base of the stand and the sensing element. The shim stock was used to ease positioning of the membrane and to prevent its contamination or damage. The membrane was put on the shim stock and thickness was measured at four points along the edge of membrane as well as at two points in the centre of the membrane sample. Subsequently, membrane samples were dried in an oven and thickness of dry membrane was measured accordingly. Error of the dial gauge is 1 µm.

Membrane Wetness in equilibrium with liquid phase was also determined by water uptake measurements. For each temperature and each membrane, three new membrane samples as well as three samples that had previously been used

for measurements at lower temperature were prepared as described above. After soaking time, one membrane sample after another was taken out of the water and the surface was carefully dried with a lint-free tissue paper. Subsequently, weight of the sample was determined using an *XS205* analytical balance from *Mettler Toledo* with a maximum error of 0.01 mg. The sample holder of *Mettler Toledo's* density kit was used for better positioning of the membrane sample. Time between taking membrane out of the water and measuring weight was minimized (below 10 s) since the membrane looses water to surrounding gas during that time. Weight loss within the first 10 s is up to 2 % of the wet membrane weight at 60 °C and up to 1 % for temperatures below 30 °C. After determination of wet weight of all samples, membrane samples were dried in an oven and afterwards weighed again as quickly as possible to avoid water uptake from surrounding gas. Membrane wetness f^{M} is calculated from mass of wet and dry membrane according to Eq. (3.4). Error of f^{M} is estimated according to Eq. (3.14) and includes the maximum error of the balance Δm as well as the standard deviation $\sigma_{f^{\mathrm{M}}}$ to account for variation of temperature and other operation conditions like gas humidity during drying:

$$\Delta f^{\mathrm{M}} = \sqrt{\left(\frac{1}{m_{\mathrm{dry}}^2} + \frac{m_{\mathrm{wet}}^2}{m_{\mathrm{dry}}^4}\right)\Delta m^2 + \sigma_{f^{\mathrm{M}}}^2} \tag{3.15}$$

This error does not account for water loss during surface drying which decreases membrane wetness.

3.3.1.2 Results

Temperature dependency of membrane thickness and membrane wetness was determined by measurements at temperatures between 25 °C and 60 °C for both membranes.

Membrane thickness does not vary with temperature. Therefore, mean values of the measured thickness of the membrane samples are not displayed in a figure but listed in Table 3.2. The values reveal that variation in membrane thickness with temperature is below 1 µm for both membranes in dry and wet conditions. Standard deviations are up to 0.5 µm while uncertainty of the shim stock is up to 2 µm. The latter might be of no consequence since the dial gauge is reset to zero before each measurement including the shim stock. However, membrane thickness is accepted to be independent of temperature since maximum error of dial gauge

Table 3.2: Mean values and standard deviation of measured membrane thickness of A201 and CMM membranes.

Tokuyama A201				
Temperature	Mean value / µm		Standard deviation / µm	
/ °C	Wet	Dry	Wet	Dry
25	30.0	26.5	0.0	0.8
30	29.9	25.9	0.5	0.3
40	30.0	26.0	0.3	0.2
50	30.2	26.0	0.6	0.7
60	30.0	25.8	0.3	0.5
CellEra's modified membrane CMM				
Temperature	Mean value / µm		Standard deviation / µm	
/ °C	Wet	Dry	Wet	Dry
25	28.8	26.9	0.4	0.3
30	28.8	26.3	0.4	0.5
40	28.8	26.9	0.4	0.2
50	28.2	26.4	0.4	0.5
60	28.3	26.7	0.5	0.5

is 1 µm. Thickness of A201 is about 30 µm in wet conditions and 26 µm in dry conditions which corresponds to a swelling ratio of approximately 15 % according to Eq. (3.5). Swelling of CMM is only half of this value (approximately 7.3 %) with thickness of approximately 28.8 µm in wet conditions and 26.6 µm in dry conditions. In ADMFCs and also in the diffusion experiments described below, membrane is in contact with liquid at one side and with gas at the other side. Since difference between thickness of wet and dry membrane is small (4 µm for A201 and 2 µm for CMM), it is assumed that membrane thickness in a fuel cell is approximately the average between thickness of dry and wet membrane. Thus, 28 µm is used as an average thickness for simulations in Chapter 4 and Chapter 5.

Membrane wetness in equilibrium with liquid water was determined by measuring weight of dry and wet membrane which are displayed in Fig. 3.2a. As expected, weight of wet membrane increases with temperature at which the mem-

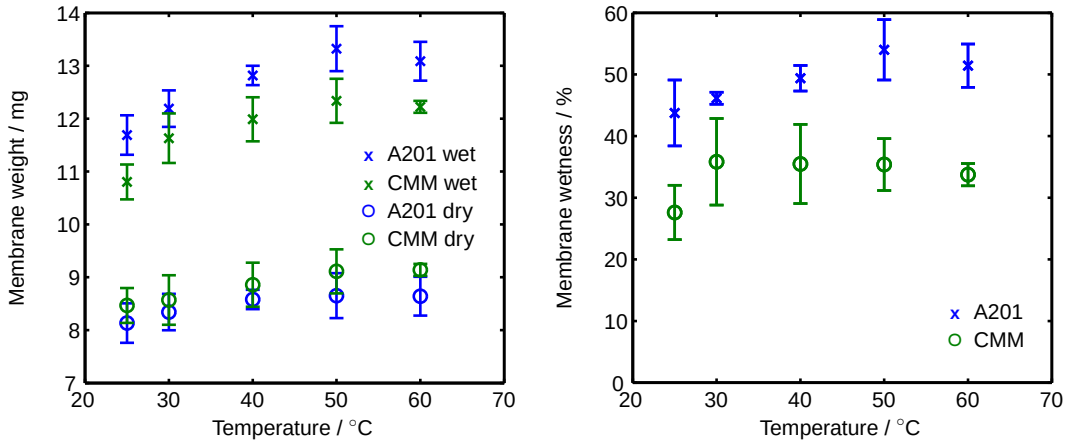

(a) (b)

Figure 3.2: Temperature dependency of water uptake measurements for A201 and CMM: (a) weight of dry and wet membrane; (b) membrane wetness f^{M}; Error bars contain standard deviation as well as error of the balance as calculated by Eq. (3.15);

brane was equilibrated with water. However, weight of dry membrane also increases slightly with this temperature which is surprising since all membrane samples are of same size and were dried at same temperature and should therefore have same dry weight. The increase in dry weight is presumably caused by water in the membrane due to insufficient drying or due to a quicker uptake of water from air between drying and measuring. Since the reason for the increase of the dry weight cannot be proved, membrane wetness is calculated with the measured values and displayed in Fig. 3.2b. The values are also listed in Table 3.3. As a consequence of the simultaneous increase of wet and dry weight, membrane wetness of A201 increases only slightly with rising temperature up to 50 °C while wetness of CMM is quite stable between 30 °C and 60 °C. Both membranes show a slight decrease of membrane wetness for 60 °C which results from a decrease in weight of wet membrane. This decrease is presumably caused by higher evaporation during surface drying and positioning on the sample holder of the balance in consequence of higher membrane temperature. As stated above, this loss of water by evaporation is quite small ($\leq 2\,\%$ of wet membrane weight) and the error is not included in the error bar which is calculated by Eq. (3.15). Therefore, actual values will be slightly above the displayed mean values for all temperatures.

A201 takes up more water than CMM which corresponds to the measured membrane swelling. Values of *Tokuyama* membrane from Table 3.3 are used for simulation of diffusion experiments in Chapter 4 and of water diffusion in the fuel cell in Chapter 5.

Table 3.3: Mean values of membrane wetness for A201 and CMM membranes equilibrated with liquid water at different temperatures.

Temperature / °C		25	30	40	50	60
Membrane wetness	A201 / %	43.8	46.1	49.4	54.0	51.4
	CMM / %	27.6	35.8	35.5	35.4	33.7

3.3.2 Gas Phase

Modelling water diffusion through membrane also requires knowledge of equilibrium between membrane wetness and humidity of surrounding gas. Therefore, water uptake from gas phase was also measured which is more complex compared to that from liquid phase.

3.3.2.1 Setup and Procedure

Equilibrium between membrane and gas phase depends on gas conditions such as temperature and gas humidity. In order to assure defined gas conditions, a small chamber of 10 cm diameter and 10 cm hight was designed which was flushed with humidified nitrogen. The nitrogen inlet flux was controlled to $0.5\,\mathrm{l_N\,min^{-1}}$ by a gas mass flow controller from *Sierra Instruments* and was humidified with help of a *Controlled Evaporator and Mixer* (CEM) from *Bronkhorst Mättig* that allows precise and continuous mixing of gas and evaporated liquids. The water flux to the CEM was measured by a *Cori Flow Meter* from *Bronkhorst Mättig* and controlled by a valve at the liquid inlet of the CEM. Humidity and temperature in the chamber were measured by a set of temperature and humidity sensor *HMT337* from *Vaisala* that are inserted into the chamber. A heating element was inserted to adjust temperature at the *HMT337* to values of 40 °C, 50 °C, 60 °C and 70 °C. The corresponding values of local temperature at the membrane sample, which were measured by a thermocouple installed close to the sample holder, are 37.4 °C, 47.5 °C, 57.7 °C and 62.9 °C. In order to avoid disturbance of gas conditions by opening the chamber and taking the membrane sample to measure the weight, the chamber was put in the weighing chamber of the *XS205* analytical balance of *Mettler Toledo*, which was used for water uptake measurements from liquid phase, and the sample holder of the density kit was directly inserted in the chamber as shown in Fig. 3.3. In addition to the heating element, an infra red light was used

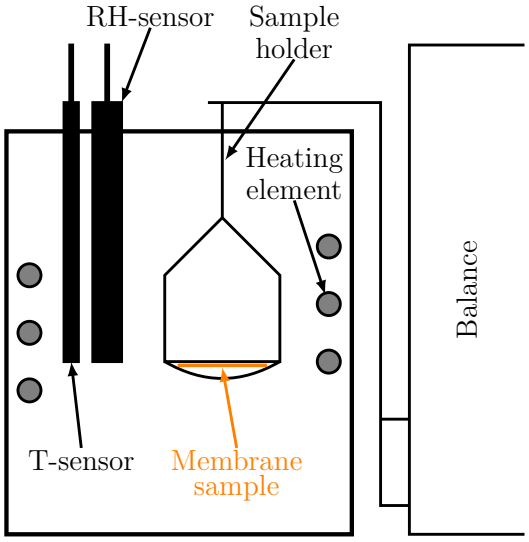

Figure 3.3: Setup for measurements of water uptake from gas phase: Sample holder of the balance is surrounded by a chamber with defined gas humidity and temperature.

to heat the surrounding to avoid condensation at the sample holder of the balance and, thus, incorrect results.

The measurements were performed only for A201 membrane from *Tokuyama*. Circular samples of 24 mm diameter were cut with a hole puncher to get membrane pieces of equal size. For each temperature, a new membrane sample was put on the sample holder and temperature as well as lowest humidity were adjusted. Keeping temperature constant, humidity was increased successively by raising water flux to the CEM. Due to the volume of the chamber, the response of relative humidity on step change of water inlet flow takes about 10 min to reach a new steady state. Weight of wet membrane was measured after all conditions were stable for at least 5 min. The small change in conditions by raising relative humidity by 10 % justifies the much shorter equilibration time of $t \gtrsim 15$ min compared to the 4 h for water uptake from liquid phase. In order to avoid disturbances, gas and liquid flow rates were turned off while reading the value of the membrane weight. After measurement with highest gas humidity, water flux to the CEM was reduced to adjust lowest humidity again and do multiple measurements. Subsequently, membrane sample was dried by flashing the chamber with dry nitrogen during night and weight of dry membrane was measured next day.

Molar fraction of water in gas phase y_w was calculated from the data of the *HMT337* using Dalton's law (see Eq. (2.38)). Due to the mixing effect of the gas inlet, the chamber was assumed to be ideally mixed (CSTR) and y_w to be

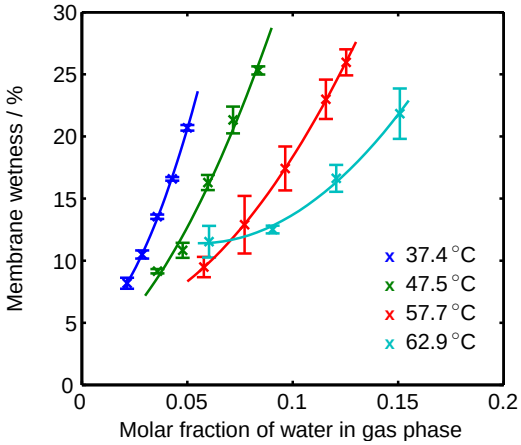

Figure 3.4: Equilibrium membrane wetness as a function of molar fraction of water in gas phase for different temperatures measured at membrane sample; Solid lines are polynomial fits of second degree.

constant within the chamber. Membrane temperature measured with the thermocouple was taken as operation temperature. For temperatures of 37.4 °C and 47.5 °C membrane weight was measured only twice for each humidity because these measurements were less prone to error. Measurements of higher temperatures of 57.7 °C and 62.9 °C were carried out six times. Membrane wetness f^{M} was calculated from weight of wet and dry membrane according Eq. (3.4). Errors were estimated as for water uptake from liquid phase, Eq. (3.15), including standard deviation of multiple measurements to account for uncertainties of humidity and temperature in the chamber.

3.3.2.2 Results

The results in Fig. 3.4 show that membrane wetness f^{M} rises with increasing molar fraction of water in gas phase y_{W} as expected. Higher temperature at same y_{W} is equivalent to lower relative humidity and, thus, leads to lower water uptake. Only exception to this is the curve of 62.9 °C for low water content in gas phase. This might be caused due to higher uncertainties of relative humidity or due to higher temperature difference between humidity sensor and membrane sample. However, this is of no consequence for analysis of water diffusion through membrane which was mainly studied for temperature of 50 °C. Similar to measurements in literature [25], dependency of membrane wetness on y_{W} follows a polynomial function and the results were fitted by least squares to a polynomial equation of degree 2 for each temperature:

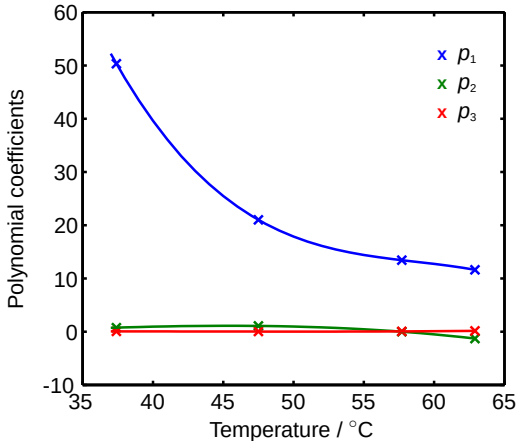

Figure 3.5: Parameter of Eq. (3.16) as a function of temperature; Solid lines are polynomial fits of degree 3.

Table 3.4: Fitted values of parameters for Eq. (3.17).

i	$a_{i,1}$ / K^{-3}	$a_{i,2}$ / K^{-2}	$a_{i,3}$ / K^{-1}	$a_{i,4}/1$
1	$-3.200 \cdot 10^{-3}$	3.151	$-\ 1.046 \cdot 10^{3}$	$1.157 \cdot 10^{5}$
2	$-9.420 \cdot 10^{-5}$	$8.380 \cdot 10^{-2}$	-24.720	$2.416 \cdot 10^{3}$
3	$3.186 \cdot 10^{-5}$	$-3.040 \cdot 10^{-2}$	9.657	$-1.023 \cdot 10^{3}$

$$f^{\mathrm{M}} = p_1(T) y_{\mathrm{W}}^2 + p_2(T) y_{\mathrm{W}} + p_3(T) \tag{3.16}$$

The coefficients $p_i(T)$ depend on temperature and are likewise fitted to polynomial functions of degree 3 of temperature as shown in Fig. 3.5 following the equation:

$$p_i = a_{i,1} T^3 + a_{i,2} T^2 + a_{i,3} T + a_{i,4} \tag{3.17}$$

Fitted parameters $a_{i,j}$ are listed in Table 3.4. With these parameters and Eqs. (3.16) and (3.17), membrane wetness $f^{\mathrm{M}}(T, y_{\mathrm{W}})$ can be calculated for any temperature $T \in [37\,^{\circ}\mathrm{C}; 63\,^{\circ}\mathrm{C}]$ and mole fractions of $y_{\mathrm{W}} \in [0.02; 0.15]$. Furthermore, weight of a dry *Tokuyama* membrane sample is 11.6 mg which results in an area density of dry membrane of $\tilde{\rho}^{\mathrm{M}}_{\mathrm{dry}} = 0.0256\,\mathrm{kg\,m^{-2}}$. This area density is needed for modelling of water diffusion in Chapters 4 and 5.

3.4 Quantification of Diffusion

As stated in Chapter 2, water diffusion through membrane is the key process for stable water management in alkaline membrane fuel cells. However, water diffusion coefficients presented in literature are determined for a simplified version of Fick's law using concentration gradient as driving force. The model approach to describe water diffusion presented in this thesis uses the gradient of membrane wetness as a driving force. Diffusion coefficients for this approach are not available in literature and are therefore determined in this thesis. Therefore, diffusive fluxes through an AEM were quantified experimentally which is content of this section.

3.4.1 Gas Chromatography Setup

A gas chromatograph (GC) was used to quantify water and methanol content in the gas phase of the diffusion experiment. The analysis of a gas sample with a GC consists of two steps. First, the gas sample flows through chromatography columns which contain a stationary phase that interacts differently with each substance and, thus, causes different retention times of the respective substances. As a consequence, a sample that moves through the columns is split up into single substances. Afterwards, the split up sample is directed to a sensor which detects all substances separately.

The results of this thesis are achieved using a GC *7890A* from *Agilent Technologies* with three different chromatography columns from *Agilent J&W*: Column 1 is an *HP-PLOT/QO4* (30 m x 0.535 mm x 40 µm), column 2 is a *DB-1* (10 m x 0.538 mm x 5.00 µm) and column 3 is an *HP-Plot Molesieve/MS6* (30 m x 0.535 mm x 25.00 µm). Due to interconnection with two switching valves, columns 1 and 3 can be included in the internal pipeline of the GC or bypassed while column 2 is always included in the pipeline as shown in Fig. 3.6. In column 1, the retention time of methanol is longer than that of water. Hence, this column is included in the pipeline for this study to separate the substances of the samples which consist of water and methanol. Furthermore, water and methanol would both poison the *Molesieve* which is consequently bypassed in all measurements done for this thesis by switching Valve 2. The sample loop is connected to Valve 1 and is bypassed most of the time. At the beginning of each run after the loop is filled with the sample, Valve 1 is switched and the sample loop is flushed by the carrier gas Helium 5.0 for 1 minute to inject the sample into the flow line of the GC.

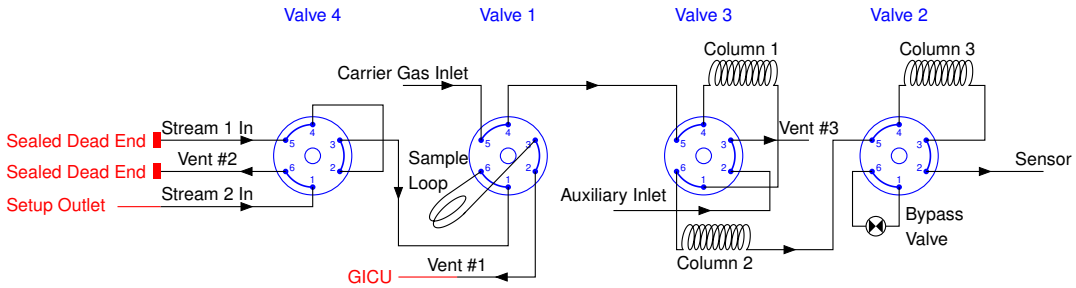

Figure 3.6: Flow chart of internal piping of the GC with the default position (off-position) of all valves. Modifications and connections for use of GICU are displayed in red colour.

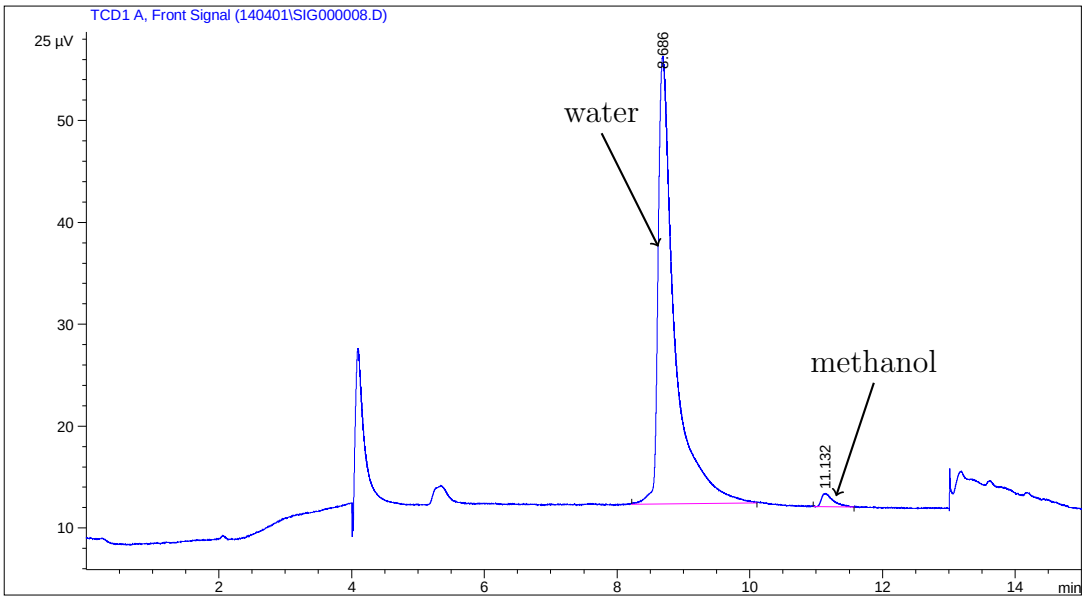

Figure 3.7: Typical chromatogram of diffusion experiments at a temperature of 50 °C and a gas flow rate of 1.4 l_N min^{-1}.

The used GC is equipped with a thermal conduction detector (TCD). This is a universal sensor in gas chromatography that can detect any substance. It measures the difference in thermal conductivity between the sample gas exiting the chromatography columns and a reference gas which is identical to the carrier gas. The sensor returns a continuous voltage signal. The temporal progress of this signal versus time is called chromatogram which shows a peak for each component of the sample. However, a typical chromatogram of the measurements done for this thesis in Fig. 3.7 shows more than the two peaks of methanol and water. The other peaks result from switching one of the valves which causes a pressure pulse that changes the thermal conductivity for a short time and, thus, temporarily

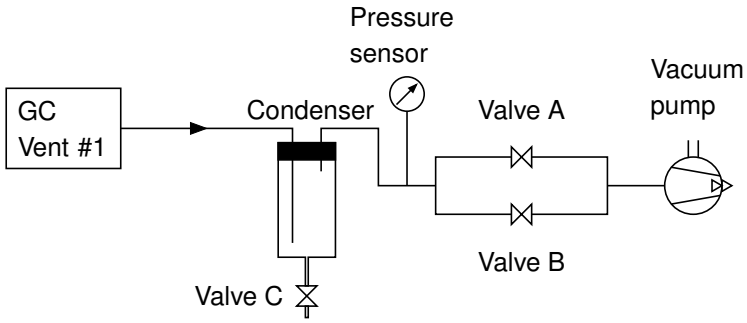

Figure 3.8: Flow chart of internal piping of the GICU.

disturbs the voltage signal. The area below a component peak represents the quantity of the respective component in the sample. For quantitative studies, a calibration curve that correlates peak area and substance quantity needs to be determined by calibration experiments described in Section 3.4.2. More details about gas chromatography and the working principle of a TCD can be found in literature [56].

Since the sample is in gas form, reproducible results can only be achieved if conditions in the sample loop are adjusted to equal values for all measurements. Temperature $T^{\mathrm{SL}} = 150\,^{\circ}\mathrm{C}$ and volume $V^{\mathrm{SL}} = 0.25\,\mathrm{ml}$ of the sample loop are predetermined by GC and are same for all measurements. Solely, the pressure cannot be adjusted by GC. Therefore, a *Gas Injection Control Unit* (GICU) from *Joint Analytical Systems GmbH (jas)* is connected to the GC sample loop. The modifications on the internal piping of the GC required for the use of the GICU are highlighted in red colour in Fig. 3.6. The internal piping of the GICU is displayed in Fig. 3.8. This device uses a vacuum pump to reduce the pressure in the sample loop up to few millibars. Valves A and B are switching valves of different size that function as controlling elements for the feedback control of the pressure. A pressure sensor upstream of these valves provides the feedback signal. In order to prevent the vacuum pump from being affected by liquids, a condenser is assembled upstream of the valves to collect condensed liquid. The condensate is removed after each measurement by opening valve C at the bottom of the condenser.

3.4.2 Calibration Experiments

Quantification by Gas Chromatography requires calibration curves for all substances in the analysed sample. These curves have to be generated by calibration

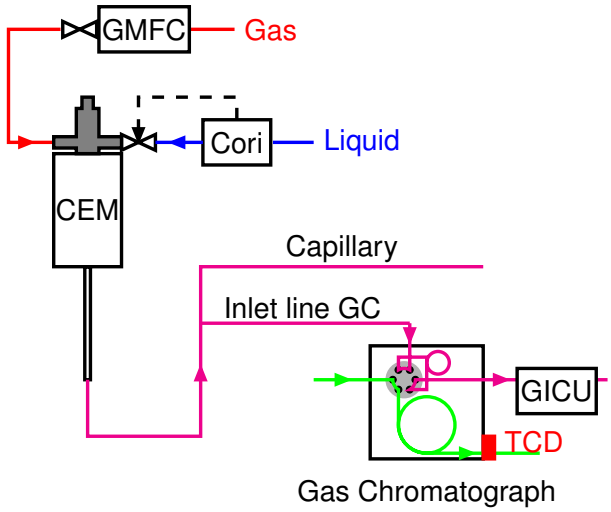

Figure 3.9: Setup for GC calibration consists of an evaporation system connected to the inlet line of the GC.

experiments which require a separate setup but have to be performed with the same GC settings as the diffusion experiments.

3.4.2.1 Setup and Procedure

Calibration experiments require samples with specific amount of substances in quantities similar to those expected for the measurement results. Therefore, the evaporation system from *Bronkhorst Mättig* that has been used for water uptake measurements from gas phase (Section 3.3.2) was used for the calibration experiments as well. As displayed in Fig. 3.9, the evaporation system consists of a gas mass flow controller for flow rates up to $4\,\mathrm{l_N\,min^{-1}}$ calibrated for Helium and a cori flow meter for liquids up to $8\,\mathrm{g\,h^{-1}}$ which feed a controlled evaporator and mixer (CEM). The exit of the CEM was connected to the GC inlet line by a T-connector.

Several combinations of liquid and gas flow rates are necessary to obtain calibration curves for water and methanol contents of a gas flow, respectively. Methanol solutions of two different concentrations were used as liquid feed for calibration: $3\,\mathrm{mol\,l^{-1}}$ and $2.55\,\mathrm{mol\,l^{-1}}$ of methanol. Helium 5.0 was used as carrier gas. All parameter settings of concentration and flow rates are listed in Table 3.5. Six to seven samples were analysed for each of these parameter settings.

Table 3.5: Parameter settings of methanol concentrations (c_{Me}) and flow rates of gas (F_{dry}) and liquid ($\dot{m}_{\mathrm{liq}}$) used to generate calibration curves for water and methanol.

Flow rates for $c_{\mathrm{Me}} = 3.0\,\mathrm{mol\,l^{-1}}$									
F_{dry} / $\mathrm{l_N\,min^{-1}}$	2.0	2.0	2.0	1.0	1.0	1.0	4.0	4.0	3.0
$\dot{m}_{\mathrm{liq}}$ / $\mathrm{g\,h^{-1}}$	2.0	4.0	1.0	2.0	4.0	6.0	2.0	1.0	2.0

Flow rates for $c_{\mathrm{Me}} = 2.55\,\mathrm{mol\,l^{-1}}$												
F_{dry} / $\mathrm{l_N\,min^{-1}}$	2.0	2.0	2.0	1.0	1.0	1.0	4.0	1.0	3.0	4.0	4.0	2.0
$\dot{m}_{\mathrm{liq}}$ / $\mathrm{g\,h^{-1}}$	2.0	4.0	1.0	2.0	1.0	4.0	2.0	6.0	2.0	1.0	2.0	0.5

Liquid volume flow rate can be calculated from water and methanol concentrations as well as mass flow of methanol solution:

$$\dot{m}_{\mathrm{liq}} = \dot{m}_{\mathrm{W}} + \dot{m}_{\mathrm{Me}} = (c_{\mathrm{W}} M_{\mathrm{W}} + c_{\mathrm{Me}} M_{\mathrm{Me}}) F_{\mathrm{liq}} \tag{3.18}$$

$$F_{\mathrm{liq}} = \frac{\dot{m}_{\mathrm{liq}}}{c_{\mathrm{W}} M_{\mathrm{W}} + c_{\mathrm{Me}} M_{\mathrm{Me}}} \tag{3.19}$$

Combining liquid and gas flow provides the molar fraction of liquid components $\alpha \in \{\mathrm{W}, \mathrm{Me}\}$ of the calibration sample:

$$y_\alpha = \frac{\dot{n}_\alpha}{\dot{n}_{\mathrm{W}} + \dot{n}_{\mathrm{Me}} + \dot{n}_{\mathrm{He}}} = \frac{c_\alpha F_{\mathrm{liq}}}{(c_{\mathrm{W}} + c_{\mathrm{Me}}) F_{\mathrm{liq}} + \frac{p_{\mathrm{N}}}{R T_{\mathrm{N}}} F_{\mathrm{gas}}} \tag{3.20}$$

With these molar fractions, the amount of water and methanol in the sample loop can be determined by:

$$n_\alpha^{\mathrm{SL}} = y_\alpha \frac{p^{\mathrm{SL}} V^{\mathrm{SL}}}{R T^{\mathrm{SL}}} \tag{3.21}$$

Some of the combinations lead to equal amount of water or methanol in the sample loop which helps to verify the results. These measurements are combined to one calibration point.

Error estimation for the calibration curve is quite complex since values of both axis are containing errors. The error of the area below the GC signal is estimated by the standard deviation of the measured area of multiple samples which is used as corresponding error in x direction. The error of the amount of moles in the sample loop is estimated by error propagation according Eq. (3.14). Regarding

Eqs. (2.33) and (2.34) which are valid for any liquid phase, the error of water concentration is calculated by:

$$\Delta c_{\mathrm{W}} = \frac{c^*_{\mathrm{W}}}{c^*_{\mathrm{Me}}} \Delta c_{\mathrm{Me}} \tag{3.22}$$

According to Eq. (3.19), the error of liquid volume flow rate is calculated by:

$$\Delta F_{\mathrm{liq}} = \sqrt{\left(\frac{\Delta \dot{m}_{\mathrm{liq}}}{c_{\mathrm{W}} M_{\mathrm{W}} + c_{\mathrm{Me}} M_{\mathrm{Me}}} \right)^2 + \frac{\dot{m}^2_{\mathrm{liq}} \left(\left(\Delta c_{\mathrm{W}} M_{\mathrm{W}} \right)^2 + \left(\Delta c_{\mathrm{Me}} M_{\mathrm{Me}} \right)^2 \right)}{\left(c_{\mathrm{W}} M_{\mathrm{W}} + c_{\mathrm{Me}} M_{\mathrm{Me}} \right)^2}} \tag{3.23}$$

Considering that methanol concentration is low compared to water concentration, Eq. (3.20) simplifies to:

$$y_\alpha = \frac{c_\alpha F_{\mathrm{liq}}}{c_{\mathrm{W}} F_{\mathrm{liq}} + \frac{p_{\mathrm{N}}}{R T_{\mathrm{N}}} F_{\mathrm{dry}}} \tag{3.24}$$

As a consequence, the estimated errors for the molar fraction in the gas phase are:

$$\Delta y_{\mathrm{W}} = \sqrt{\frac{\left(\frac{p_{\mathrm{N}}}{R T_{\mathrm{N}}} \right)^2}{\left(c_{\mathrm{W}} F_{\mathrm{liq}} + \frac{p_{\mathrm{N}}}{R T_{\mathrm{N}}} F_{\mathrm{dry}} \right)^4} \left(\left(F_{\mathrm{dry}} F_{\mathrm{liq}} \Delta c_{\mathrm{W}} \right)^2 + \left(c_{\mathrm{W}} F_{\mathrm{dry}} \Delta F_{\mathrm{liq}} \right)^2 + \ldots \right.} \left. \begin{array}{c} \\ \ldots + \left(c_{\mathrm{W}} F_{\mathrm{liq}} \Delta F_{\mathrm{dry}} \right)^2 \end{array} \right) \tag{3.25}$$

$$\Delta y_{\mathrm{Me}} = \sqrt{\begin{array}{l} \left(\frac{F_{\mathrm{liq}} \Delta c_{\mathrm{Me}}}{c_{\mathrm{W}} F_{\mathrm{liq}} + \frac{p_{\mathrm{N}}}{R T_{\mathrm{N}}} F_{\mathrm{dry}}} \right)^2 + \frac{\left(c_{\mathrm{Me}} F^2_{\mathrm{liq}} \Delta c_{\mathrm{W}} \right)^2}{\left(c_{\mathrm{W}} F_{\mathrm{liq}} + \frac{p_{\mathrm{N}}}{R T_{\mathrm{N}}} F_{\mathrm{dry}} \right)^4} + \ldots \\ \quad \ldots + \left(\frac{p_{\mathrm{N}} c_{\mathrm{Me}}}{R T_{\mathrm{N}}} \right)^2 \frac{(F_{\mathrm{dry}} \Delta F_{\mathrm{liq}})^2 + (F_{\mathrm{liq}} \Delta F_{\mathrm{dry}})^2}{\left(c_{\mathrm{W}} F_{\mathrm{liq}} + \frac{p_{\mathrm{N}}}{R T_{\mathrm{N}}} F_{\mathrm{dry}} \right)^4} \end{array}} \tag{3.26}$$

Based on Eq. (3.21), the error of the amount of moles of a component α in the sample loop can finally be calculated by:

$$\Delta n^{\mathrm{SL}}_\alpha = \sqrt{\left(\frac{p^{\mathrm{SL}} V^{\mathrm{SL}}}{R T^{\mathrm{SL}}} \Delta y_\alpha \right)^2 + \left(\frac{y_\alpha V^{\mathrm{SL}}}{R T^{\mathrm{SL}}} \Delta p^{\mathrm{SL}} \right)^2 + \left(\frac{y_\alpha p^{\mathrm{SL}}}{R T^{\mathrm{SL}}} \Delta V^{\mathrm{SL}} \right)^2 + \ldots} \left. \begin{array}{c} \\ \ldots + \left(\frac{y_\alpha p^{\mathrm{SL}} V^{\mathrm{SL}}}{R T^{\mathrm{SL}2}} \Delta T^{\mathrm{SL}} \right)^2 \end{array} \right) \tag{3.27}$$

Uncertainties of the measured values are displayed in Table 3.1.

3.4.2.2 Results

Calibration curves for water and methanol are displayed in Fig. 3.10. As expected, the amount of moles in the sample loop increases with the measured peak area

Table 3.6: Fittet parameters to calculate calibration curves.

	$p^{\mathrm{cc}}_{\alpha,1}$	$p^{\mathrm{cc}}_{\alpha,2}$	$p^{\mathrm{cc}}_{\alpha,3}$
Water	$2.48 \cdot 10^{-14}$	$3.98 \cdot 10^{-10}$	$-2.62 \cdot 10^{-9}$
Methanol	$-3.18 \cdot 10^{-13}$	$3.10 \cdot 10^{-10}$	$1.81 \cdot 10^{-9}$

or vice versa. A trendline which is displayed as solid line shows a polynomial behaviour and was therefore fitted to the data points by the polyfit function of Matlab with power 2. This function uses least squares to tune the parameter of the following polynomial function:

$$n^{\mathrm{cc}}_{\alpha}(A) = p^{\mathrm{cc}}_{\alpha,1} A^2 + p^{\mathrm{cc}}_{\alpha,2} A + p^{\mathrm{cc}}_{\alpha,3} \tag{3.28}$$

Parameters $p^{\mathrm{cc}}_{\alpha,\mathrm{i}}$ are listed in Table 3.6. Equation (3.28) and the tuned parameters are used for evaluation of GC signals for the samples of diffusion measurements.

Errors of the area below the GC signal (x-data) and of the amount of moles in the sample loop (y-data) are depicted as rectangles around the mean value with an edge length of twice the corresponding error. Calibration curves are used to determine the amount of moles in the sample loop from the measured peak areas of the samples of diffusion measurements. Converting the uncertainty of the peak area A into an error of amount of moles in the sample loop results in:

$$\Delta\tilde{n}^{\mathrm{SL}}_{\alpha} = 2p_{\alpha,1}\overline{A}_{\alpha}\Delta A_{\alpha} + p_{\alpha,2}\overline{A}_{\alpha} \tag{3.29}$$

For error propagation of diffusion measurements, it is necessary to estimate one error of the calibration curves which is calculated from the maximum value of $\Delta n^{\mathrm{SL}}_{\alpha}$ and the mean value of $\Delta\tilde{n}^{\mathrm{SL}}_{\alpha}$ by:

$$\Delta n^{\mathrm{cc}}_{\alpha} = \sqrt{{\Delta n^{\mathrm{SL}}_{\alpha,\max}}^2 + \overline{\Delta\tilde{n}^{\mathrm{SL}}_{\alpha}}^2} \tag{3.30}$$

This error is a kind of confidence interval which is depicted by the dashed lines framing the trendline in Figs. 3.10a and 3.10b. It is used for further error propagation of the results of diffusion experiments.

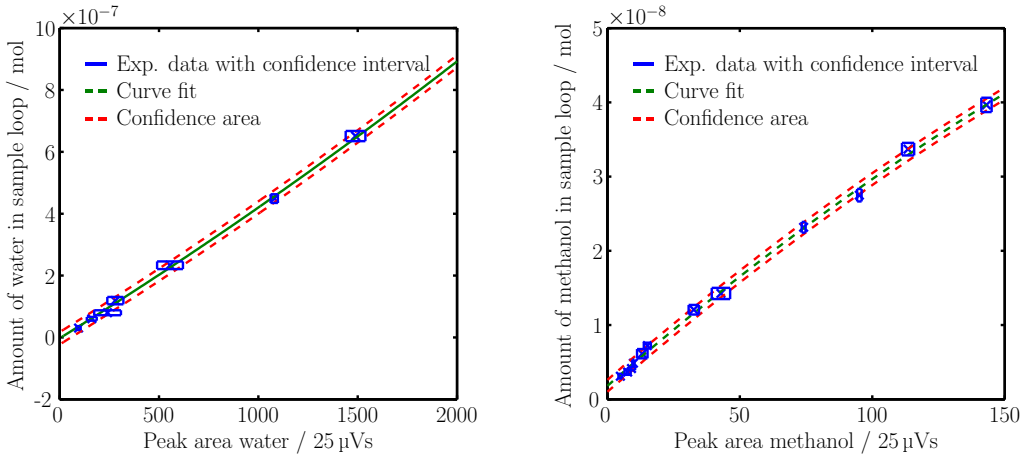

(a) Water. (b) Methanol.

Figure 3.10: Calibration curves for water and methanol showing area below the signal peak of the TCD in µVs versus amount of substance in the sample loop in µmol; Squares represent errors and the dashed lines depict the confidential interval of the solid trendline;

3.4.3 Diffusion Experiments

Water and methanol content in a helium flow were quantified with the same GC setup and settings as used for the calibration experiments. However, the setup that generates a methanol and water vapour flow by diffusion of these substances through a membrane is obviously different to the calibration setup.

3.4.3.1 Setup and Procedure

The setup for measuring diffusion through membrane contains a diffusion cell which was designed as two chambers that are separated by the membrane sample. Therefore, a frame was made from two circular slices of PEEK with a circular window of 22.5 mm diameter in which a piece of membrane with a diameter of 33 mm can be clamped in between as shown in Fig. 3.11. Two rings of PTFE foil are used for sealing, one at each side of the membrane. The frame is sandwiched by two chambers of different size. These chambers are shaped as rectangular cuboids which are open to one side. Both chambers have a flange of the same size as the frame around the open side. Flanges and frame are pressed together with a pair of retainer screw and retainer nut pulled over the flanges. The assembly of the diffusion cell is shown in Fig. 3.12.

A flow chart of the entire diffusion setup is shown in Fig. 3.13. The liquid chamber with a volume of 0.5 l is filled with 1 molar methanol solution and put

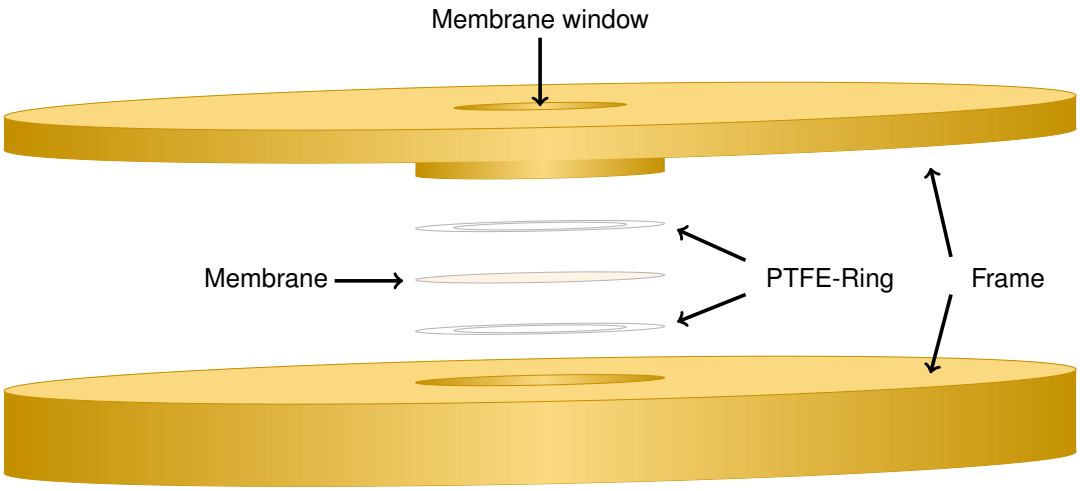

Figure 3.11: Membrane sample and two rings of PTFE-foil for sealing are assembled in a frame made of PEEK.

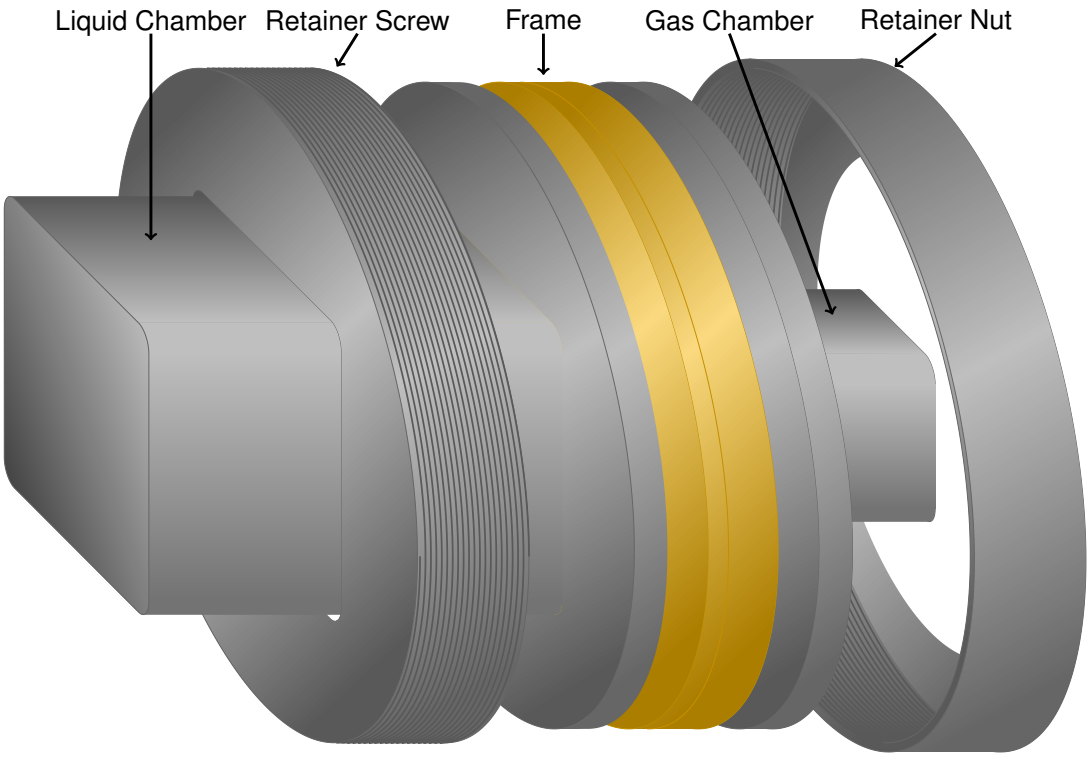

Figure 3.12: Assembly of diffusion cell: the frame is sandwiched by the two chambers fixed with retainer screw and retainer nut.

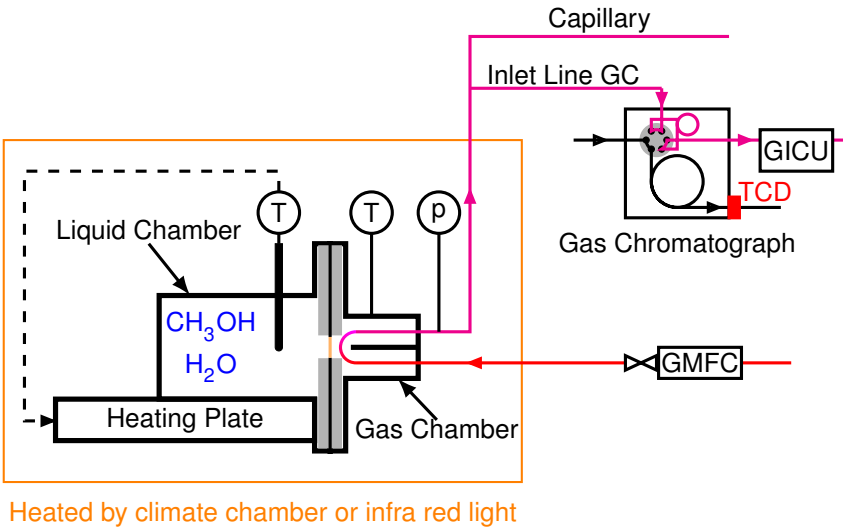

Figure 3.13: Assembly and flow chart of the diffusion setup

on a heating plate. The temperature sensor of the heating plate which is dipped in the liquid is sealed to avoid evaporation or gas dissolution. Hence, the liquid chamber is sealed except for the membrane window. The gas chamber is flushed with pure Helium 5.0. A pressure sensor and a thermocouple are installed to measure pressure and temperature in the gas chamber. Inlet and outlet pipes as well as the two sensors are also sealed to avoid loss of gas and impurities in the sample. A T-connector links the setup outlet to the inlet line of the GC to enable continuous sample-taking. After the T-connector, the gas exits to environment through a capillary of 1 mm diameter and 1 m length. The inlet line of the GC and capillary are heated with a heating cord to temperatures above 70 °C to avoid condensation.

Measurements were performed in two different sessions. In the first session, flow rate of helium was set to values up to $1\,\mathrm{l_N\,min^{-1}}$. The pressure sensor was installed at the outlet directly after the chamber connected by T-connector. The gas line of about 15 cm from setup to inlet line of GC was heated by the infra red light which was also used to heat the gas chamber of the setup. This kind of heating has no feedback control and, thus, was difficult to adjust. Therefore, the setup was put in a climate chamber for the second session instead of using infra red light. Helium flow rate was set to values between $1\,\mathrm{l_N\,min^{-1}}$ and $2\,\mathrm{l_N\,min^{-1}}$ and the pressure sensor was directly connected to the gas chamber. The distance from setup to inlet line of the GC was longer in the second session compared to the first session and, thus, was additionally heated with help of a heating cord between climate chamber and bypass to GC.

In both sessions, the setup was heated up before the measurements started. Measurements were performed for three temperatures: 40 °C, 50 °C and 60 °C. When the setup temperature reached measurement temperature, the GICU-software was started which was programmed to take several samples in sequence. For each sample, the sample loop of the GC was first flushed three times. After that, the sample was taken and the pressure in the sample loop was adjusted to 900 mbar. When pressure in sample loop was stable, the GC method was started and Valve 1 in Fig. 3.6 was switched to inject the sample. After GC method was running for 9 min, the GICU started to flush the sample loop again to prepare for the next sample. For the first flow rate that was measured after heating up, at least 7 samples were taken to make sure conditions are stable. After taking the last sample of a flow rate, the flow rate was changed to a lower value and at least 6 samples were taken for each following gas flow rate. However, only data without visible trend were taken for analysis since other data was not in steady state. Gas flow rates were varied from $0.3\,\mathrm{l_N\,min^{-1}}$ to $2\,\mathrm{l_N\,min^{-1}}$ for this analysis for each temperature.

With help of Eq. (3.28), the amount of moles in the sample loop n_α^{SL} is calculated from the peak areas of the TCD signal. Solving Eq. (3.21) for y_α provides molar fractions of water and methanol in the sample loop which are equal to the molar fractions of the gas leaving the setup. Since inlet gas flow consists of pure helium, molar fluxes of water and methanol through membrane and molar fluxes leaving the gas chamber are equal in steady state. Hence, the diffusive fluxes of water and methanol can be calculated by:

$$\dot{n}_\alpha^{\mathrm{M,diff}} = \frac{y_\alpha}{1 - y_{\mathrm{Me}} - y_{\mathrm{W}}} \frac{p_{\mathrm{N}}}{RT_{\mathrm{N}}} F_{\mathrm{in}} \tag{3.31}$$

with $\alpha \in \{\mathrm{W,Me}\}$.

However, the aim of the experimental study is to provide data for determination of coefficients for water and methanol diffusion through AEMs. According to Fick's diffusion, determination of diffusion coefficients D_α^{M} requires knowledge of the driving force F_α^{d} for diffusion across the membrane in addition to the measured diffusive fluxes:

$$\dot{n}_\alpha^{\mathrm{M,diff}} = D_\alpha^{\mathrm{M}} \zeta_\alpha F_\alpha^{\mathrm{d}} \tag{3.32}$$

With a substitution term ζ_α that contains several variables like area or density of dry membrane depending on the driving force. In case of methanol, the driving force is the concentration gradient across the membrane which combines concen-

tration in the gas chamber $c^{\mathrm{G}}_{\mathrm{Me}}$ and in the liquid camber $c^{\mathrm{L}}_{\mathrm{Me}}$. In case of water, the driving force is the gradient of membrane wetness between wetness at membrane gas interface $f^{\mathrm{M,G}}$ and at membrane liquid interface $f^{\mathrm{M,L}}$.

$$F^{\mathrm{d}}_{\mathrm{Me}} = \frac{\partial c^{\mathrm{M}}_{\mathrm{Me}}}{\partial z} \approx \frac{c^{\mathrm{G}}_{\mathrm{Me}} - c^{\mathrm{L}}_{\mathrm{Me}}}{d^{\mathrm{M}}} \tag{3.33}$$

$$F^{\mathrm{d}}_{\mathrm{W}} = \frac{\partial f^{\mathrm{M}}}{\partial z} \approx \frac{f^{\mathrm{M,G}} - f^{\mathrm{M,L}}}{d^{\mathrm{M}}} \tag{3.34}$$

Membrane wetness at liquid side is known from water uptake experiments in Section 3.3.1 and methanol concentration is $1\,\mathrm{mol\,l^{-1}}$. However, since conditions at membrane gas interface cannot be detected, methanol concentration and membrane wetness at gas side of the membrane are unknown. The common way to solve this problem is to measure the maximal possible diffusion through the membrane which corresponds to the maximum gradient across the membrane. In this case, methanol concentration and membrane wetness at gas side are assumed to be zero and the gradient can be determined. In theory, an increase in helium flow rate leads to lower methanol concentration and membrane wetness at the membrane gas interface until both are zero and the maximum gradients are reached. Further increase of helium flow rate would not change the diffusive flux through the membrane. Consequently, the gas flow rate has to be increased until diffusive flux does no longer change with gas flow rate because maximum diffusive flux was reached.

Errors of the results are calculated by error propagation. The amount of substance in the sample loop is identified with help of calibration curve. Therefore, the error of the calibration curves $\Delta n^{\mathrm{cc}}_{\alpha}$ calculated by Eq. (3.30) represents the uncertainty of the parameters $p_{\alpha,\mathrm{i}}$ of the calibration curve and is one part of the error of n^{SL}_{α}. Another error that needs to be considered is the standard deviation of the measured peak area which is propagated considering Eq. (3.28). Thus, the error of n^{SL}_{α} is calculated by:

$$\Delta n^{\mathrm{SL}}_{\alpha} = \sqrt{\Delta {n^{\mathrm{cc}}_{\alpha}}^2 + \left(\left(2p_{\alpha,1}\overline{A}_{\alpha} + p_{\alpha,2}\right)\Delta A_{\alpha}\right)^2} \tag{3.35}$$

For diffusion measurements, the error for the molar fraction in gas phase is based on Eq. (3.21) solved by y_{α}:

$$\Delta y_{\alpha} = \sqrt{\begin{array}{c}\left(\frac{RT^{\mathrm{SL}}}{p^{\mathrm{SL}}V^{\mathrm{SL}}}\Delta n^{\mathrm{SL}}_{\alpha}\right)^2 + \left(\frac{n^{\mathrm{SL}}_{\alpha}R}{p^{\mathrm{SL}}V^{\mathrm{SL}}}\Delta T^{\mathrm{SL}}\right)^2 + \left(\frac{n^{\mathrm{SL}}_{\alpha}RT^{\mathrm{SL}}}{{p^{\mathrm{SL}}}^2V^{\mathrm{SL}}}\Delta p^{\mathrm{SL}}\right)^2 + \ldots \\ \ldots + \left(\frac{n^{\mathrm{SL}}_{\alpha}RT^{\mathrm{SL}}}{p^{\mathrm{SL}}{V^{\mathrm{SL}}}^2}\Delta V^{\mathrm{SL}}\right)^2\end{array}} \tag{3.36}$$

Considering Eq. (3.31), errors for molar flux of water and methanol are calculated by:

$$\Delta n_{\mathrm{W}}^{\mathrm{diff}} = \sqrt{\begin{array}{c} \frac{((1-y_{\mathrm{Me}})\Delta y_{\mathrm{W}})^2+(y_{\mathrm{W}}\Delta y_{\mathrm{Me}})^2}{(1-y_{\mathrm{W}}-y_{\mathrm{Me}})^4}\left(\frac{p_{\mathrm{N}}F_{\mathrm{dry}}}{RT_{\mathrm{N}}}\right)^2+\ldots \\ \ldots+\left(\frac{y_{\mathrm{W}}}{1-y_{\mathrm{W}}-y_{\mathrm{Me}}}\frac{p_{\mathrm{N}}\Delta F_{\mathrm{dry}}}{RT_{\mathrm{N}}}\right)^2 \end{array}} \tag{3.37}$$

$$\Delta n_{\mathrm{Me}}^{\mathrm{diff}} = \sqrt{\begin{array}{c} \frac{((1-y_{\mathrm{W}})\Delta y_{\mathrm{Me}})^2+(y_{\mathrm{Me}}\Delta y_{\mathrm{W}})^2}{(1-y_{\mathrm{W}}-y_{\mathrm{Me}})^4}\left(\frac{p_{\mathrm{N}}F_{\mathrm{dry}}}{RT_{\mathrm{N}}}\right)^2+\ldots \\ \ldots+\left(\frac{y_{\mathrm{Me}}}{1-y_{\mathrm{W}}-y_{\mathrm{Me}}}\frac{p_{\mathrm{N}}\Delta F_{\mathrm{dry}}}{RT_{\mathrm{N}}}\right)^2 \end{array}} \tag{3.38}$$

3.4.4 Experimental Results

The diffusive fluxes of methanol and water through membrane were determined for *A201* from *Tokuyama* and of *CMM* from *CellEra*. Figure 3.14 shows that diffusive flux of water through membrane increases with temperature for both membranes. In case of A201, the expected maximum diffusive flux of water is only reached at 40 °C for flow rates up to $2\,\mathrm{l_N\,min^{-1}}$. For 50 °C and 60 °C, water flux through A201 shows a monotonous increase with increasing gas flow rate. In case of CMM, water flux shows a maximum at approximately $1.5\,\mathrm{l_N\,min^{-1}}$. The decrease of diffusive flux for high gas flow rates may arise from a dry membrane at gas side. If membrane gets too dry, mobility of water molecules can decrease and, thus, water transport is reduced. However, this cannot be ascertained without additional experiments. Methanol diffusion shows similar behaviour for both membranes as shown in Fig. 3.15. Diffusive flux of methanol increases with rising temperature as expected and in case of A201, it also increases with increasing gas flow rate while diffusive methanol flux through CMM shows a maximum. Mass transport of water and methanol from liquid side to gas side is actually a combination of three processes: diffusion through membrane, evaporation to gas phase and diffusion through a boundary layer in the gas phase. The latter follows Fick's law of diffusion with the concentration gradient as driving force. The measured increasing mass transport requires a simultaneous increase of all three processes with rising gas flow rate. Since membrane wetness and methanol concentration at liquid side are fixed, an increase of diffusion through membrane requires a decrease of membrane wetness and methanol concentration at membrane gas interface. Evaporation takes place to achieve equilibrium between membrane and gas phase at the interface. Hence, lower membrane wetness and methanol con-

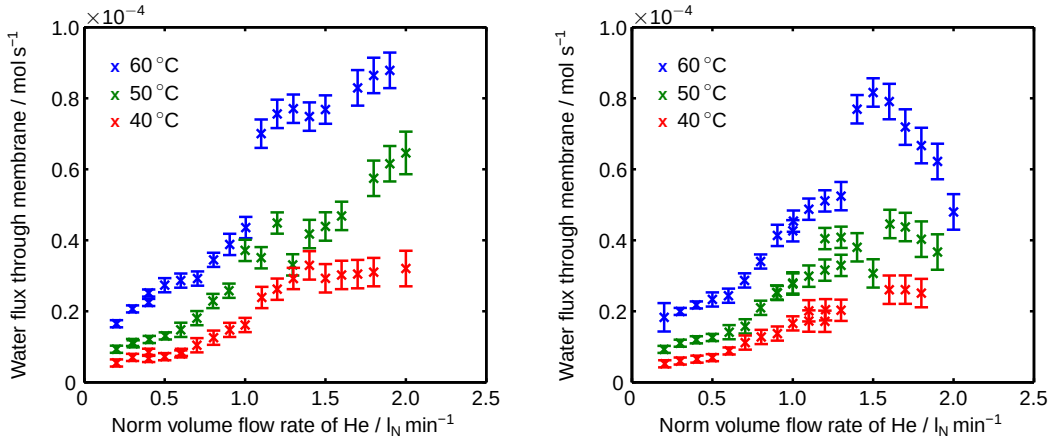

Figure 3.14: Diffusive flux of water through (a) A201 from Tokuyama and (b) CellEra's modified membrane (CMM) versus norm volume flow rate of gas.

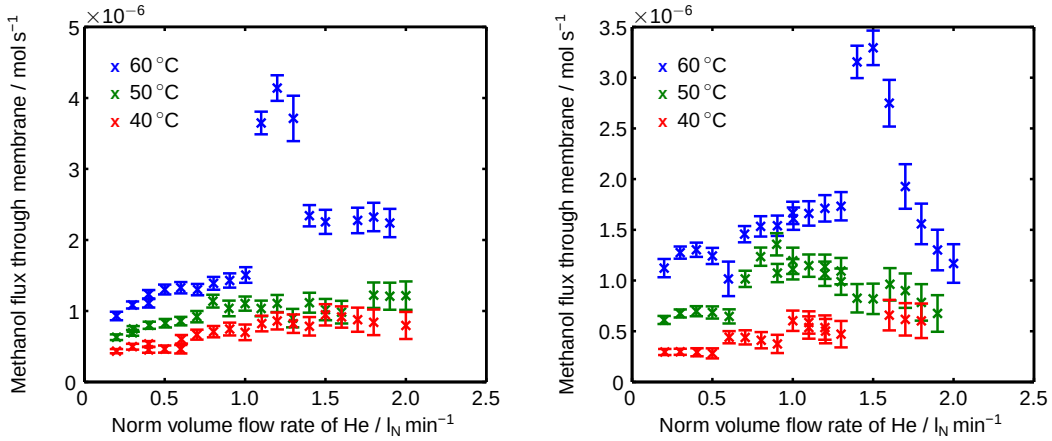

Figure 3.15: Diffusive flux of methanol through (a) A201 from Tokuyama and (b) CellEra's modified membrane (CMM) versus norm volume flow rate of gas.

centration in the membrane require lower molar fractions in the gas at membrane gas interface. Consequently, molar fraction of water and methanol in the gas chamber also need to decrease which is anyway expected due to a smaller retention time in the gas chamber. Figure 3.17 reveals that methanol molar fraction shows the expected behaviour for all flow rates and both membranes. The three data points that step out of line for each membrane are measurements that have been performed at two days (one for each membrane). Since the corresponding diffusive fluxes are also stepping out of line, it is believed that at these days some

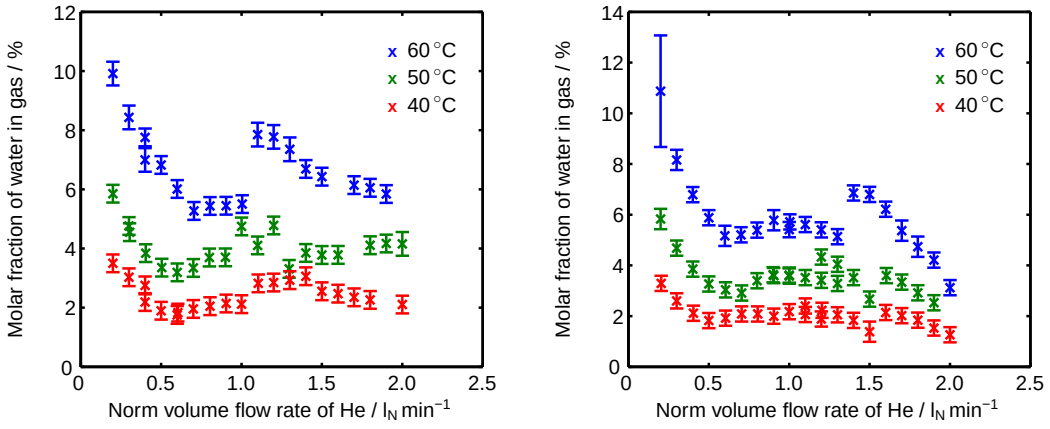

Figure 3.16: Molar fraction of water in gas phase versus norm volume flow rate of gas for (a) A201 from Tokuyama and (b) CellEra's modified membrane (CMM).

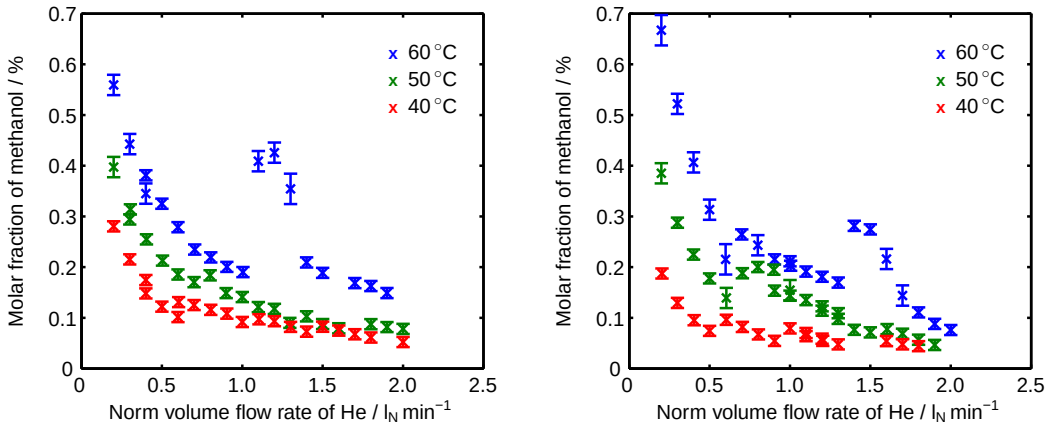

Figure 3.17: Molar fraction of methanol in gas phase versus norm volume flow rate of gas for (a) A201 from Tokuyama and (b) CellEra's modified membrane (CMM).

leakage or hole in the membrane increased the transport of water and methanol through the membrane. However, Fig. 3.16 reveals that molar fraction of water only decreases for flow rates up to $0.5\,l_N\,min^{-1}$. At higher flow rates, molar fraction of water more or less stays constant or rather increases slightly. The increase of water diffusion in spite of smaller concentration difference should be explained by a decrease of boundary layer thickness. Due to the higher gas flow rate, the boundary layer is thinner and, therefore, concentration gradient across the boundary layer increases which leads to a higher diffusive flux. This indicates

that water content of membrane at membrane gas interface cannot be decreased to zero even if the limit of water diffusion is reached unless concentration of water in gas phase is also zero and cannot be measured anymore. Hence, the simplification to assume zero methanol concentration and zero membrane wetness at membrane gas interface is not justified. Therefore, the processes in the diffusion cell are modelled in Chapter 4 in order to evaluate experimental data and determine diffusion coefficients.

CHAPTER 4

Determination of Diffusion Coefficients

The diffusive fluxes through membrane measured in the experiments described in Chapter 3 continuously increase with gas flow rate while molar fraction of water in the gas phase remains rather steady. Hence, explicit calculation of diffusion coefficients from experimental results is not possible. Therefore, the diffusion setup is modelled to determine diffusion coefficients by comparison of modelling and experimental results. Figure 4.1 displays a sketch of the setup model which is segmented into four zones: liquid chamber (L), membrane (M), diffusion layer (DL) and gas chamber (G). Bahrami and Faghri [57] already revealed that concentration profiles between anode and cathode are nonlinear. Thus, the membrane needs to be discretised in z direction. Due to the circular shape of the membrane window (see Fig. 3.11), the diffusion layer is conically hollowed out by the gas flow in the gas chamber as indicated in Fig. 4.1. As a result, concentrations not only change in z direction but also change with radius r and angle φ of the membrane window and, thus, membrane as well as diffusion layer need to be modelled in three dimensional cylindrical coordinates which makes the model quite complex. Therefore, this chapter starts with a detailed model description, followed by the determination of diffusion layer thickness. Finally, diffusion coefficients of water and methanol through membrane are determined for *Tokuyama A201* membrane which is the most established AEM for fuel cell application and is therefore intended to be used as standard for further modelling.

4.1 Model of Diffusion Cell

The diffusion cell is segmented into four different zones as shown in Fig. 4.1. Due to the large volume of the liquid chamber, methanol concentration in liquid phase stays nearly constant during measurements. The high diffusivity of methanol in water diminishes local gradients which justifies the assumption that the liquid chamber is well mixed. Hence, it is assumed that liquid chamber contains infinite amount of methanol solution with constant composition and is only

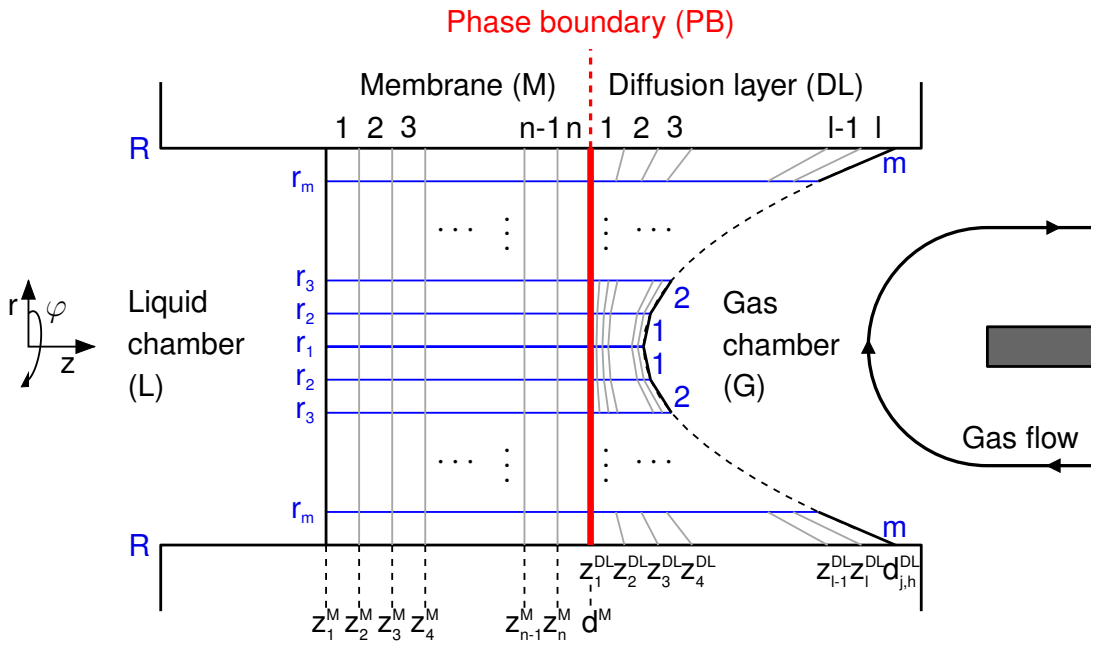

Figure 4.1: Sketch of the discretisation grid of membrane and gas diffusion layer;

considered for boundary conditions of membrane at liquid side. The other three zones (membrane, diffusion layer and gas chamber) are modelled separately and coupled only by the fluxes across the interfaces between the zones. The processes which occur in the diffusion cell are diffusion of water and methanol from liquid chamber through membrane and diffusion layer to the gas chamber and the only convective flux flows through the gas chamber. Since no reactions take place, no sources or sinks occur in any of the zones and the general mass balance in the original integral form reduces to:

$$\int_V \frac{\partial \rho_\alpha}{\partial t} \mathrm{d}V = -\int_A \left(\rho_\alpha v_k + j_{k,\alpha} M_\alpha\right) \vec{n}_k \mathrm{d}A \tag{4.1}$$

with density ρ_α and molar mass M_α of component α, velocity v_k in direction k, the diffusive flux $j_{k,\alpha}$ as well as volume integral $\int \mathrm{d}V$ and surface integral $\int \mathrm{d}A$ including the face normal $\vec{n}_k$. Focus of this chapter is to determine diffusion coefficients D_α^M of water and methanol through membrane for a modified approach of Fick's law which is suitable for water management analysis. The simplified version of Fick's law used for scenario modelling in Chapter 2, which assumes concentration gradients to be the driving force for diffusion, is neither suitable for diffusion through membrane nor for diffusion in the gas phase. For the latter, it is not suitable because that version is only valid for dilute solutions for which total density does not change. In case of water vapour diffusion through helium

gas, density cannot be considered as constant. For diffusion through membrane, the approach is not suitable since it combines liquid concentration of the liquid chamber with much lower concentrations of the gas phase. Therefore, further analysis in this thesis uses approaches for diffusive fluxes that are based on a version of Fick's law used by Jischa [58] which does not assume that total density stays constant:

$$j_{k,\alpha} = -\frac{D_\alpha \rho}{M_\alpha} \frac{\partial w_\alpha}{\partial z_k} \tag{4.2}$$

with the mass fraction of component α:

$$w_\alpha = \frac{\rho_\alpha}{\rho} \tag{4.3}$$

Pressure is assumed to be constant in the whole setup while temperatures of liquid and gas may differ slightly. However, due to the high heat conductivity of water it is assumed that temperature within the liquid chamber is constant and membrane temperature is equal to liquid temperature. Temperature of the gas phase is also assumed to be constant because of the mixing effect of the gas flow. Gas phase is assumed to follow the ideal gas law.

The model is implemented in *Matlab* using *ode15s* which can be used to solve differential algebraic equation systems (DAE-systems) but cannot solve partial differential equations (PDEs). Hence, the PDEs of the zones in which local gradients cannot be neglected are converted to ODEs by finite volume method assuming linear profiles between the volume elements. Some help variables are required for more than one location. To avoid multiple declarations, these variables are defined for a general location loc. If loc represents a zone which is discretised by finite volume method, it also contains the indices ijh of the corresponding volume element.

Geometry variables used for simulation are defined as:

$$A^{\mathrm{M}} = (R^{\mathrm{MW}})^2 \pi \tag{4.4}$$

$$V^{\mathrm{G}} = A^{\mathrm{M}} d^{\mathrm{G}} - \sum_{i,j,h} \left(0.5 \left(r^2_{j+1h} - r^2_{jh}\right) \Delta z^{\mathrm{DL}}_{jh} \Delta\varphi\right) \tag{4.5}$$

$$\Delta\varphi = \frac{2\pi}{a} \tag{4.6}$$

$$\Delta z^{\mathrm{M}} = \frac{d^{\mathrm{M}}}{n} \tag{4.7}$$

Table 4.1: Sets of parameters measured in experiments and used for simulation of diffusion setup.

$T^{\mathrm{liq}} = 40\,^{\circ}\mathrm{C}$, $f^{\mathrm{Ml}} = 49.4\,\%$						
$F_{\mathrm{in}}^{\mathrm{G}}$ / $\mathrm{l_N\,min^{-1}}$	0.5	0.8	1.0	1.2	1.5	2.0
T^{gas} / °C	40.5	40.3	43.0	38.7	38.5	38.1
p / 10^5Pa	1.197	1.404	1.467	1.086	1.121	1.179
$T^{\mathrm{liq}} = 50\,^{\circ}\mathrm{C}$, $f^{\mathrm{Ml}} = 54\,\%$						
$F_{\mathrm{in}}^{\mathrm{G}}$ / $\mathrm{l_N\,min^{-1}}$	0.5	0.8	1.0	1.2	1.5	2.0
T^{gas} / °C	50.0	50.0	48.4	48.0	46.6	47.2
p / 10^5Pa	1.270	1.320	1.075	1.096	1.140	1.200

$$\Delta r = \frac{R^{\mathrm{MW}}}{m} \tag{4.8}$$

$$\Delta z_{jh}^{\mathrm{DL}} = \frac{d_{jh}^{\mathrm{DL}}}{l} \tag{4.9}$$

where d_{jh}^{DL} is the diffusion layer thickness in the middle of the volume element after discretisation. Diffusion layer thickness is described by a function of r and φ determined in section Section 4.2. Mass of the dry membrane is constant. Assuming that membrane diameter is also constant with respect to membrane wetness, density of the dry membrane $\rho_{\mathrm{dry}}^{\mathrm{M}}$ solely changes with membrane thickness:

$$\rho_{\mathrm{dry}}^{\mathrm{M}} = \frac{\tilde{\rho}_{\mathrm{dry}}^{\mathrm{M}}}{d^{\mathrm{M}}} \tag{4.10}$$

The area density of dry membrane $\tilde{\rho}_{\mathrm{dry}}^{\mathrm{M}}$ is determined experimentally in Section 3.3. Equations for gas concentration, vapour pressure and binary diffusion coefficients in gas phase are listed in Table 2.1.

The model is simulated for the sets of parameters listed in Table 4.1. Further parameters for simulation are listed in Table 4.2. Chemical data of water and methanol as well as universal constants which are missing in this table are listed in Table 2.2.

4.1.1 Membrane

The membrane is the most important zone since diffusion coefficients through membrane are determined by this model. Area of diffusion is defined by the

Table 4.2: Parameters used for simulation of the experimental setup.

Geometry and Discretisation:					
n	=	10	m	=	9
a	=	12	l	=	10
R^{MW}	=	11.25 mm	d^{M}	=	28 µm
d^{G}	=	12 mm			
Concentrations and densities:					
$c^{\mathrm{L}}_{\mathrm{Me}}$	=	$1\,\mathrm{mol\,l^{-1}}$	$c^{\mathrm{L}}_{\mathrm{W}}$	=	$53.15\,\mathrm{mol\,l^{-1}}$
$\tilde{\rho}^{\mathrm{M}}_{\mathrm{dry}}$	=	$0.0256\,\mathrm{kg\,m^{-2}}$			

circular membrane window shown in Fig. 3.11 and the membrane is shaped as a very flat cylinder. Concentration or density of methanol and water in the membrane may change in all spatial directions and, thus, all three dimensions of membrane need to be considered. It is assumed that mass transport in the membrane is only caused by diffusion and diffusion coefficients are independent of the direction of diffusion. With help of Gauß's theorem, the mass balance Eq. (4.1) of a component in local form reads:

$$\frac{\partial \rho^{\mathrm{M}}_{\alpha}}{\partial t} = -M_{\alpha}\frac{\partial j^{\mathrm{M}}_{k,\alpha}}{\partial z_k} \tag{4.11}$$

Since the membrane separates two different phases, gradient of membrane wetness is assumed to be the driving force for water diffusion through membrane. This concept is derived from the model of Wolfgang Neubrand [59] who used gradient of water content of the membrane as driving force which is defined as the amount of moles of water based on the amount of counter ions in the membrane. In this thesis, water content is replaced by membrane wetness f^{M} which can be determined experimentally. It is defined as:

$$f^{\mathrm{M}} = \frac{m^{\mathrm{M}}_{\mathrm{wet}} - m^{\mathrm{M}}_{\mathrm{dry}}}{m^{\mathrm{M}}_{\mathrm{dry}}} = \frac{\rho^{\mathrm{M}}_{\mathrm{W}}}{\rho^{\mathrm{M}}_{\mathrm{dry}}} \tag{4.12}$$

where $m^{\mathrm{M}}_{\mathrm{wet}}$ and $m^{\mathrm{M}}_{\mathrm{dry}}$ are mass of wet and dry membrane respectively, $\rho^{\mathrm{M}}_{\mathrm{W}}$ is the density of water in the membrane zone and $\rho^{\mathrm{M}}_{\mathrm{dry}}$ is the density of the dry membrane. Total density in the membrane zone is defined as:

$$\rho^{\mathrm{M}} = \rho^{\mathrm{M}}_{\mathrm{dry}} + \rho^{\mathrm{M}}_{\mathrm{W}} + \rho^{\mathrm{M}}_{\mathrm{Me}} = (1 + f^{\mathrm{M}})\rho^{\mathrm{M}}_{\mathrm{dry}} + \rho^{\mathrm{M}}_{\mathrm{Me}} \tag{4.13}$$

Since density of methanol in the membrane is very small compared to density of water and dry membrane ($\approx 1\,\%$), methanol is neglected for calculation of water diffusion which leads to a mass fraction of:

$$w^{\mathrm{M}}_{\mathrm{W}} = \frac{\rho^{\mathrm{M}}_{\mathrm{W}}}{\rho^{\mathrm{M}}} \approx \frac{f^{\mathrm{M}}}{1 + f^{\mathrm{M}}} \tag{4.14}$$

Including this in Eq. (4.2) for water through membrane and in the mass balance Eq. (4.11) of water and considering $\rho^{\mathrm{M}}_{\mathrm{dry}} = const$ results in:

$$j^{\mathrm{M}}_{k,\mathrm{W}} = -\frac{D^{\mathrm{M}}_{\mathrm{W}}}{M_{\mathrm{W}}} \frac{\rho^{\mathrm{M}}_{\mathrm{dry}}}{1 + f^{\mathrm{M}}} \frac{\partial f^{\mathrm{M}}}{\partial z_k} \tag{4.15}$$

$$\frac{\partial f^{\mathrm{M}}}{\partial t} = \frac{\partial}{\partial z_k}\left(D^{\mathrm{M}}_{\mathrm{W}} \frac{1}{1 + f^{\mathrm{M}}} \frac{\partial f^{\mathrm{M}}}{\partial z_k} \right) \tag{4.16}$$

Methanol is diluted compared to water. Therefore, methanol diffusion is commonly described by the simplified version of Fick's law using concentration gradient as driving force. In this thesis, methanol diffusion is also described by Eq. (4.2) considering all three components (methanol, water and dry membrane) for calculation of the total density:

$$j^{\mathrm{M}}_{k,\mathrm{Me}} = -\frac{D^{\mathrm{M}}_{\mathrm{Me}}}{M_{\mathrm{Me}}} \frac{\rho^{\mathrm{M}}_{\mathrm{dry}}}{\rho^{\mathrm{M}}} \left((1 + f^{\mathrm{M}}) \frac{\partial \rho^{\mathrm{M}}_{\mathrm{Me}}}{\partial z_k} - \rho^{\mathrm{M}}_{\mathrm{Me}} \frac{\partial f^{\mathrm{M}}}{\partial z_k} \right) \tag{4.17}$$

Since density of methanol can be converted to methanol concentration by dividing through molar mass M_{Me}, the mass balance Eq. (4.11) in the membrane is transferred to a differential equation for methanol concentration in the membrane based on volume of the membrane:

$$\frac{\partial c^{\mathrm{M}}_{\mathrm{Me}}}{\partial t} = \frac{\partial}{\partial z_k}\left(D^{\mathrm{M}}_{\mathrm{Me}} \frac{\rho^{\mathrm{M}}_{\mathrm{dry}}}{\rho^{\mathrm{M}}} \left((1 + f^{\mathrm{M}}) \frac{\partial c^{\mathrm{M}}_{\mathrm{Me}}}{\partial z_k} - c^{\mathrm{M}}_{\mathrm{Me}} \frac{\partial f^{\mathrm{M}}}{\partial z_k} \right) \right) \tag{4.18}$$

Transformation of Eqs. (4.16) and (4.18) to cylindrical coordinates as described in Appendix A.3 results in:

$$\begin{aligned}\frac{\partial f^{\mathrm{M}}}{\partial t} =& D_{\mathrm{W}}^{\mathrm{M}} \left(\frac{\partial}{\partial z} \left(\frac{1}{1+f^{\mathrm{M}}} \frac{\partial f^{\mathrm{M}}}{\partial z} \right) + \frac{1}{r} \frac{\partial}{\partial r} \left(\frac{r}{1+f^{\mathrm{M}}} \frac{\partial f^{\mathrm{M}}}{\partial r} \right) \ldots \right. \\ & \left. \ldots + \frac{1}{r^2} \frac{\partial}{\partial \varphi} \left(\frac{1}{1+f^{\mathrm{M}}} \frac{\partial f^{\mathrm{M}}}{\partial \varphi} \right) \right) \end{aligned} \tag{4.19}$$

$$\begin{aligned}\frac{\partial c_{\mathrm{Me}}^{\mathrm{M}}}{\partial t} =& D_{\mathrm{Me}}^{\mathrm{M}} \left[\frac{\partial}{\partial z} \left(\frac{\rho_{\mathrm{dry}}^{\mathrm{M}}}{\rho^{\mathrm{M}}} \left((1+f^{\mathrm{M}}) \frac{\partial c_{\mathrm{Me}}^{\mathrm{M}}}{\partial z^{\mathrm{M}}} - c_{\mathrm{Me}}^{\mathrm{M}} \frac{\partial f^{\mathrm{M}}}{\partial z^{\mathrm{M}}} \right) \right) \ldots \right. \\ & \ldots + \frac{1}{r} \frac{\partial}{\partial r} \left(r \frac{\rho_{\mathrm{dry}}^{\mathrm{M}}}{\rho^{\mathrm{M}}} \left((1+f^{\mathrm{M}}) \frac{\partial c_{\mathrm{Me}}^{\mathrm{M}}}{\partial r} - c_{\mathrm{Me}}^{\mathrm{M}} \frac{\partial f^{\mathrm{M}}}{\partial r} \right) \right) \ldots \\ & \left. \ldots + \frac{1}{r^2} \frac{\partial}{\partial \varphi} \left(\frac{\rho_{\mathrm{dry}}^{\mathrm{M}}}{\rho^{\mathrm{M}}} \left((1+f^{\mathrm{M}}) \frac{\partial c_{\mathrm{Me}}^{\mathrm{M}}}{\partial \varphi} - c_{\mathrm{Me}}^{\mathrm{M}} \frac{\partial f^{\mathrm{M}}}{\partial \varphi} \right) \right) \right] \end{aligned} \tag{4.20}$$

with the same boundary conditions for both states in the membrane $x^{\mathrm{M}} \in \{f^{\mathrm{M}}, c_{\mathrm{Me}}^{\mathrm{M}}\}$:

$$x^{\mathrm{M}}\big|_{z=0} = x^{\mathrm{Ml}} \tag{4.21}$$

$$x^{\mathrm{M}}\big|_{z=d^{\mathrm{M}}} = x^{\mathrm{Mg}} \tag{4.22}$$

$$\left.\frac{\partial x^{\mathrm{M}}}{\partial r}\right|_{r=0} = \left.\frac{\partial x^{\mathrm{M}}}{\partial r}\right|_{r=R^{\mathrm{MW}}} = 0 \tag{4.23}$$

$$\left.\frac{\partial x^{\mathrm{M}}}{\partial \varphi}\right|_{\varphi=0} = \left.\frac{\partial x^{\mathrm{M}}}{\partial \varphi}\right|_{\varphi=2\pi} \tag{4.24}$$

$$\left.\frac{\partial x^{\mathrm{M}}}{\partial \varphi}\right|_{r=0} = 0 \tag{4.25}$$

with membrane thickness d^{M} and radius R^{MW} of membrane window. x^{Ml} and x^{Mg} denote values of state variable x in the membrane in equilibrium with liquid phase or gas phase, respectively. Since volume elements in the centre of the membrane with radius $r < \Delta r$ are very small, change of concentration with angle φ is insignificant in these elements and Eq. (4.25) is assumed to be valid for all volume elements in membrane centre. Discretisation of Eqs. (4.19) and (4.20) results in:

$$\frac{\partial f_{ijh}^{\mathrm{M}}}{\partial t} = 2 D_{\mathrm{W}}^{\mathrm{M}} \left(I_{\mathrm{W},ijh}^{\mathrm{M,a}} - I_{\mathrm{W},ijh}^{\mathrm{M,b}} + I_{\mathrm{W},ijh}^{\mathrm{M,c}} - I_{\mathrm{W},ijh}^{\mathrm{M,d}} + I_{\mathrm{W},ijh}^{\mathrm{M,e}} - I_{\mathrm{W},ijh}^{\mathrm{M,f}} \right) \tag{4.26}$$

$$\frac{\partial c_{\mathrm{Me},ijh}^{\mathrm{M}}}{\partial t} = 2 D_{\mathrm{Me}}^{\mathrm{M}} \rho_{\mathrm{dry}}^{\mathrm{M}} \left(I_{\mathrm{Me},ijh}^{\mathrm{M,a}} - I_{\mathrm{Me},ijh}^{\mathrm{M,b}} + I_{\mathrm{Me},ijh}^{\mathrm{M,c}} - I_{\mathrm{Me},ijh}^{\mathrm{M,d}} + I_{\mathrm{Me},ijh}^{\mathrm{M,e}} - I_{\mathrm{Me},ijh}^{\mathrm{M,f}} \right) \tag{4.27}$$

$I^{\mathrm{M,a\text{-}f}}_{\alpha,\,ijh}$ are introduced in order to reduce size of the above equations. They are defined in Appendix A.2. Indices i, j, h represent the volume element number in z, r, φ direction respectively.

4.1.2 Diffusion Layer

The diffusion layer is modelled as a separate zone but it is actually part of the gas chamber. The convective flux through the gas chamber flows towards the membrane and is redirected when hitting the membrane to leave the chamber in the opposite direction. This causes a boundary layer of inhomogeneous thickness between membrane and gas phase as indicated in Fig. 4.1 and requires a three dimensional model. In the diffusion layer, diffusive transport dominates convective transport which is neglected. The gas mainly consists of helium and molar fractions of water and methanol vapour are below 10 %. Therefore, diffusive fluxes are described by Eq. (4.2) using binary diffusion coefficients of water in helium and methanol in helium which are available in literature. Due to the large molar mass of water ($18\,\mathrm{g\,mol^{-1}}$) and methanol ($32\,\mathrm{g\,mol^{-1}}$) compared to molar mass of helium ($4\,\mathrm{g\,mol^{-1}}$), even small molar fractions of water or methanol have a significant impact on total density. Hence, total density of gas is not constant which results in the following modification of Eq. (4.2):

$$j^{\mathrm{DL}}_{k,\,\alpha} = -D^{\mathrm{DL}}_{\alpha}\left(\frac{\partial c^{\mathrm{DL}}_{\alpha}}{\partial z_k} - \frac{c^{\mathrm{DL}}_{\alpha}}{\rho^{\mathrm{DL}}}\frac{\partial \rho^{\mathrm{DL}}}{\partial z_k}\right) \tag{4.28}$$

For the entire gas phase in the diffusion cell it holds that:

$$\rho^{\mathrm{loc}} = \rho^{\mathrm{loc}}_{\mathrm{Me}} + \rho^{\mathrm{loc}}_{\mathrm{W}} + \rho^{\mathrm{loc}}_{\mathrm{He}} = M^{\mathrm{loc}}_{\mathrm{gas}} c^{\mathrm{loc}}_{\mathrm{gas}} \tag{4.29}$$

$$M^{\mathrm{loc}}_{\mathrm{gas}} = M_{\mathrm{Me}} y^{\mathrm{loc}}_{\mathrm{Me}} + M_{\mathrm{W}} y^{\mathrm{loc}}_{\mathrm{W}} + M_{\mathrm{He}}\left(1 - y^{\mathrm{loc}}_{\mathrm{Me}} - y^{\mathrm{loc}}_{\mathrm{W}}\right) \tag{4.30}$$

Combining these equations results in:

$$j^{\mathrm{DL}}_{k,\,\alpha} = -D^{\mathrm{DL}}_{\alpha}\left(\frac{M_{\mathrm{He}} + \left(M_{\beta} - M_{\mathrm{He}}\right) y^{\mathrm{DL}}_{\beta}}{M^{\mathrm{DL}}_{\mathrm{gas}}}\frac{\partial c^{\mathrm{DL}}_{\alpha}}{\partial z_k} - \frac{\left(M_{\beta} - M_{\mathrm{He}}\right) y^{\mathrm{DL}}_{\alpha}}{M^{\mathrm{DL}}_{\mathrm{gas}}}\frac{\partial c^{\mathrm{DL}}_{\beta}}{\partial z_k}\right) \tag{4.31}$$

$$= -D^{\mathrm{DL}}_{\alpha}\left(B^{\mathrm{DL}}_{\beta}\frac{\partial c^{\mathrm{DL}}_{\alpha}}{\partial z_k} - B^{\mathrm{DL}}_{\alpha}\frac{\partial c^{\mathrm{DL}}_{\beta}}{\partial z_k}\right) \tag{4.32}$$

for $\alpha \neq \beta \in \{\mathrm{W}, \mathrm{Me}\}$. The substitutions B_β^{DL} and B_α^{DL} are introduced to reduce equation sizes in the following. Transformation of Eq. (4.32) to cylinder coordinates results in:

$$j_{1,\alpha} = -D_\alpha^{\mathrm{DL}} \left(B_\beta^{\mathrm{DL}} \frac{\partial c_\alpha^{\mathrm{DL}}}{\partial z} - B_\alpha^{\mathrm{DL}} \frac{\partial c_\beta^{\mathrm{DL}}}{\partial z} \right) \tag{4.33}$$

$$\begin{aligned} j_{2,\alpha} = -D_\alpha^{\mathrm{DL}} \Bigg(& \cos\varphi \left(B_\beta^{\mathrm{DL}} \frac{\partial c_\alpha^{\mathrm{DL}}}{\partial r} - B_\alpha^{\mathrm{DL}} \frac{\partial c_\beta^{\mathrm{DL}}}{\partial r} \right) \ldots \\ & \ldots - \frac{\sin\varphi}{r} \left(B_\beta^{\mathrm{DL}} \frac{\partial c_\alpha^{\mathrm{DL}}}{\partial \varphi} - B_\alpha^{\mathrm{DL}} \frac{\partial c_\beta^{\mathrm{DL}}}{\partial \varphi} \right) \Bigg) \end{aligned} \tag{4.34}$$

$$\begin{aligned} j_{3,\alpha} = -D_\alpha^{\mathrm{DL}} \Bigg(& \sin\varphi \left(B_\beta^{\mathrm{DL}} \frac{\partial c_\alpha^{\mathrm{DL}}}{\partial r} - B_\alpha^{\mathrm{DL}} \frac{\partial c_\beta^{\mathrm{DL}}}{\partial r} \right) \ldots \\ & \ldots + \frac{\cos\varphi}{r} \left(B_\beta^{\mathrm{DL}} \frac{\partial c_\alpha^{\mathrm{DL}}}{\partial \varphi} - B_\alpha^{\mathrm{DL}} \frac{\partial c_\beta^{\mathrm{DL}}}{\partial \varphi} \right) \Bigg) \end{aligned} \tag{4.35}$$

The resulting PDE-system is discretised by finite volume method. Although diffusion layer thickness (z direction) changes with r and φ, the number of volume elements in z direction is set constant. As a consequence, the thickness of the volume elements, Δz^{DL}, and with it the surfaces of the volume elements vary with r and φ. Therefore, the surface of a volume element is segmented in six surface areas $A_{\mathrm{s}}^{\mathrm{DL}}$ at $z_i, z_{i+1}, r_j, r_{j+1}, \varphi_h, \varphi_{h+1}$. Replacing the surface integral in Eq. (4.1) by a sum of six surface integrals – one for each surface segment – provides the molar balance for a volume element:

$$\int_{V_{\mathrm{VE}}^{\mathrm{DL}}} \frac{\partial c_\alpha^{\mathrm{DL}}}{\partial t} \mathrm{d}V = - \int_{A_{\mathrm{VE}}^{\mathrm{DL}}} \frac{\partial j_{k,\alpha}^{\mathrm{DL}}}{\partial z_k} n_k \mathrm{d}A = - \sum_{\mathrm{s}} \int_{A_{\mathrm{s}}^{\mathrm{DL}}} \frac{\partial j_{k,\alpha}^{\mathrm{DL}}}{\partial z_k} n_{\mathrm{s},k} \mathrm{d}A \tag{4.36}$$

With the surface normals:

$$\vec{n}|_{z_{i+1}} = -\vec{n}|_{z_i} = \begin{pmatrix} 1 & 0 & 0 \end{pmatrix}^{\mathrm{T}} \tag{4.37}$$

$$\vec{n}|_{r_{j+1}} = -\vec{n}|_{r_j} = \begin{pmatrix} 0 & \cos\varphi & \sin\varphi \end{pmatrix}^{\mathrm{T}} \tag{4.38}$$

$$\vec{n}|_{\varphi_{h+1}} = -\vec{n}|_{\varphi_h} = \begin{pmatrix} 0 & -\sin\varphi & \cos\varphi \end{pmatrix}^{\mathrm{T}} \tag{4.39}$$

Eq. (4.36) results in:

$$\begin{aligned}\int \frac{\partial c_\alpha^{\mathrm{DL}}}{\partial t}\mathrm{d}V = &\left[\left[\int_{\varphi_h}^{\varphi_{h+1}}\int_{r_j}^{r_{j+1}}\left(B_\beta^{\mathrm{DL}}\frac{\partial c_\alpha^{\mathrm{DL}}}{\partial z} - B_\alpha^{\mathrm{DL}}\frac{\partial c_\beta^{\mathrm{DL}}}{\partial z}\right) r\,\mathrm{d}r\mathrm{d}\varphi\right]_{z_i}^{z_{i+1}} \ldots\right. \\ &\ldots + \left[\int_{\varphi_h}^{\varphi_{h+1}}\int_{z_i}^{z_{i+1}}\left(B_\beta^{\mathrm{DL}}\frac{\partial c_\alpha^{\mathrm{DL}}}{\partial r} - B_\alpha^{\mathrm{DL}}\frac{\partial c_\beta^{\mathrm{DL}}}{\partial r}\right) r\,\mathrm{d}z\mathrm{d}\varphi\right]_{r_j}^{r_{j+1}} \ldots \\ &\left.\ldots + \left[\int_{r_j}^{r_{j+1}}\int_{z_i}^{z_{i+1}}\left(B_\beta^{\mathrm{DL}}\frac{\partial c_\alpha^{\mathrm{DL}}}{\partial \varphi} - B_\alpha^{\mathrm{DL}}\frac{\partial c_\beta^{\mathrm{DL}}}{\partial \varphi}\right)\frac{1}{r}\,\mathrm{d}z\mathrm{d}r\right]_{\varphi_h}^{\varphi_{h+1}}\right] \cdot D_\alpha^{\mathrm{DL}} \end{aligned} \tag{4.40}$$

A detailed derivation of Eq. (4.40) is given in Appendix A.3.

Boundary conditions for this zone are similar to those for membrane:

$$c_\alpha^{\mathrm{DL}}\big|_{z^{\mathrm{DL}}=0} = c_\alpha^{\mathrm{PB}} \tag{4.41}$$

$$c_\alpha^{\mathrm{DL}}\big|_{z^{\mathrm{DL}}=d^{\mathrm{DL}}} = c_\alpha^{\mathrm{G}} \tag{4.42}$$

$$\left.\frac{\partial c_\alpha^{\mathrm{DL}}}{\partial r}\right|_{r=0} = \left.\frac{\partial c_\alpha^{\mathrm{DL}}}{\partial r}\right|_{r=R^{\mathrm{MW}}} = 0 \tag{4.43}$$

$$\left.\frac{\partial c_\alpha^{\mathrm{DL}}}{\partial \varphi}\right|_{\varphi=0} = \left.\frac{\partial c_\alpha^{\mathrm{DL}}}{\partial \varphi}\right|_{\varphi=2\pi} \tag{4.44}$$

$$\left.\frac{\partial c_\alpha^{\mathrm{DL}}}{\partial \varphi}\right|_{r=0} = 0 \tag{4.45}$$

d^{DL} is the thickness of diffusion layer, c_α^{PB} is the gas concentration at the phase boundary between membrane and gas phase and c^{G} denotes concentration in the gas chamber. After discretisation Eq. (4.45) is assumed to be true for all volume elements in the centre with radius $r < \Delta r$. Integration of Eq. (4.40) leads to:

$$\frac{\mathrm{d}c_\alpha^{\mathrm{DL}}}{\mathrm{d}t} = D_\alpha^{\mathrm{DL}}\left(I_{\alpha,ijh}^{\mathrm{a}} - I_{\alpha,ijh}^{\mathrm{b}} + \frac{2}{r_{j+1}^2 - r_j^2}\left(\frac{I_{\alpha,ijh}^{\mathrm{c}} - I_{\alpha,ijh}^{\mathrm{d}}}{\Delta r\ \Delta z_{jh}^{\mathrm{DL}}} + \frac{I_{\alpha,ijh}^{\mathrm{e}} - I_{\alpha,ijh}^{\mathrm{f}}}{\Delta\varphi^2\ \Delta z_{jh}^{\mathrm{DL}}}\right)\right) \tag{4.46}$$

$I^{\text{a-f}}_{\alpha,ijh}$ are specified in Appendix A.2. Since linear profiles are assumed between the volume elements, concentration c^{DL}_{α} at the boundary between two elements are approximated by the mean values of molar fractions in the two elements.

$$c^{\text{DL}}_{\alpha jh}\big|_i = \frac{c^{\text{DL}}_{\alpha,ijh} + c^{\text{DL}}_{\alpha,i-1jh}}{2} \tag{4.47}$$

$$c^{\text{DL}}_{\alpha ih}\big|_j = \frac{c^{\text{DL}}_{\alpha,ijh} + c^{\text{DL}}_{\alpha,ij-1h}}{2} \tag{4.48}$$

$$c^{\text{DL}}_{\alpha ij}\big|_h = \frac{c^{\text{DL}}_{\alpha,ijh} + c^{\text{DL}}_{\alpha,ijh-1}}{2} \tag{4.49}$$

Boundary conditions are considered for boundary elements.

4.1.3 Phase Boundaries

The model is analysed in steady state conditions. Therefore, it is assumed that membrane is always in equilibrium with gas or liquid phase at the corresponding interface. Only exception to this is the case that membrane wetness at membrane gas interface is higher than the equilibrium wetness for water saturated gas. This exception is explained in more detail below (see Eq. (4.56)).

Conditions in liquid chamber are assumed to remain constant during operation. Consequently, equilibrium values of membrane wetness and methanol concentration in membrane at this phase boundary are also constant. Due to the low molar fraction of methanol in the liquid chamber ($< 2\,\%$), presence of methanol is assumed to have negligible influence on the equilibrium between liquid water and membrane wetness. Thus, membrane wetness at membrane liquid interface is equal to equilibrium wetness f^{Ml} that has been determined by water uptake measurements described in Section 3.3. The values are listed in Table 3.3.

Assuming that affinity of membrane to take up methanol is similar to affinity to take up water, ratio between methanol and water concentration in the membrane at membrane liquid interface is equal to the ratio in the liquid chamber:

$$\frac{c^{\text{Ml}}_{\text{Me}}}{\frac{f^{\text{Ml}}\rho^{\text{M}}_{\text{dry}}}{M_{\text{W}}}} = \frac{c^{\text{L}}_{\text{Me}}}{c^{\text{L}}_{\text{W}}} \tag{4.50}$$

Solving this equation for methanol concentration in the membrane results in:

$$c^{\text{Ml}}_{\text{Me}} = \frac{c^{\text{L}}_{\text{Me}}}{c^{\text{L}}_{\text{W}}} \frac{f^{\text{Ml}}\rho^{\text{M}}_{\text{dry}}}{M_{\text{W}}} \tag{4.51}$$

Membrane is believed to be a solid polymer structure that forms pores which are filled with the liquid components water and methanol that are taken up by the membrane. Hence, equilibrium between methanol in membrane and gas phase at the phase boundary (PB) is assumed to follow Raoult and Dalton:

$$y_{\mathrm{Me}}^{\mathrm{PB}} = X_{\mathrm{Me}}^{\mathrm{Mg}} \frac{p_{\mathrm{Me}}^{\mathrm{o}}(T^{\mathrm{gas}})}{p} \quad \Rightarrow \quad c_{\mathrm{Me}}^{\mathrm{PB}} = X_{\mathrm{Me}}^{\mathrm{Mg}} \frac{p_{\mathrm{Me}}^{\mathrm{o}}(T^{\mathrm{gas}})}{p} c_{\mathrm{gas}} \tag{4.52}$$

where $X_{\mathrm{Me}}^{\mathrm{Mg}}$ is the molar fraction of methanol based on liquid components water and methanol:

$$X_{\mathrm{Me}}^{\mathrm{Mg}} = \frac{c_{\mathrm{Me}}^{\mathrm{Mg}}}{c_{\mathrm{Me}}^{\mathrm{Mg}} + \frac{\rho_{\mathrm{dry}} f^{\mathrm{Mg}}}{M_{\mathrm{W}}}} \tag{4.53}$$

Similar to the other phase boundary, equilibrium of water at the membrane gas interface was measured in water uptake experiments presented in Section 3.3. The determined correlation of membrane wetness f^{Mg} and molar fraction of water vapour $y_{\mathrm{W},jh}^{\mathrm{DL,eq}}$ at phase boundary between membrane and gas is described by Eq. (3.16) and is solved for the molar fraction of water:

$$y_{\mathrm{W},jh}^{\mathrm{DL,eq}} = \frac{-p_2 \pm \sqrt{p_2^2 - 4p_1(p_3 - f_{jh}^{\mathrm{Mg}})}}{2p_1} \tag{4.54}$$

p_1, p_2 and p_3 are functions of temperature and described by Eq. (3.17). Parameters of this function are listed in Table 3.4. These parameters are only valid if membrane wetness is in equilibrium with the gas phase. Since membrane is equilibrating with liquid at one side, f^{Mg} may rise above equilibrium with water saturated gas. In this case, Eq. (4.54) would lead to humidities above 100 % which is not feasible. However, evaporation only takes place up to 100 % humidity. This is implemented by limiting $y_{\mathrm{W},jh}^{\mathrm{DL,eq}}$ to the maximum molar fraction of water saturated gas:

$$y_{\mathrm{W}}^{\mathrm{max}} = \frac{p_{\mathrm{W}}^{\mathrm{o}}(T)}{p} \tag{4.55}$$

$$y_{\mathrm{W},jh}^{\mathrm{PB}} = \min\left(y_{\mathrm{W},jh}^{\mathrm{DL,eq}}, y_{\mathrm{W}}^{\mathrm{max}}\right) \tag{4.56}$$

As long as f^{Mg} stays below equilibrium value at membrane liquid interface f^{Ml}, there is no driving force to release liquid water at membrane gas interface. Since diffusion will stop in case that $f^{\mathrm{Mg}} = f^{\mathrm{Ml}}$, water diffusion will never cause flooding at the gas side.

The corresponding values of water and methanol content in the membrane at this phase boundary are determined assuming that phase boundary has no volume and, thus, diffusion through membrane to phase boundary needs to be equal to diffusion through diffusion layer from phase boundary.

$$j^{\mathrm{M}}_{\alpha,\,jh}\Big|_{z^{\mathrm{M}}=d^{\mathrm{M}}} = j^{\mathrm{DL}}_{\alpha,\,jh}\Big|_{z^{\mathrm{DL}}=0} \tag{4.57}$$

Inserting Eq. (4.33) and Eq. (4.17) or Eq. (4.15), respectively, and approximating concentration gradients at the phase boundary as:

$$\left.\frac{\partial c^{\mathrm{DL}}_{\alpha}}{\partial z}\right|_{z^{\mathrm{DL}}=0} \approx \frac{c^{\mathrm{DL}}_{\alpha,\,1jh} - c^{\mathrm{PB}}_{\alpha,\,jh}}{\frac{\Delta z^{\mathrm{DL}}_{jh}}{2}} \tag{4.58}$$

$$\left.\frac{\partial c^{\mathrm{M}}_{\mathrm{Me}}}{\partial z}\right|_{z^{\mathrm{M}}=d^{\mathrm{M}}} \approx \frac{c^{\mathrm{Mg}}_{\mathrm{Me},\,jh} - c^{\mathrm{M}}_{\mathrm{Me},\,njh}}{\frac{\Delta z^{\mathrm{M}}}{2}} \tag{4.59}$$

$$\left.\frac{\partial f^{\mathrm{M}}}{\partial z}\right|_{z^{\mathrm{M}}=d^{\mathrm{M}}} \approx \frac{f^{\mathrm{Mg}}_{jh} - f^{\mathrm{M}}_{njh}}{\frac{\Delta z^{\mathrm{M}}}{2}} \tag{4.60}$$

results in:

$$\begin{aligned} 0 =& \frac{D^{\mathrm{DL}}_{\mathrm{Me}}}{M^{\mathrm{PB}}_{\mathrm{gas},\,jh}} \left(M_{\mathrm{He}} \frac{c^{\mathrm{DL}}_{\mathrm{Me},\,1jh} - c^{\mathrm{PB}}_{\mathrm{Me},\,jh}}{\frac{\Delta z^{\mathrm{DL}}_{jh}}{2}} + (M_{\mathrm{W}} - M_{\mathrm{He}}) \frac{c^{\mathrm{PB}}_{\mathrm{W},\,jh} c^{\mathrm{DL}}_{\mathrm{Me},\,1jh} - c^{\mathrm{PB}}_{\mathrm{Me},\,jh} c^{\mathrm{DL}}_{\mathrm{W},\,1jh}}{c_{\mathrm{gas}} \frac{\Delta z^{\mathrm{DL}}_{jh}}{2}} \right) ... \\ & ... - D^{\mathrm{M}}_{\mathrm{Me}} \frac{\rho^{\mathrm{M}}_{\mathrm{dry}}}{\rho^{\mathrm{Mg}}_{jh}} \frac{\left(1 + f^{\mathrm{M}}_{njh}\right) c^{\mathrm{Mg}}_{\mathrm{Me},\,jh} - \left(1 + f^{\mathrm{Mg}}_{jh}\right) c^{\mathrm{M}}_{\mathrm{Me},\,njh}}{\frac{\Delta z^{\mathrm{M}}}{2}} \end{aligned} \tag{4.61}$$

$$\begin{aligned} 0 =& \frac{D^{\mathrm{DL}}_{\mathrm{W}}}{M^{\mathrm{PB}}_{\mathrm{gas},\,jh} \frac{\Delta z^{\mathrm{DL}}_{jh}}{2}} \left(M_{\mathrm{He}} \left(c^{\mathrm{DL}}_{\mathrm{W},\,1jh} - c^{\mathrm{PB}}_{\mathrm{W},\,jh} \right) + (M_{\mathrm{Me}} - M_{\mathrm{He}}) \left(y^{\mathrm{PB}}_{\mathrm{Me},\,jh} c^{\mathrm{DL}}_{\mathrm{W},\,1jh} - y^{\mathrm{PB}}_{\mathrm{W},\,jh} c^{\mathrm{DL}}_{\mathrm{Me},\,1jh} \right) \right) ... \\ & ... - \frac{D^{\mathrm{M}}_{\mathrm{W}}}{M_{\mathrm{W}}} \frac{\rho^{\mathrm{M}}_{\mathrm{dry}}}{1 + f^{\mathrm{Mg}}_{jh}} \frac{f^{\mathrm{Mg}}_{jh} - f^{\mathrm{M}}_{njh}}{\frac{\Delta z^{\mathrm{M}}}{2}} \end{aligned} \tag{4.62}$$

Both equations yield nonlinear equations that are solved for $c^{\mathrm{Mg}}_{\mathrm{Me},\,jh}$ and f^{Mg}_{jh} respectively.

4.1.4 Convective Domain and Geometry Definitions

The gas chamber is the only zone with convective transport. This zone includes the part of the gas chamber in which convection dominates diffusion, i.e. modelled gas chamber excluding diffusion layer. It is assumed that convection leads to an ideal mixing of components in the gas chamber which is modelled as a CSTR.

Since pure helium is fed to the gas chamber, mass balances in the gas chamber reduce to:

$$\frac{\mathrm{d}c_{\alpha}^{\mathrm{G}}}{\mathrm{d}t} = \frac{\dot{n}_{\alpha}^{\mathrm{diff}} - F_{\mathrm{out}}^{\mathrm{G}} c_{\alpha}^{\mathrm{G}}}{V^{\mathrm{G}}} \tag{4.63}$$

with $\alpha \in \{\mathrm{W}, \mathrm{Me}\}$ and

$$\begin{aligned}\dot{n}_{\alpha}^{\mathrm{diff}} = \sum_{j} \sum_{h} -D_{\alpha}^{\mathrm{DL}} \Bigg(& \frac{M_{\mathrm{He}} + (M_{\beta} - M_{\mathrm{He}})\, y_{\beta,\,jh}^{\mathrm{G}}}{M_{\mathrm{gas}}^{\mathrm{G}}\, \Delta z_{jh}^{\mathrm{DL}}} \left(c_{\alpha}^{\mathrm{G}} - c_{\alpha,\,ljh}^{\mathrm{DL}}\right) \ldots \\ & \ldots - \frac{(M_{\beta} - M_{\mathrm{He}})\, y_{\alpha,\,jh}^{\mathrm{G}}}{M_{\mathrm{gas}}^{\mathrm{G}}\, \Delta z_{jh}^{\mathrm{DL}}} \left(c_{\beta}^{\mathrm{G}} - c_{\beta,\,ljh}^{\mathrm{DL}}\right) \Bigg) \left(r_{j+1h}^{2} - r_{jh}^{2}\right) \Delta\varphi \end{aligned} \tag{4.64}$$

and $\alpha \neq \beta$. The volume flow rate exiting gas chamber is calculated according to Eq. (2.23):

$$F_{\mathrm{out}}^{\mathrm{G}} = F_{\mathrm{in}}^{\mathrm{G}} + \frac{\dot{n}_{\mathrm{Me}}^{\mathrm{diff}} + \dot{n}_{\mathrm{W}}^{\mathrm{diff}}}{c_{\mathrm{gas}}} \tag{4.65}$$

4.2 Identification of Diffusion Layer Thickness

As mentioned above, the diffusion layer in this model is the boundary layer between convective flux and membrane and is therefore shaped by the gas flow through the gas chamber. Since temperature dependency of convective flux is insignificant in the investigated range of temperature (40 °C to 50 °C), diffusion layer is assumed to be independent of temperature as well. However, boundary layer thickness decreases with increasing gas flow rate and is therefore determined for all flow rates used for simulation which are listed in Table 4.1.

Among other things, thickness and shape of boundary layer between solid phase and gas stream depend on geometry of the solid phase. For several standard geometries, e.g. a plane plate, boundary layer thickness is specified in literature. However, these definitions cannot be applied to the boundary layer in the diffusion cell since geometry of the gas chamber is non standard. The model of the diffusion cell assumes that no convection occurs in the diffusion layer and no diffusion occurs in the convective domain. This assumption is based on the film theory by Whitman [60] which assumes a stagnant film without convection between a well mixed bulk fluid and the phase boundary. Steady state concentration profile across the stagnant film is assumed to be linear. The slope of this linear profile is equal to the slope at the wall ($s = 0$). Therefore, the effective boundary layer thickness is defined as the distance from the phase boundary at which the tangent

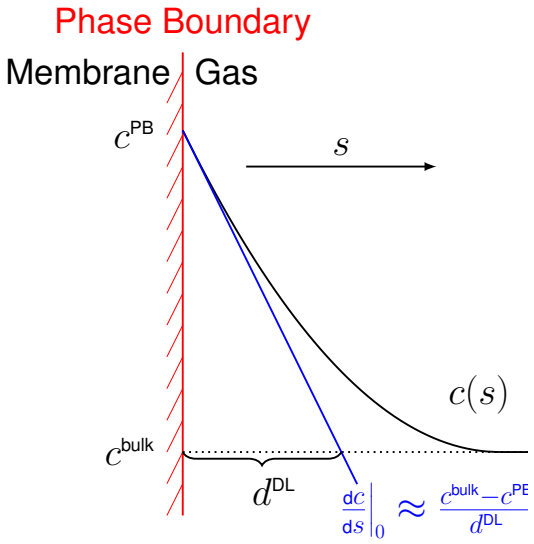

Figure 4.2: Definition of effective boundary layer with linear concentration profile according film theory

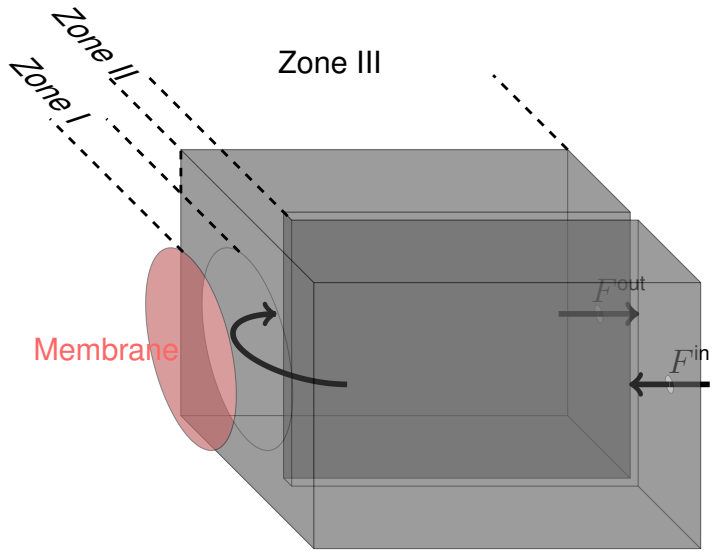

Figure 4.3: Geometry of gas chamber implemented in *Comsol*

to the concentration profile at the phase boundary reaches bulk concentration c^{bulk} as shown in Fig. 4.2.

In order to apply this theory to the diffusion layer of the experimental setup, it is necessary to determine a three dimensional steady state concentration distribution in the gas chamber. Therefore, the entire geometry of the gas chamber as shown in Fig. 4.3 is implemented in *Comsol Multiphysics 4.3b* in three dimensions to simulate a two component flow of helium and water vapour through the gas chamber for several flow rates. The membrane is implemented as a plane wall

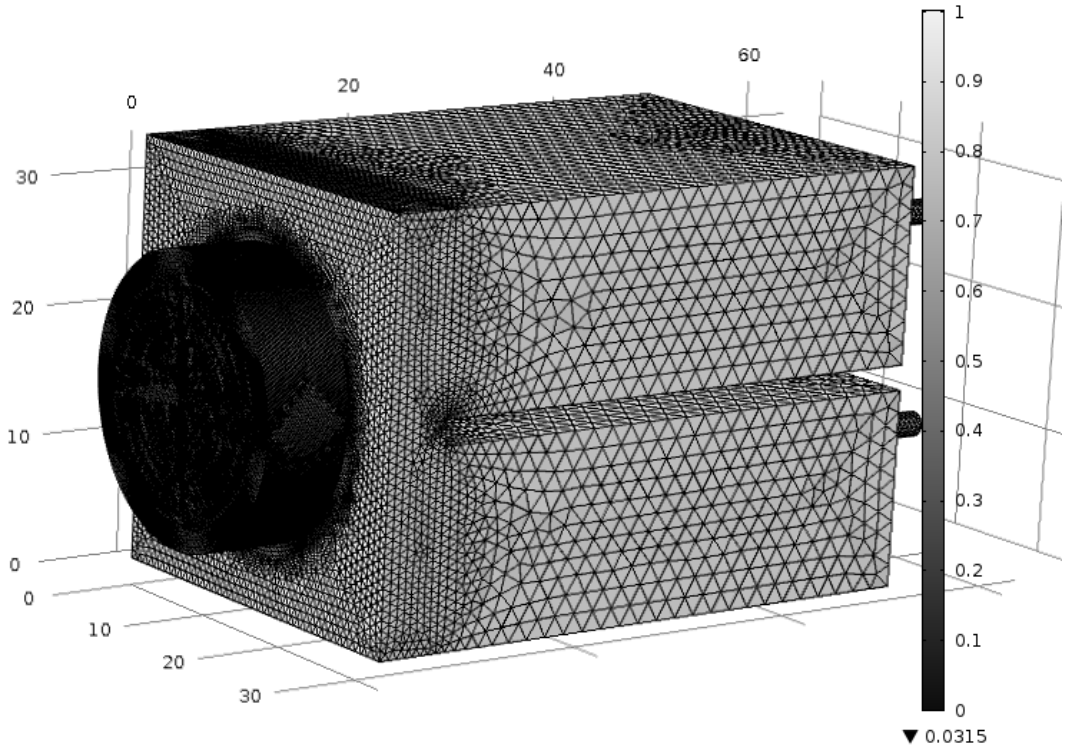

Figure 4.4: User defined mesh for gas chamber geometry with very fine mesh in the membrane window.

with the boundary condition that concentration of water is constant at saturation concentration at simulation temperature of 50 °C while inlet gas consists of pure helium. As a consequence, water vapour diffuses from membrane through the boundary layer to the chamber forming a three dimensional concentration profile.

Mesh independency tests reveal that element size needs to be lower than 0.3 mm. Applying this to a standard mesh of *Comsol* causes simulation times above 1 day and displaying and saving data of the required concentration profiles takes several hours. Since diffusion process mainly occurs in the circular membrane window (zone I in Fig. 4.3), a user defined mesh as shown in Fig. 4.4 is generated which changes maximum element size to 0.3 mm, 0.8 mm and 1.75 mm in zone I, zone II and zone III respectively. Mesh independency tests prove these element sizes sufficiently small and simulation times decrease to few hours.

Concentration profile is evaluated along several straight lines perpendicular to membrane (z-direction) at all combinations of $\varphi \in \left\{0, \frac{\pi}{8}, \frac{2\pi}{8}, ..., 2\pi\right\}$ and $r \in \{0, 2, 4, 7, 9, 11\}$ in mm. Some profiles overshoot slightly to a minimum concentration and rise again as the profile of $r = 4$ mm in Fig. 4.5. This happens due to

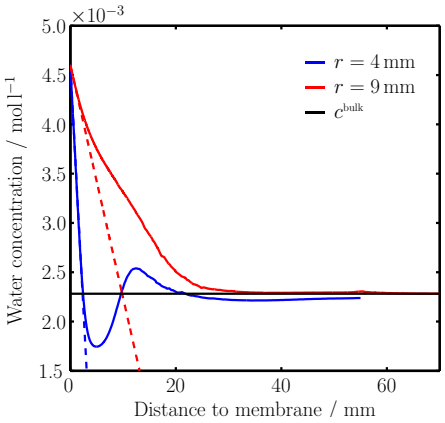

Figure 4.5: Profiles of water concentration in z-direction for a helium flow rate of $2\,\mathrm{l_N\,min^{-1}}$ at $\varphi = 0$ and $r = 4\,\mathrm{mm}$ or $r = 9\,\mathrm{mm}$, respectively.

a high flux of dry helium from the inlet at these places which can reduce water concentration locally. However, the simulation is used to approximate a diffusion layer thickness according to film theory which assumes a well mixed bulk flow with constant concentration. Hence, bulk concentration needs to be equal for all combinations of φ and r and is defined as the concentration at outlet of the gas chamber which is the value at $z \approx 70\,\mathrm{mm}, r = 9\,\mathrm{mm}, \varphi = 0$ as depicted in Fig. 4.5.

The local profiles are analysed with *Matlab* according to the film theory depicted in Fig. 4.2 providing local values of $d^{\mathrm{DL}}(r,\varphi)$. Diffusion layer thickness $d^{\mathrm{DL}}(r,\varphi)$ is fitted by least squares to a polynomial of order o in r with angle depending coefficients:

$$d^{\mathrm{DL}}(r,\varphi) = \sum_{\kappa=1}^{o+1} r^{\kappa-1} b_\kappa(\varphi) \tag{4.66}$$

Dependencies of coefficients b_κ from angle φ are sinusoidal as shown in Fig. 4.6. Therefore, coefficients b_κ are expressed by superposition of cosine oscillation of different frequency $f_{\kappa,\epsilon}$, different amplitude $\mathcal{A}_{\kappa,\epsilon}$ and different phase shift $\psi_{\kappa,\epsilon}$:

$$b_\kappa(\varphi) = \mathcal{A}_\kappa^0 + \sum_\epsilon \mathcal{A}_{\kappa,\epsilon} \cos\left(\varphi_h f_{\kappa,\epsilon} + \psi_{\kappa,\epsilon}\right) \tag{4.67}$$

$\mathcal{A}_\kappa^0$ is the mean value of the oscillation of coefficient b_κ. Frequencies, amplitudes and phase shifts of these superposed cosine functions are determined by fast Fourier transform (FFT) function in *Matlab* for each flow rate. The resulting fits of $b_\kappa(\varphi)$ for $F_{\mathrm{in}}^{\mathrm{G}} = 1\,\mathrm{l_N\,min^{-1}}$ are displayed as solid lines in Fig. 4.6. Inserting

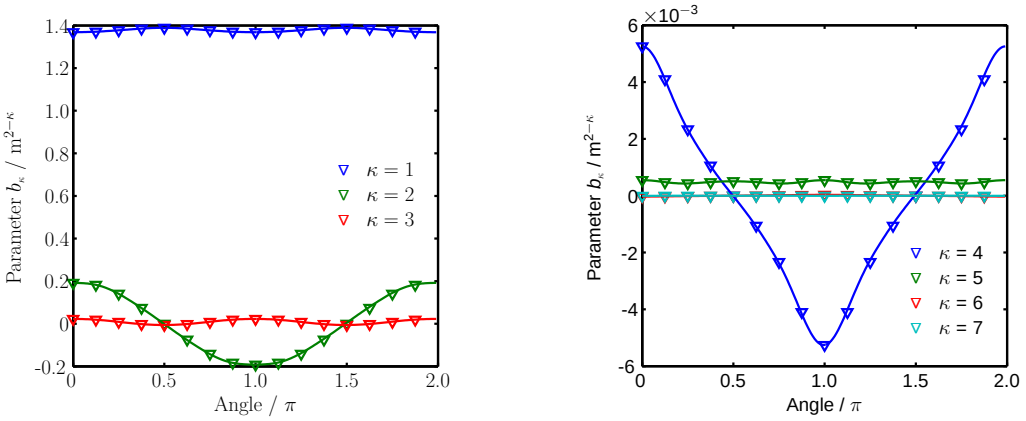

(a) Parameters b_1, b_2 and b_3 (b) Parameters b_4, b_5, b_6 and b_7

Figure 4.6: Parameters b_κ fitted to calculate diffusion layer thickness for various φ (symbols) and fit of parameters b_κ by FFT as a function of angle φ (solid lines) for $F_{\text{in}}^{\text{G}} = 1\,\text{l}_\text{N}\,\text{min}^{-1}$

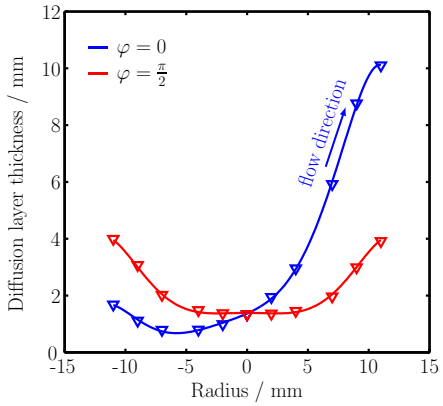

Figure 4.7: Profiles of diffusion layer in flow direction ($\varphi = 0$) and perpendicular to flow direction ($\varphi = \frac{\pi}{2}$) determined by cfd simulation (symbols) and by curve fitting (solid lines) for $F_{\text{in}}^{\text{G}} = 1\,\text{l}_\text{N}\,\text{min}^{-1}$

these parameters in Eq. (4.66) results in a three dimensional reproduction of the diffusion layer thickness $d^{\text{DL}}(r, \varphi)$ which is used in simulations. Figure 4.7 shows diffusion layer thickness along the radius in direction of gas flow ($\varphi = 0$) and perpendicular to flow direction ($\varphi = \frac{\pi}{2}$) for a gas flow rate of $F_{\text{in}}^{\text{G}} = 1\,\text{l}_\text{N}\,\text{min}^{-1}$. As expected, the profile perpendicular to flow direction is symmetrical while profile in flow direction is asymmetrical.

A slight decrease of diffusion layer thickness for high radii may happen due to the high order polynomial fit. In this case, thickness is assumed to stay constant at the highest value calculated for the specific angle.

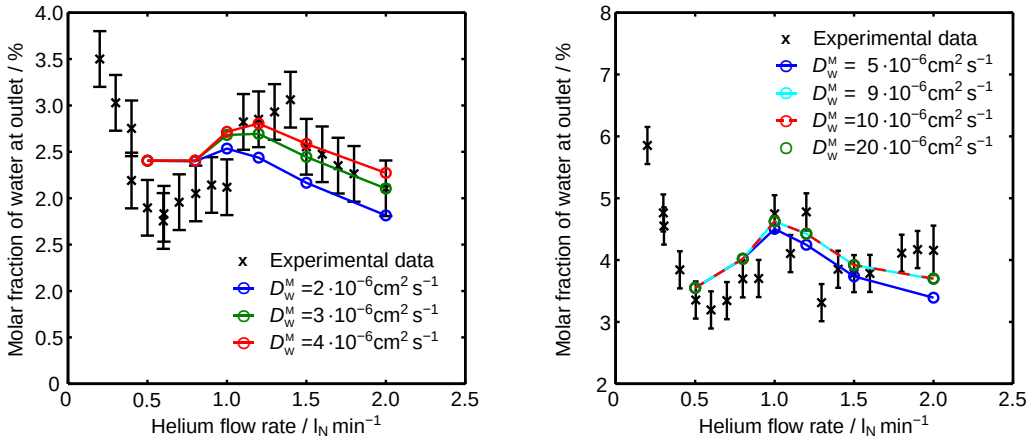

(a) (b)

Figure 4.8: Measured and simulated molar fractions of water vapour in the gas chamber at a temperature of (a) 40 °C and (b) 50 °C.

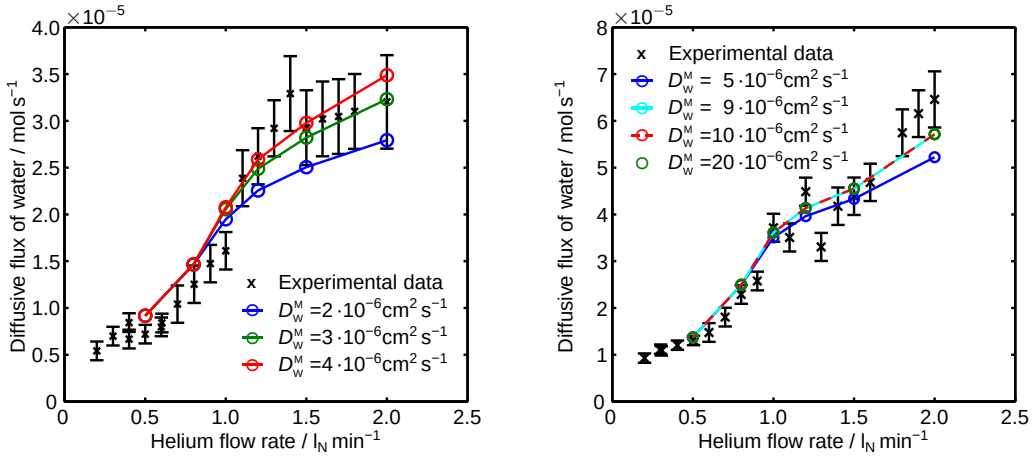

(a) (b)

Figure 4.9: Measured and simulated diffusive fluxes of water from liquid chamber to gas chamber for various water diffusion coefficients through membrane at a temperature of (a) 40 °C and (b) 50 °C.

4.3 Comparison of Experiment and Model

A comparison of experimental data and simulation results for various values of water and methanol diffusion coefficients at temperatures of 40 °C and 50 °C is displayed in Figs. 4.8 to 4.11. Quantitative model predictions of diffusive fluxes and molar fractions in the gas chamber are very close to measured values. The model even predicts the unexpected trend of molar fraction of water vapour in the gas phase Fig. 4.8. Molar flux of water and the corresponding water vapour fraction in gas phase are solely underestimated for 2 l_N min^{-1} helium flow rate at

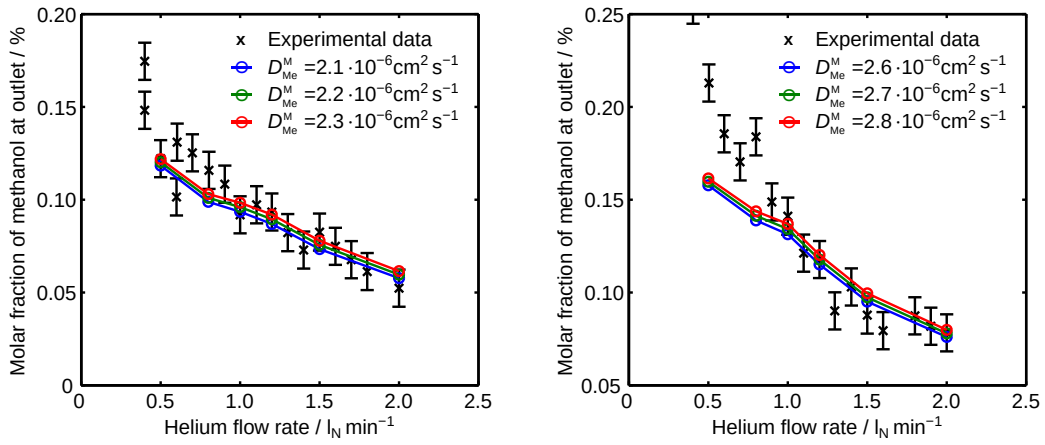

(a) (b)

Figure 4.10: Measured and simulated molar fractions of methanol vapour in the gas chamber at a temperature of (a) 40 °C and (b) 50 °C.

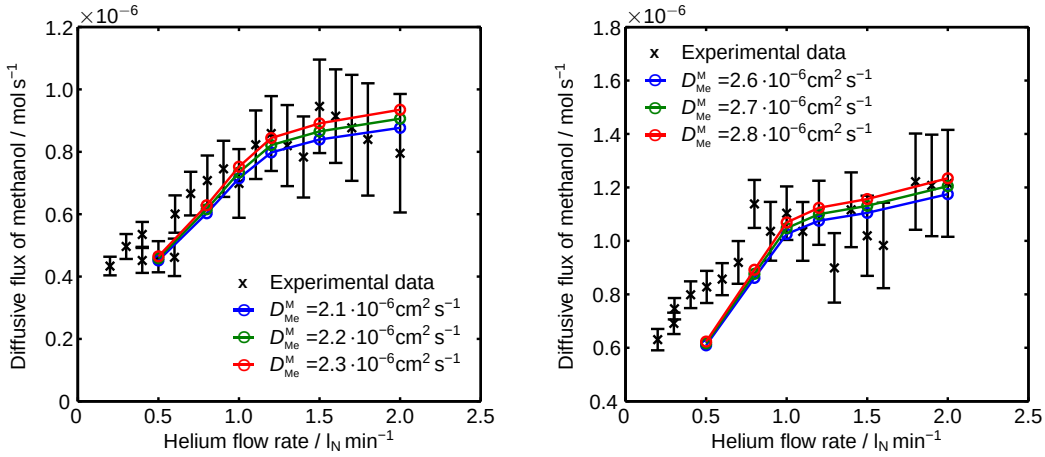

(a) (b)

Figure 4.11: Measured and simulated diffusive fluxes of methanol from liquid chamber to gas chamber for various methanol diffusion coefficients through membrane at a temperature of (a) 40 °C and (b) 50 °C.

a temperature of 50 °C as shown by Fig. 4.9. Among others, one possible reason for that is a local temperature change in the gas chamber. Temperature of gas at phase boundary is assumed to be equal to the measured gas temperature which is slightly lower than liquid temperature. As a consequence, calculated maximum concentration of water in the gas phase is lower than it might be in reality. Thus, diffusive flux calculated by simulations is lower than the experimentally determined flux in cases in which gas at membrane gas interface is saturated with water. The temperature difference is bigger for higher flow rates as shown in Table 4.1. Further model uncertainties are attributed to determined diffusion

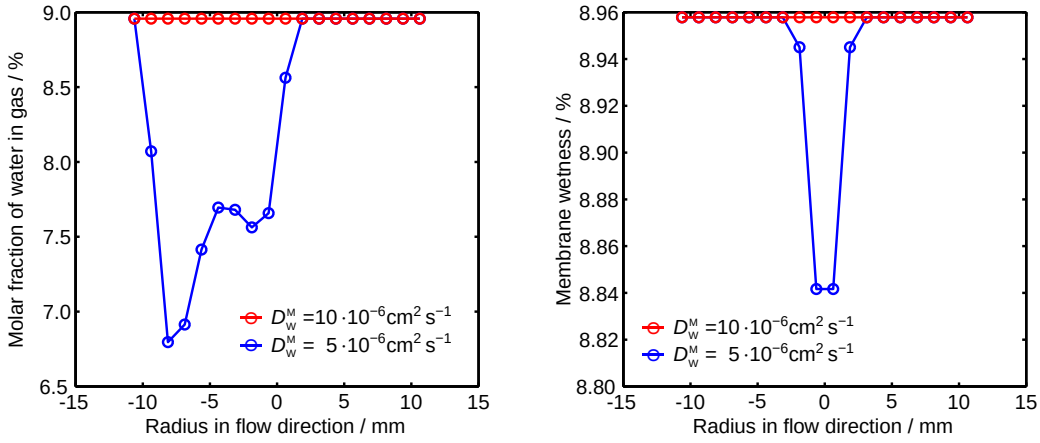

(a) (b)

Figure 4.12: Simulated molar fraction of water vapour at membrane gas interface at T =50 °C and for 2 l_N min^{-1} helium flow rate (a) in flow direction and (b) perpendicular to flow direction.

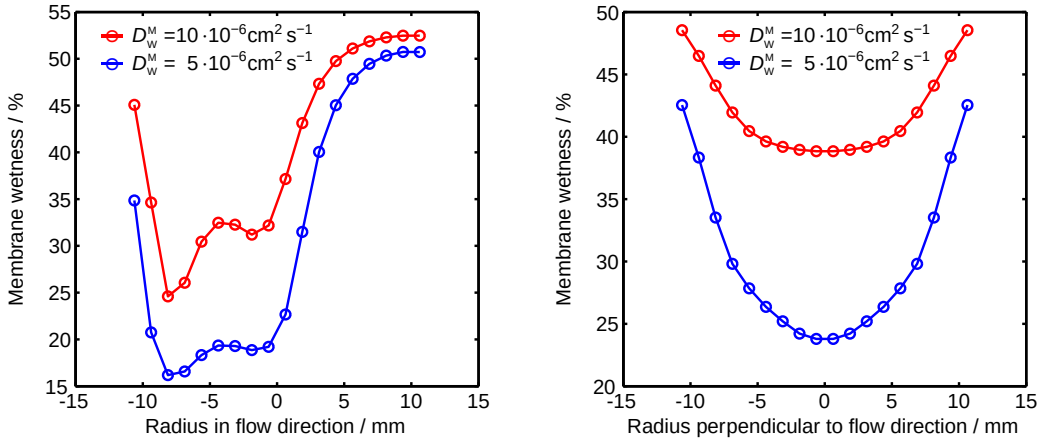

(a) (b)

Figure 4.13: Simulated profiles of membrane wetness at membrane gas interface at T =50 °C and for 2 l_N min^{-1} helium flow rate (a) in flow direction and (b) perpendicular to flow direction.

layer thickness and equilibrium between gas and liquid phase. However, even for 2 l_N min^{-1}, the difference between model predicted and experimentally determined values is about 10 % which is acceptable. Prediction of diffusive flux and molar fraction of methanol are even closer to experimental results than that of water which proves the used approach of diffusive fluxes to be suitable to describe diffusion through membrane.

The used assumption of film theory is mainly applicable for flow rates which are high enough to cause a well mixed bulk phase in the gas chamber. This

explains the slightly higher discrepancy between experiment and simulation for low gas flow rates. Furthermore, low gas flow rates cause thick boundary layers and result in limitation of mass transport by diffusion through boundary layer and saturation of gas at membrane gas interface instead of limitation by diffusion through membrane. In these cases, gas at membrane gas interface is saturated with water and, consequently, increasing diffusion coefficients through membrane has no effect on concentrations in gas phase. For higher flow rates, the gas at the membrane gas interface is not saturated and, thus, diffusion through membrane effects gas concentration. However, the profiles of molar fraction of water vapour at membrane gas interface in flow direction and perpendicular to flow direction in Fig. 4.12 reveal that at a gas flow rate of $2\,\mathrm{l_N\,min^{-1}}$ and a temperature of 50 °C, gas is saturated with water at the whole interface for diffusion coefficient of $10\cdot10^{-6}\ \mathrm{cm^2\,s^{-1}}$ while $D_{\mathrm{W}}^{\mathrm{M}}$ =$5\cdot10^{-6}\ \mathrm{cm^2\,s^{-1}}$ leads to lower molar fractions of water at part of the membrane gas interface. Hence, further increase of $D_{\mathrm{W}}^{\mathrm{M}}$ has no effect on the water concentration in the gas chamber whereas membrane wetness is not same all over the interface and may change with further increase of water diffusion coefficient as shown in Fig. 4.13. Therefore, it is difficult to determine a diffusion coefficient of water through membrane for 50 °C. For further studies, diffusion coefficient of water is set to $D_{\mathrm{W}}^{\mathrm{M}}(50\,^{\circ}\mathrm{C}) = 10\cdot10^{-6}\,\mathrm{cm^2\,s^{-1}}$ which is at least the correct dimension but might be slightly lower than the correct value.

For water at 40 °C and for methanol at both temperatures, a change of diffusion coefficients through membrane effects the calculated diffusive flux. However, this effect is lower than the estimated error of the experimental results. Therefore, diffusion coefficients are not determined by parameter optimisation but estimated roughly at $D_{\mathrm{W}}^{\mathrm{M}}(40\,^{\circ}\mathrm{C}) = 3\cdot10^{-6}\,\mathrm{cm^2\,s^{-1}}$, $D_{\mathrm{Me}}^{\mathrm{M}}(40\,^{\circ}\mathrm{C}) = 2.2\cdot10^{-6}\,\mathrm{cm^2\,s^{-1}}$ and $D_{\mathrm{Me}}^{\mathrm{M}}(50\,^{\circ}\mathrm{C}) = 2.7\cdot10^{-6}\,\mathrm{cm^2\,s^{-1}}$ respectively. It should be mentioned that these values are fitted to the special approach of diffusive flux used in this study and may not be compared to the diffusion coefficients for common Fick's diffusion. The used approach to describe diffusion assumes that diffusion coefficients are independent of concentration and nonlinear behaviour of diffusion solely arises from the change of total density with membrane wetness. Other approaches believe that diffusion coefficient is influenced by concentration or membrane wetness [25, 61] but this dependency cannot be determined by the experimental results from Chapter 3 since membrane wetness and methanol concentration in the membrane were not detected in the experiments.

The results also indicate that the assumption of dry membrane at gas side would have caused high errors since membrane wetness at gas side is even higher than at equilibrium with water saturated gas.

CHAPTER 5

Enhanced Transport Model of an ADMFC

Results of Chapter 2 identify mass transport through membrane as an essential process in ADMFCs. This chapter combines the fuel cell model of Chapter 2 with the detailed description of diffusion processes of Chapter 4 for further analysis of water management in ADMFCs. Aim is to study the two challenges mentioned in Chapter 2 with a more realistic model as well as the impact of uncertainties of the experimentally determined parameters.

5.1 Mathematical Modelling

Four zones are described by this model: anode chamber, membrane, cathode chamber and a gas diffusion layer between membrane and cathode chamber. As in the extreme case scenarios (Chapter 2), anode and cathode chambers are as-

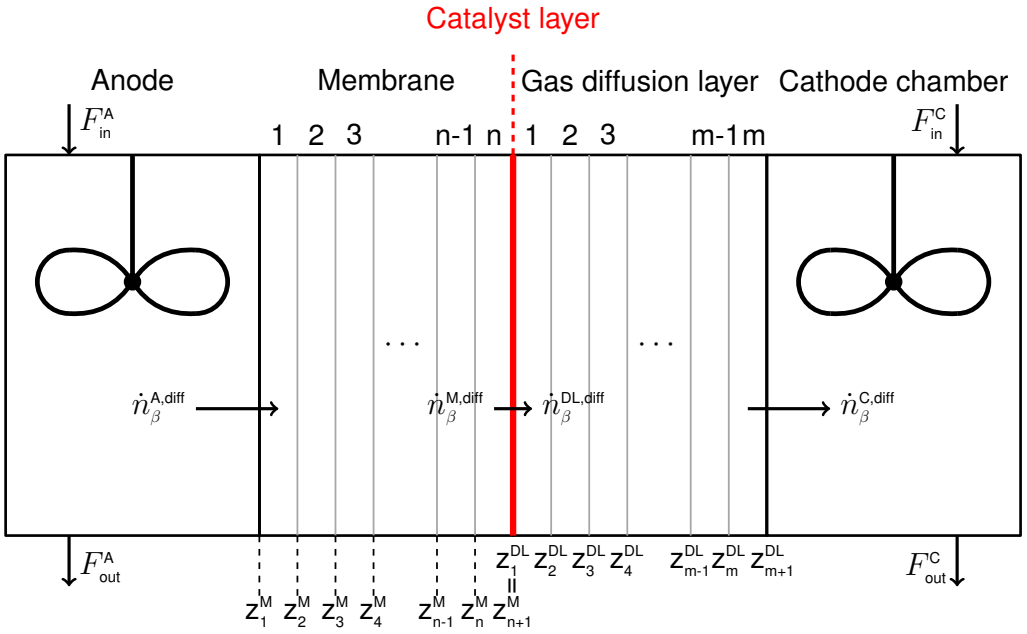

Figure 5.1: Sketch of the ADMFC model with detailed description of diffusive transport from anode to cathode.

sumed to be ideally mixed and are modelled as CSTRs with constant temperature and pressure. Contrary to the model of the diffusion cell in Chapter 4, gas diffusion layer thickness is constant across the active area of the membrane. As a consequence, solely gradients in through plane direction z are significant which reduces the dimension of membrane and GDL to one spatial dimension as shown in Fig. 5.1. In fuel cells, phase boundary between membrane and gas phase is located in the catalyst layer and is assumed to have an area equal to the effective membrane area for this model. Neither catalyst layer nor diffusion layer at anode is considered because they have insignificant influence on water transport through membrane.

Differential equations for all zones arise from local mass balances as in the models derived in the previous chapters. Mass balances in anode and cathode chamber are similar to those in Chapter 2:

$$V^{\mathrm{A}}\frac{dc_{\alpha}^{\mathrm{A}}}{dt} = F_{\mathrm{in}}^{\mathrm{A}}c_{\alpha,\mathrm{in}}^{\mathrm{A}} - F_{\mathrm{out}}^{\mathrm{A}}c_{\alpha}^{\mathrm{A}} + \dot{n}_{\alpha}^{\mathrm{A,diff}} + \sigma_{\alpha}^{\mathrm{A}} \tag{5.1}$$

$$V^{\mathrm{C}}\frac{dc_{\gamma}^{\mathrm{C}}}{dt} = F_{\mathrm{in}}^{\mathrm{A}}c_{\gamma,\mathrm{in}}^{\mathrm{C}} - F_{\mathrm{out}}^{\mathrm{A}}c_{\gamma}^{\mathrm{C}} + \dot{n}_{\gamma}^{\mathrm{C,diff}} + \sigma_{\gamma}^{\mathrm{C}} \tag{5.2}$$

for $\alpha \in \{\mathrm{W,Me,W^g,Me^g,CO_2}\}$ at anode and $\gamma \in \{\mathrm{N_2,O_2,CO_2,W^g}\}$ at cathode. Since cathode chamber and cathode catalyst layer are separated by the GDL, no sources or sinks occur in the cathode chamber $\sigma_{\gamma}^{\mathrm{C}} = 0$. In contrast, anode chamber, anode GDL and anode CL are modelled as one CSTR in which sources and sinks occur $\sigma_{\alpha}^{\mathrm{A}} = \sigma_{\alpha}^{\mathrm{ACL}}$.

Assuming constant and equal pressure in anode and cathode chambers as well as cathode GDL and CL, mass transport from anode to cathode chamber is solely based on diffusion in addition to ionic transport and the corresponding electro-osmotic drag through membrane as in the previously derived models. Convection solely takes place as inlet and outlet of anode and cathode chamber. Diffusion through membrane is described as in the model of the diffusion cell neglecting presence of methanol for calculation of water diffusion. Hence, differential equations for membrane wetness and concentration of methanol in the membrane are equal to those derived in Chapter 4:

$$\frac{\partial f^{\mathrm{M}}}{\partial t} = \frac{\partial}{\partial z}\left(D_{\mathrm{W}}^{\mathrm{M}}\frac{1}{1+f^{\mathrm{M}}}\frac{\partial f^{\mathrm{M}}}{\partial z}\right) \tag{5.3}$$

$$\frac{\partial c_{\mathrm{Me}}^{\mathrm{M}}}{\partial t} = \frac{\partial}{\partial z}\left(D_{\mathrm{Me}}^{\mathrm{M}}\frac{\rho_{\mathrm{dry}}^{\mathrm{M}}}{\rho^{\mathrm{M}}}\left((1+f^{\mathrm{M}})\frac{\partial c_{\mathrm{Me}}^{\mathrm{M}}}{\partial z} - c_{\mathrm{Me}}^{\mathrm{M}}\frac{\partial f^{\mathrm{M}}}{\partial z}\right)\right) \tag{5.4}$$

Boundary conditions are defined as f^{Ml} and $c_{\mathrm{Me}}^{\mathrm{Ml}}$ at anode side and f^{Mg} and $c_{\mathrm{Me}}^{\mathrm{Mg}}$ at cathode side.

Since temperature as well as pressure in the cathode chamber are constant and molar masses of gas components at cathode do not differ much from the molar mass of the main component nitrogen, over all density of cathodic gas is assumed to stay constant contrary to the model in Chapter 4. Moreover, it is neglected that cathodic gas consists of more than two components and binary diffusion coefficients of CO_2 in air, H_2O in air and O_2 in N_2 are used for calculation of diffusive fluxes through GDL. As a consequence, the diffusion is described by the standard approach of Fick's diffusion and the mass balance of gas components $\gamma \in \{\mathrm{N_2,O_2,CO_2,W^g}\}$ reduces to:

$$\frac{\partial c_\gamma^{\mathrm{DL}}}{\partial t} = -\frac{\partial}{\partial z}\left(-D_\gamma^{\mathrm{DL}}\frac{\partial c_\gamma^{\mathrm{DL}}}{\partial z}\right) \tag{5.5}$$

Boundary conditions for this equation are gas concentrations in the catalyst layer c_γ^{CL} and in the cathode chamber c_γ^{C}. Equations (5.3) to (5.5) are discretised by standard finite volume method assuming linear profiles between equidistant volume elements in membrane and GDL respectively:

$$V_{\mathrm{VE}}^{\mathrm{M}} = A^{\mathrm{M}}\Delta z^{\mathrm{M}} \tag{5.6}$$

$$V_{\mathrm{VE}}^{\mathrm{DL}} = \epsilon^{\mathrm{DL}} A^{\mathrm{M}}\Delta z^{\mathrm{DL}} \tag{5.7}$$

Phases at anode are assumed to be in equilibrium. Hence, f^{Ml} is taken from water uptake measurements neglecting presence of methanol and $c_{\mathrm{Me}}^{\mathrm{Ml}}$ is calculated analogous to Eq. (4.51) by:

$$c_{\mathrm{Me}}^{\mathrm{Ml}} = \frac{c_{\mathrm{Me}}^{\mathrm{A}}}{c_{\mathrm{W}}^{\mathrm{A}}}\frac{f^{\mathrm{Ml}}\rho_{\mathrm{dry}}^{\mathrm{M}}}{M_{\mathrm{W}}} \tag{5.8}$$

Similar to the phase boundary in Chapter 4, cathode catalyst layer is modelled as a phase boundary between membrane and gas phase without volume at which electrochemical reactions as well as chemical oxidation of methanol take place. Methanol diffusing through membrane is assumed to be immediately oxidised at cathode CL which results in $c_{\mathrm{Me}}^{\mathrm{Mg}} = 0$ and no methanol evaporation takes place. Furthermore, it is assumed that phases are also in equilibrium at cathode catalyst layer with only one exception: If gas in the cathode CL is saturated with water, membrane wetness at the membrane gas interface f^{Mg} may rise above equilibrium wetness as explained in Chapter 4. Hence, the equilibrium between membrane

wetness and gas humidity is taken from water uptake experiments analogous to Eq. (4.54):

$$y_{\mathrm{W}}^{\mathrm{DL,eq}} = \frac{-p_2 \pm \sqrt{p_2^2 - 4p_1(p_3 - f^{\mathrm{Mg}})}}{2p_1} \tag{5.9}$$

but molar fraction of water vapour is limited to the molar fraction at water saturation of the gas:

$$y_{\mathrm{W}}^{\mathrm{max}} = \frac{p_{\mathrm{W}}^{\mathrm{o}}}{p} \tag{5.10}$$

$$y_{\mathrm{W}}^{\mathrm{CL}} = \min\left(y_{\mathrm{W}}^{\mathrm{DL,eq}}, y_{\mathrm{W}}^{\mathrm{max}}\right) \tag{5.11}$$

Since cathode catalyst layer has no volume, accumulation of substances at cathode CL is prohibited and water diffusing through membrane from anode to cathode $\dot{n}_{\mathrm{W}}^{\mathrm{M,diff}}$ is either consumed by electrochemical reactions or evaporates to equilibrate membrane wetness and gas humidity. Evaporated water diffuses from cathode CL through cathode GDL to cathode chamber $\dot{n}_{\mathrm{W}}^{\mathrm{DL,diff}}$. Hence, mass balance of water in cathode CL results in:

$$0 = \dot{n}_{\mathrm{W}}^{\mathrm{M,diff}} - \dot{n}_{\mathrm{W}}^{\mathrm{DL,diff}} + \sigma_{\mathrm{W}}^{\mathrm{CCL}} \tag{5.12}$$

The sources and sinks term $\sigma_{\mathrm{W}}^{\mathrm{CCL}}$ includes water consumption by electrochemical reduction reaction, water production due to methanol oxidation resulting from cross-over and electro-osmotic drag of water. It is equal to that used for scenario modelling in Chapter 2 and defined by Eq. (2.13). Inserting equations for diffusive fluxes which are defined below, Eq. (5.12) results in an algebraic equation that is solved for f^{Mg}.

Mass balances for other gas components $\gamma \in \{\mathrm{O_2}, \mathrm{CO_2}\}$ at cathodic catalyst layer result in:

$$\dot{n}_{\gamma}^{\mathrm{DL,diff}} = \sigma_{\gamma}^{\mathrm{CCL}} \tag{5.13}$$

Diffusive fluxes are specified from anode to membrane $\dot{n}_{\alpha}^{\mathrm{A,diff}}$, from membrane to cathode CL $\dot{n}_{\alpha}^{\mathrm{M,diff}}$, from cathode CL to GDL $\dot{n}_{\gamma}^{\mathrm{DL,diff}}$ and from cathode GDL to cathode chamber $\dot{n}_{\gamma}^{\mathrm{C,diff}}$ as depicted in Fig. 5.1. Due to the one dimensional

discretisation with the assumption of linear profiles between volume elements, these diffusive fluxes are defined as:

$$\dot{n}_{\mathrm{Me}}^{\mathrm{A,diff}} = D_{\mathrm{Me}}^{\mathrm{M}} A^{\mathrm{M}} \frac{\rho_{\mathrm{dry}}^{\mathrm{M}}}{\frac{\Delta z^{\mathrm{M}}}{2}} \frac{c_{\mathrm{Me},1}^{\mathrm{M}} \left(1 + f^{\mathrm{Ml}}\right) - c_{\mathrm{Me}}^{\mathrm{Ml}} \left(1 + f_1^{\mathrm{M}}\right)}{\left(1 + f^{\mathrm{Ml}}\right) \rho_{\mathrm{dry}}^{\mathrm{M}} + c_{\mathrm{Me}}^{\mathrm{Ml}} M_{\mathrm{Me}}} \tag{5.14}$$

$$\dot{n}_{\mathrm{W}}^{\mathrm{A,diff}} = D_{\mathrm{W}}^{\mathrm{M}} A^{\mathrm{M}} \frac{\rho_{\mathrm{dry}}^{\mathrm{M}}}{M_{\mathrm{W}}} \frac{1}{1 + f^{\mathrm{Ml}}} \frac{f_1^{\mathrm{M}} - f^{\mathrm{Ml}}}{\frac{\Delta z^{\mathrm{M}}}{2}} \tag{5.15}$$

$$\dot{n}_{\alpha}^{\mathrm{A,diff}} = 0 \qquad \forall \alpha \in \left\{\mathrm{Me^g, W^g, CO_2}\right\} \tag{5.16}$$

$$\dot{n}_{\mathrm{Me}}^{\mathrm{M,diff}} = -D_{\mathrm{Me}}^{\mathrm{M}} A^{\mathrm{M}} \frac{\rho_{\mathrm{dry}}^{\mathrm{M}}}{\frac{\Delta z^{\mathrm{M}}}{2}} \frac{c_{\mathrm{Me}}^{\mathrm{Mg}} \left(1 + f_{\mathrm{n}}^{\mathrm{M}}\right) - c_{\mathrm{Me,n}}^{\mathrm{M}} \left(1 + f^{\mathrm{Mg}}\right)}{\left(1 + f^{\mathrm{Mg}}\right) \rho_{\mathrm{dry}}^{\mathrm{M}} + c_{\mathrm{Me}}^{\mathrm{Mg}} M_{\mathrm{Me}}} \tag{5.17}$$

$$\dot{n}_{\mathrm{W}}^{\mathrm{M,diff}} = -D_{\mathrm{W}}^{\mathrm{M}} A^{\mathrm{M}} \frac{\rho_{\mathrm{dry}}^{\mathrm{M}}}{M_{\mathrm{W}}} \frac{1}{1 + f^{\mathrm{Mg}}} \frac{f^{\mathrm{Mg}} - f_{\mathrm{n}}^{\mathrm{M}}}{\frac{\Delta z^{\mathrm{M}}}{2}} \tag{5.18}$$

$$\dot{n}_{\gamma}^{\mathrm{DL,diff}} = -D_{\gamma}^{\mathrm{DL}} \epsilon^{\mathrm{DL}} A^{\mathrm{M}} \frac{c_{\gamma,1}^{\mathrm{DL}} - c_{\gamma}^{\mathrm{CL}}}{\frac{\Delta z^{\mathrm{DL}}}{2}} \quad \forall \gamma \in \left\{\mathrm{O_2,CO_2,W^g}\right\} \tag{5.19}$$

$$\dot{n}_{\gamma}^{\mathrm{C,diff}} = -D_{\gamma}^{\mathrm{DL}} \epsilon^{\mathrm{DL}} A^{\mathrm{M}} \frac{c_{\gamma}^{\mathrm{C}} - c_{\gamma,\mathrm{n}}^{\mathrm{DL}}}{\frac{\Delta z^{\mathrm{DL}}}{2}} \quad \forall \gamma \in \left\{\mathrm{N_2,O_2,CO_2,W^g}\right\} \tag{5.20}$$

Total density at any location in the membrane $\mathrm{loc} \in \{\mathrm{M,Mg,Ml}\}$ is defined as:

$$\rho^{\mathrm{loc}} = (1 + f^{\mathrm{loc}}) \rho_{\mathrm{dry}}^{\mathrm{M}} + c_{\mathrm{Me}}^{\mathrm{loc}} M_{\mathrm{Me}} \tag{5.21}$$

Density of dry membrane, $\rho_{\mathrm{dry}}^{\mathrm{M}}$, is calculated regarding Eq. (4.10).

For analysis of water management, the change of anodic water level is defined as the difference between convective water flux leaving anode chamber and convective flux entering anode chamber:

$$\xi_{\mathrm{W}} = c_{\mathrm{W}}^{\mathrm{A}} F_{\mathrm{out}}^{\mathrm{A}} - c_{\mathrm{W,in}}^{\mathrm{A}} F_{\mathrm{in}}^{\mathrm{A}} \tag{5.22}$$

For calculation of methanol efficiency it is assumed that entire methanol flux at the anodic exit is recycled. Hence, methanol efficiency is defined as:

$$\eta_{\mathrm{Me}} = \frac{\frac{A^{\mathrm{M}} i}{6F}}{-\sigma_{\mathrm{Me}}^{\mathrm{ACL}} - \sigma_{\mathrm{Me}}^{\mathrm{CCL}}} \tag{5.23}$$

Analogous, oxygen efficiency is calculated by:

$$\eta_{\mathrm{O_2}} = \frac{\frac{A^{\mathrm{M}} i}{4F}}{-\sigma_{\mathrm{O_2}}^{\mathrm{CCL}}} \tag{5.24}$$

Further equations are equivalent to those for scenario modelling in Chapter 2: Sources and sinks are defined in Eqs. (2.5) to (2.15), volume flow rates and inlet

Table 5.1: Reference set of parameters used for simulation.

Geometry and material parameters:					
V^{A}	=	$12.5\,\mathrm{ml}$	V^{C}	=	$12.5\,\mathrm{ml}$
d^{M}	=	$28\,\mu\mathrm{m}$	d^{DL}	=	$500\,\mu\mathrm{m}$
A^{M}	=	$25\,\mathrm{cm}^2$	ϵ^{DL}	=	0.8
n	=	100	m	=	500
$D^{\mathrm{M}}_{\mathrm{W}}$	=	$10\cdot10^{-6}\mathrm{cm}^2\,\mathrm{s}^{-1}$	$D^{\mathrm{M}}_{\mathrm{Me}}$	=	$2.7\cdot10^{-6}\mathrm{cm}^2\,\mathrm{s}^{-1}$
f^{Ml}	=	54 %	$\tilde{\rho}^{\mathrm{M}}_{\mathrm{dry}}$	=	$0.0256\,\mathrm{kg\,m}^{-2}$
κ	=	4			
Inlet data:					
$c^{\mathrm{A}}_{\mathrm{Me,in}}$	=	$1\,\mathrm{mol\,l}^{-1}$	$c^{\mathrm{A}}_{\mathrm{W,in}}$	=	$53.15\,\mathrm{mol\,l}^{-1}$
$c^{\mathrm{A}}_{\mathrm{Me^g,in}}$	=	$0\,\mathrm{mol\,l}^{-1}$	$c^{\mathrm{A}}_{\mathrm{W^g,in}}$	=	$0\,\mathrm{mol\,l}^{-1}$
$c^{\mathrm{A}}_{\mathrm{CO_2,in}}$	=	$0\,\mathrm{mol\,l}^{-1}$	$c^{\mathrm{C}}_{\mathrm{CO_2,in}}$	=	$0\,\mathrm{mol\,l}^{-1}$
λ^{A}	=	4	λ^{C}	=	10
$T^{\mathrm{C}}_{\mathrm{in}}$	=	$20\,^{\circ}\mathrm{C}$	$p^{\mathrm{C}}_{\mathrm{in}}$	=	$1.013\,\mathrm{bar}$
$RH^{\mathrm{C}}_{\mathrm{in}}$	=	60 %			
Operating conditions:					
p^{A}	=	$1.013\,\mathrm{bar}$	T^{A}	=	$50\,^{\circ}\mathrm{C}$
p^{C}	=	$1.013\,\mathrm{bar}$	T^{C}	=	$50\,^{\circ}\mathrm{C}$

conditions are defined in Eqs. (2.18) to (2.23) and definitions of binary diffusion coefficients etc. are listed in Table 2.1. Constants and data on chemical media are taken from Table 2.2, all other parameters of this model are listed inTable 5.1. The DAE-system is simulated with *Matlab* using the solver *ode15s*.

5.2 Results and Discussion

This model is used to analyse water management with a realistic implementation of water transport through membrane and to study influence of measured parameters. As shown in Fig. 5.2, concentration of water in cathode chamber is smaller than at catalyst layer for current densities below $1570\,\mathrm{mA\,cm}^{-2}$. For these current densities, excess water evaporates at cathode catalyst layer and

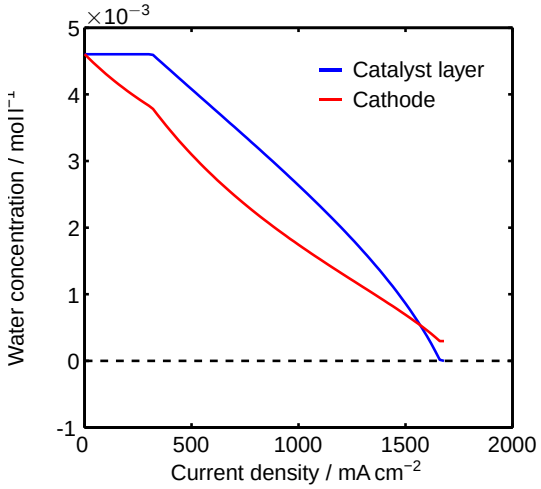

Figure 5.2: Water concentration in cathode catalyst layer and cathode chamber as a function of current density for reference set of parameters;

diffuses from CL to cathode chamber. This only takes place if water diffusion through membrane in ADMFCs is sufficient to fulfil cathodic water demand related to electrochemical reduction reaction and electro-osmotic drag of water and to additionally humidify cathodic gas. For higher current densities, water concentration in cathode chamber is higher than at catalyst layer. In this case, water transport through membrane does not supply sufficient water to cathode and water from cathodic gas is additionally needed for electrochemical reaction to provide these high current densities. However, when using ambient air with inlet temperature of $T_{\mathrm{in}}^{\mathrm{C}} = 20\,^{\circ}\mathrm{C}$ and humidity of $RH_{\mathrm{in}}^{\mathrm{C}} = 60\,\%$, gas in cathode CL is totally dehumidified at a current density of $i_{\mathrm{lim}} \approx 1660\,\mathrm{mA\,m^{-2}}$. Higher current densities cannot be provided without additional humidification of cathodic inlet gas. Current densities below $300\,\mathrm{mA\,cm^{-2}}$ lead to saturation of gas with water at catalyst layer and therefore to the highest gas humidification possible with the used set of parameters. Since real ADMFCs only provide current densities up to $100\,\mathrm{mA\,cm^{-2}}$ so far, cathodic water supply is not the limiting factor of present ADMFC performance. It should be mentioned that water transport through ionomer in the cathode catalyst layer is not considered in this model and might cause additional limitations of water transport which cannot be identified by this model.

Due to the thin membrane, methanol transport through membrane is very high and reduces methanol efficiency to values below 50 % for current densities below $140\,\mathrm{mA\,cm^{-2}}$ as shown in Fig. 5.3. Methanol efficiency increases with rising current density though it is not exceeding 90 % even for limiting current

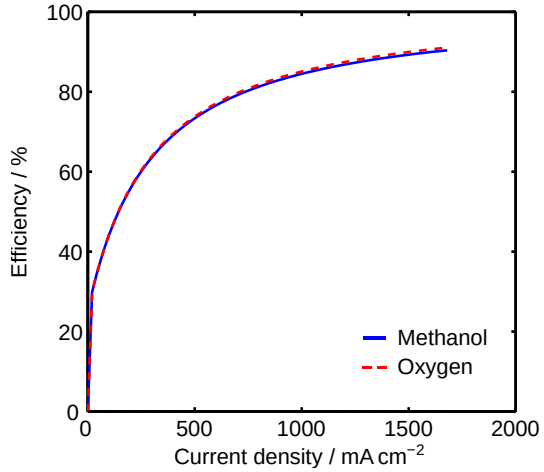

Figure 5.3: Methanol efficiency as well as oxygen efficiency as a function of current density for reference set of parameters;

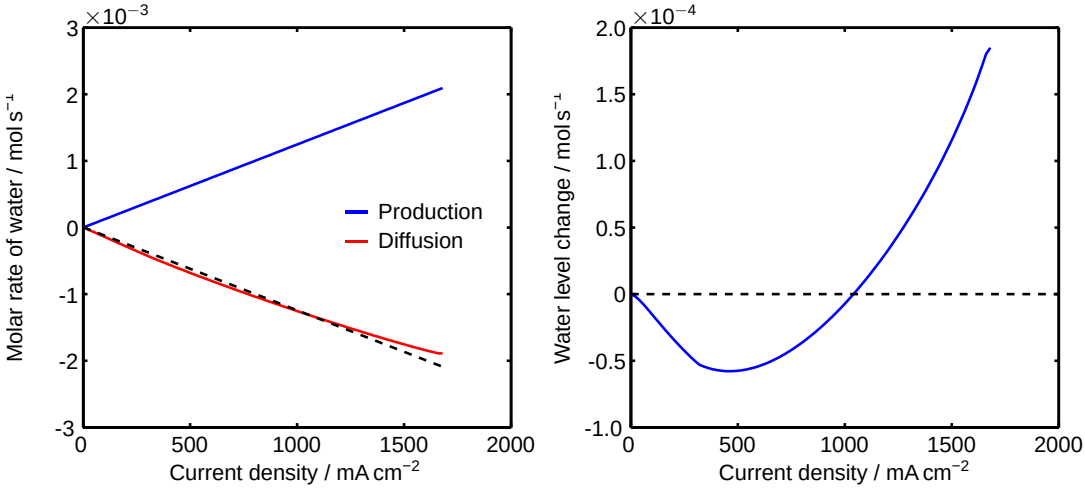

(a) (b)

Figure 5.4: Steady state values as function of current density for reference set of parameters: (a) Water production at anode and water diffusion through membrane, dashed line is water production with inverted sign; (b) Change of water level at anode;

density. Since oxygen is consumed by electrochemical reduction reaction and oxidation of methanol transported through membrane by cross-over, difference between oxygen efficiency and methanol efficiency represents efficiency loss due to methanol evaporation at anode. This efficiency loss is negligible compared to the loss by methanol cross-over. Hence, mixed potential caused by methanol cross-over [12] might be a strong limitation of ADMFC performance.

The above analysed methanol efficiency is only valid if methanol is recycled, e.g. by looping the methanol solution at anode. This leads to the challenge of

stable water level at anode of an ADMFC which is not effecting cell performance directly but is essential for stable long term operation. Stable water level in the recycling loop is reached if water flux at anode outlet is equal to water flux at anode inlet and, thus, no water is accumulated or lost. Considering the mass balance at anode Eq. (5.1) for water at steady state, definition of water level change by Eq. (5.22) is equivalent to the sum of water sources and sinks at anode, hereafter called water production, and water diffusion through membrane. As shown in Fig. 5.4a, water production at anode, which also includes water drag, increases linearly with current density while water diffusion is negative and decreases nonlinearly with current density. Water production with inverted sign is also included as dashed line to illustrate the nonlinear behaviour of water diffusion rate and to ease comparison of the two rates. For low current densities, value of water diffusion is higher than water production rate which results in water loss at anode represented by negative change of water level in Fig. 5.4b. At $i_\mathrm{s} \approx 1040\,\mathrm{mA\,cm^{-2}}$, water diffusion and production are equal and water level change is zero for the used set of parameters. Higher current densities lead to positive change of water level. Hence, to stabilise water level at anode, diffusion needs to be decreased for low current densities and increased for high current densities if possible.

Water diffusion through membrane can be influenced by water consumption at cathode, e.g. by changing cathodic evaporation rate. One operation parameter that influences water evaporation at cathode and which can easily be varied during fuel cell operation is the air excess ratio. As revealed by Scenario 4 in Section 2.3.1, specific combinations of air excess ratio and relative humidity at cathode outlet are needed to remove the required amount of water from the fuel cell that results in stable water level at anode. These pairs of values depend on current density and are displayed as dashed lines in Fig. 5.5a for current densities of $100\,\mathrm{mA\,cm^{-2}}$, $400\,\mathrm{mA\,cm^{-2}}$ and $1000\,\mathrm{mA\,cm^{-2}}$ as nominal values for stable water level. Relative humidities calculated by the model of this chapter as a function of air excess ratio are displayed as solid lines. The point of intersection of nominal values and actual values reveals the air excess ratio $\lambda_\mathrm{s}^\mathrm{C}$ for which real fuel cells with the used material can be operated at stable anodic water level. Change of water level in Fig. 5.5b proves that water level is stable for $\lambda^\mathrm{C} = \lambda_\mathrm{s}^\mathrm{C}$. As mentioned above, water level at anode is influenced by water production and water diffusion through membrane. The former linearly increases with current density and is not affected by air excess ratio while water diffusion converges to a maximum value $\dot{n}_\mathrm{W,max}^\mathrm{M,diff}$ for very high air excess ratios. Since maximum diffusion

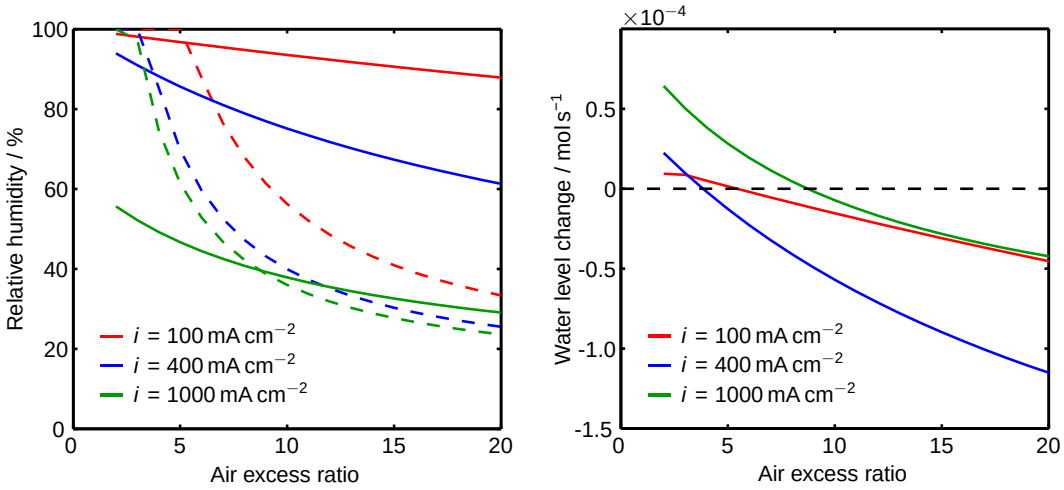

(a) (b)

Figure 5.5: Steady state values as function of air excess ratio for current densities of $100\,\mathrm{mA\,cm^{-2}}$, $400\,\mathrm{mA\,cm^{-2}}$ and $1000\,\mathrm{mA\,cm^{-2}}$: (a) Relative humidity in cathode chamber, dashed lines indicate humidity for stable water level at anode; (b) Change of water level at anode;

corresponds to maximum gradient through membrane which is independent of current density, $\dot{n}_{\mathrm{W,max}}^{\mathrm{M,diff}}$ is same for all current densities. However, the higher the current density, the higher is the diffusive flux for a fixed air excess ratio and the lower is the air excess ratio at which maximum diffusion is reached. Therefore, it is reasonable that $\lambda_{\mathrm{s}}^{\mathrm{C}}$ rises with increasing current density from $400\,\mathrm{mA\,cm^{-2}}$ to $1000\,\mathrm{mA\,cm^{-2}}$. For low current densities, water production at cathode resulting from methanol cross-over decreases water diffusion through membrane significantly and, thus, increases $\lambda_{\mathrm{s}}^{\mathrm{C}}$. As a result, $\lambda_{\mathrm{s}}^{\mathrm{C}}$ shows a minimum around $400\,\mathrm{mA\,cm^{-2}}$. As a consequence, $\lambda_{\mathrm{s}}^{\mathrm{C}}$ decreases with i for small current densities and increases for high current densities and the curve of water accumulation for current density of $100\,\mathrm{mA\,cm^{-2}}$ lies in between curves for current density of $400\,\mathrm{mA\,cm^{-2}}$ and $1000\,\mathrm{mA\,cm^{-2}}$. Nevertheless, $\lambda_{\mathrm{s}}^{\mathrm{C}}$ lies between 4 and 10 for current densities below $1000\,\mathrm{mA\,cm^{-2}}$ which are reasonable values for air excess ratio that can be adjusted.

Other parameters that influence water transport from anode to cathode chamber and, thus, influence stability of anodic water level in ADMFCs are humidity and temperature of cathodic inlet gas, thickness and porosity of GDL and membrane thickness. Influence of these parameters for $i = 400\,\mathrm{mA\,cm^{-2}}$ is depicted in Figs. 5.6a and 5.6b. Doubling thickness of GDL or membrane decreases the diffusive flux and leads to a slightly higher value of $\lambda_{\mathrm{s}}^{\mathrm{C}}$ because the achieved relative humidities at cathode are lower. Impact of membrane thickness variation is

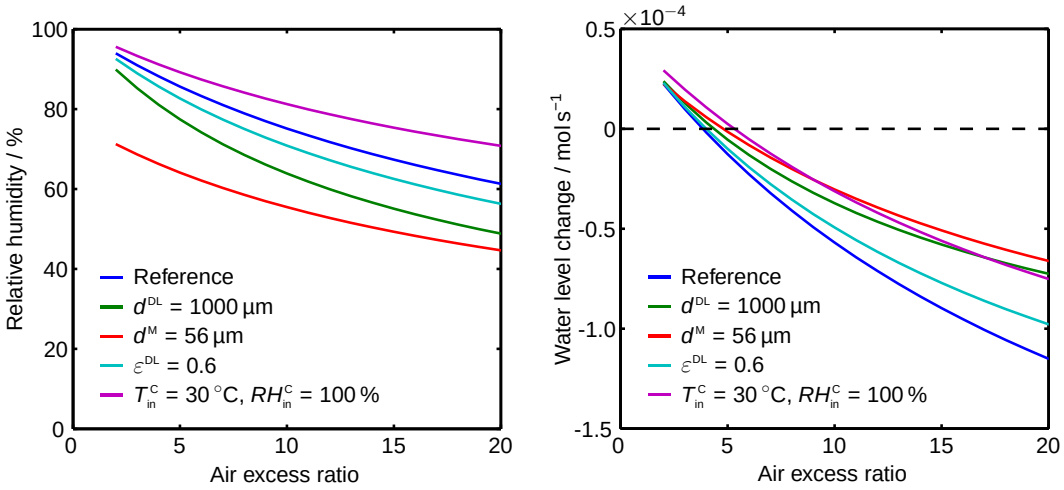

(a) (b)

Figure 5.6: Steady state values as a function of air excess ratio for reference conditions ($d^{DL} = 500\,\mu m$, $d^{M} = 28\,\mu m$, $\epsilon^{DL} = 0.8$, $T^{C}_{in} = 20\,°C$ and $RH^{C}_{in} = 60\,\%$) and for cases with varying diffusion layer thickness, membrane thickness, porosity of DL or inlet temperature and humidity: (a) Relative humidity in cathode chamber; (b) Change of water level at anode;

stronger than that of GDL thickness variation which on the one hand comes from a bigger resistance for transport through membrane than through GDL and on the other hand from a lower methanol cross-over and, thus, less water production at cathode. Influence of decreasing GDL porosity from 0.8 to 0.6 is negligible for low air excess ratios but the effect increases with λ^{C}. Less water is lost in case of lower porosities because mass transport through GDL is reduced and achieved humidity at cathode is also lower. The biggest influence on λ^{C}_{s} is observed in case of varied inlet conditions, temperature from $T^{C}_{in} = 20\,°C$ to $T^{C}_{in} = 30\,°C$ and humidity from $RH^{C}_{in} = 60\,\%$ to $RH^{C}_{in} = 100\,\%$. Since more water enters cathode chamber, relative humidity increases which reduces diffusive transport through GDL and results in $\lambda^{C}_{s} \gtrsim 5$ However, λ^{C}_{s} lies between 4 and 6 for all investigated sets of parameters and $i = 400\,mA\,cm^{-2}$.

Simulation results obviously depend on parameter values. These parameters contain uncertainties as described in Chapter 3 and can change e.g. when using different membrane material. Sensitivity of results to uncertainties of some measured parameters are depicted in Figs. 5.7 and 5.8. The former shows that methanol efficiency is mainly reduced by methanol cross-over. Efficiency without cross-over is about 99 % for the investigated range of current density. However, variation of methanol diffusion coefficient within the determined range of possi-

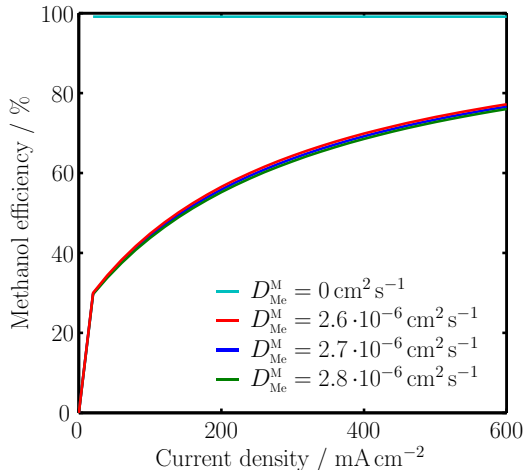

Figure 5.7: Sensitivity of methanol efficiency to methanol diffusion coefficient

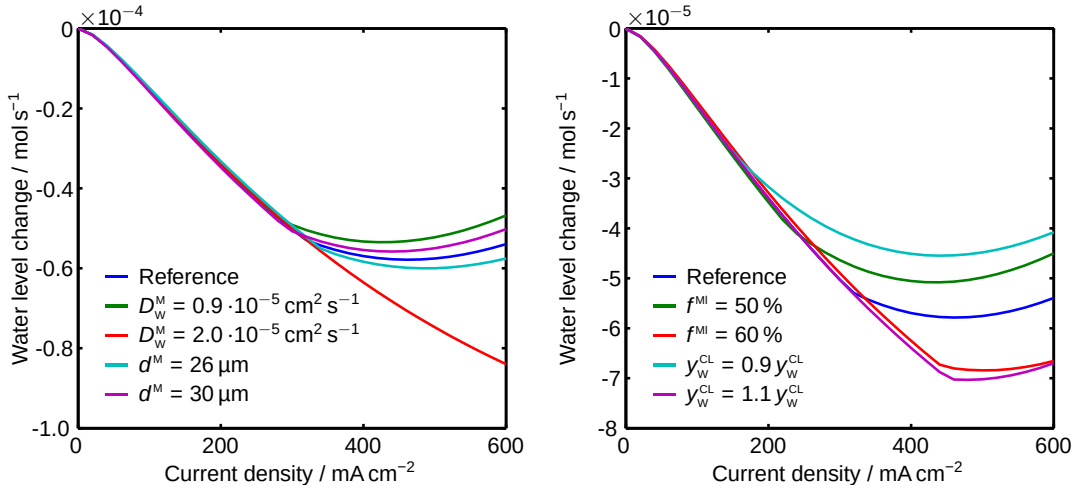

(a) (b)

Figure 5.8: Sensitivity of water level change at anode to: (a) variation of water diffusion coefficient and membrane thickness; (b) uncertainties of phase equilibria;

ble values of D^{M}_{Me} have insignificant effect on methanol efficiency. Sensitivity of water anodic level change to parameters that influence water diffusion through membrane is depicted in Fig. 5.8. Change of membrane thickness by 2 µm has already significant effect on change of water level. Even stronger influence is observed for change of phase equilibrium values by 10 % which is equivalent to a change of gradients in membrane and GDL respectively. The biggest source of error is the diffusion coefficient of water since the determined value is solely a minimum value and real value can be its multiple which also results in lower values for λ^{C}_{s} and higher limiting current densities. Therefore, simulations with

a precise set of parameters of a real fuel cell are needed for quantitative studies. However, qualitatively it can be concluded that water transport through membrane is not the rate determining step in present ADMFCs because it supplies sufficient water to cathode for the low current densities achieved in experiments so far. Furthermore, anodic water level can be stabilised by adjusting air excess ratio to reasonable values, though this also influences cell performance which also needs to be considered when operating ADMFCs. The required λ_s^C for stable water level strongly depends on fuel cell structure and operation conditions. Last but not least, methanol cross-over seems to be a big challenge in ADMFCs and might be the reason for the low performance. To prove this, a detailed analysis on the effect of methanol cross-over on cathode performance is required for which the model of this chapter may be modified in future projects.

CHAPTER 6

Summary and Outlook

This doctoral thesis focusses on the analysis of water management in alkaline direct methanol fuel cells to identify potential limitations of fuel cell performance by water management. Water production at anode and water consumption at cathode of an alkaline fuel cell lead to two challenges regarding water management in ADMFCs: sufficient water supply to cathode and water level stabilisation at anode. These challenges are analysed in three steps. In the first step, five extreme case scenarios which are based on a simplified model of an ADMFC were used to detect limitations, to identify important processes and to study options and requirements to meet the challenges. Simulations of the scenarios reveal the necessity of stable water level at anode for long term operation with reasonable methanol efficiency and identify water diffusion through membrane as key process of both challenges. Parameters for a detailed model of mass transport through anion exchange membranes are missing in literature and, thus, are determined in the second step. This includes the experimental quantification of diffusive fluxes through membrane and determination of equilibria between membrane and liquid or gas phase. Since explicit computation of diffusion coefficients from the experimental data is not possible, a three dimensional model of the used diffusion cell is derived in cylindrical coordinates to estimate specific coefficients for the used diffusion approach. In the final step, determined parameters are included in a fuel cell model with detailed description of mass transport through membrane to analyse the two challenges in more detail.

Results of this three step analysis reveal that water supply solely by cathodic inlet gas is insufficient for reasonable air excess ratios. In ADMFCs that use the investigated membrane, water diffusion through membrane supplies sufficient water to cathode for current densities up to $1570\,\mathrm{mA\,cm^{-2}}$ which is much higher than the maximum current density achieved in ADMFCs so far if solely an AEM is used as electrolyte. Hence, water diffusion is not the limiting factor of present ADMFCs. Methanol cross-over which also contributes to cathodic water supply and increases maximum current density is high for the used membrane material.

This causes high methanol losses and significantly reduces methanol efficiency especially for low current densities and in case that methanol concentration at anode rises due to water loss by diffusion. The latter is intensified if methanol solution is recycled which is necessary to achieve reasonable efficiencies. Therefore, stable water level in the methanol recycling loop is required to achieve high efficiencies during long term operation. Anodic water level can be stabilised by adjusting air excess ratio to a specific value which depends on current density and is influenced by several parameters such as thickness of GDL and membrane, GDL porosity, diffusion coefficients and cathodic inlet conditions.

Water transport through membrane is essential for operation of alkaline anion exchange membrane fuel cells and should therefore be considered when designing new membrane material. However, membrane thickness is also an important parameter and if diffusivity of methanol cannot be reduced, it should be considered to increase membrane thickness in order to reduce methanol cross-over although thicker membrane also reduces water diffusion and increases membrane resistance. For further analysis e.g. of the influence of methanol cross-over on fuel cell performance, the model of Chapter 5 should be extended by including reaction kinetics as well as adsorption kinetics of reactants, especially of oxygen. The influence of methanol concentration or GDL at anode on methanol cross-over and, thus, on methanol efficiency and fuel cell performance are also open questions. Furthermore, this thesis considers water transport through membrane but neglects water transport from membrane to reaction zone at catalyst particles through ionomer which can also be a limiting step. To analyse at which part of the catalyst layer water supply is sufficient, a local description of cathodic catalyst layer is required. Thus, further studies that also consider detailed description of catalyst layer are desired. However, a lot of specific experiments are necessary to gain parameters that are required for this extension of the model.

Bibliography

[1] J.H. Reid. Process of generating electricity. *United States patent*, 1903. Aug 11. US 736016.

[2] J.H. Reid. Gas battery. *United States patent*, 1903. Aug 11. US 736017.

[3] J.H. Reid. Gas battery. *United States patent*, 1904. Apr 19. US 757637.

[4] F.T. Bacon. Fuel cells, past, present and future. *Electrochimica Acta*, 14(7):569 – 585, 1969.

[5] N.H. Behling. Chapter 3 - history of alkaline fuel cells. In N.H. Behling, editor, *Fuel Cells*, pages 37 – 51. Elsevier, 2013.

[6] M. Warshay and P.R. Prokopius. The fuel cell in space: Yesterday, today and tomorrow. *NASA Technical Memorandum*, 102366, 1989.

[7] W.T. Grubb. Fuel cell. *United States patent*, 1959. Nov 17. US 2913511.

[8] W.G. Grot. Laminates of support material and fluorinated polymer containing pendant side chains containing sulfonyl groups. *United States patent*, 1973. Nov 06. US 3770567.

[9] E. Agel, J. Bouet, and J.F. Fauvarque. Characterization and use of anionic membranes for alkaline fuel cells. *Journal of Power Sources*, 101(2):267 – 274, 2001.

[10] J.R. Varcoe, R.C.T. Slade, and E. Lam How Yee. An alkaline polymer electrochemical interface: a breakthrough in application of alkaline anion-exchange membranes in fuel cells. *Chemical Communications*, (13):1428–1429, 2006.

[11] C. Weinzierl and U. Krewer. Model-based analysis of water management in alkaline direct methanol fuel cells. *Journal of Power Sources*, 268:911 – 921, 2014.

[12] C. Y. Du, T. S. Zhao, and W. W. Yang. Effect of methanol crossover on the cathode behavior of a DMFC: A half-cell investigation. *Electrochemica Acta*, 52(16):5266–5271, APR 30 2007.

[13] G. Merle, M. Wessling, and K. Nijmeijer. Anion exchange membranes for alkaline fuel cells: A review. *Journal of Membrane Science*, 377(12):1 – 35, 2011.

[14] E. Antolini and E.R. Gonzalez. Alkaline direct alcohol fuel cells. *Journal of Power Sources*, 195(11):3431 – 3450, 2010.

[15] P.B. Antanassov, D.R. Dekel, A.M. Herring, M.A. Hickner, P.A. Kohl, A.R. Kucernak, W.E. Mustain, K. Nijmeijer, K. Scott, J.R. Varcoe, T. Xu, and L. Zhuang. Anion-exchange membranes in electrochemical energy systems. *Energy & environmental science*, 7(10):3135 – 3191, 2014.

[16] S.D. Sajjad, D. Liu, Z. Wei, S. Sakri, Y. Shen, Y. Hong, and F. Liu. Guanidinium based blend anion exchange membranes for direct methanol alkaline fuel cells (dmafcs). *Journal of Power Sources*, 300:95 – 103, 2015.

[17] A.H.N. Rao, H.J. Kim, S. Nam, and T.H. Kim. Cardo poly(arylene ether sulfone) block copolymers with pendant imidazolium side chains as novel anion exchange membranes for direct methanol alkaline fuel cell. *Polymer*, 54(26):6918 – 6928, 2013.

[18] L. Wu and T. Xu. Improving anion exchange membranes for dmafcs by inter-crosslinking cppo/bppo blends. *Journal of Membrane Science*, 322(2):286 – 292, 2008.

[19] Y. Wang, L. Li, L. Hu, L. Zhuang, J. Lu, and B. Xu. A feasibility analysis for alkaline membrane direct methanol fuel cell: thermodynamic disadvantages versus kinetic advantages. *Electrochemistry Communications*, 5(8):662 – 666, 2003.

[20] E.H. Yu, U. Krewer, and K. Scott. Principles and materials aspects of direct alkaline alcohol fuel cells. *Energies*, 3(8):1499–1528, 2010.

[21] C. Domínguez, F.J. Pérez-Alonso, M.A. Salam, S.A. Al-Thabaiti, M.A. Peña, F.J. García-García, L. Barrio, and S. Rojas. Repercussion of the carbon matrix for the activity and stability of Fe/N/C electrocatalysts for the oxygen reduction reaction. *Applied Catalysis B: Environmental*, 183:185 – 196, 2016.

[22] T. Jurzinsky, P. Kammerer, C. Cremers, K. Pinkwart, and J. Tübke. Investigation of ruthenium promoted palladium catalysts for methanol electrooxidation in alkaline media. *Journal of Power Sources*, 303:182 – 193, 2016.

[23] K. Scott, E. Yu, G. Vlachogiannopoulos, M. Shivare, and N. Duteanu. Performance of a direct methanol alkaline membrane fuel cell. *Journal of Power Sources*, 175(1):452 – 457, 2008.

[24] S.D. Poynton, J.P. Kizewski, R.C.T. Slade, and J.R. Varcoe. Novel electrolyte membranes and non-Pt catalysts for low temperature fuel cells. *Solid State Ionics*, 181(3-4, SI):219–222, FEB 24 2010. 14th International Conference on Solid State Protonic Conductors (SSPC-14), Kyoto, Japan, Sep 07-11, 2008.

[25] Y.S. Li, T.S. Zhao, and W.W. Yang. Measurements of water uptake and transport properties in anion-exchange membranes. *International Journal of Hydrogen Energy*, 35(11):5656 – 5665, 2010. 3rd Argentinean and 2nd Latin American Congress inHydrogen and Sustainable Energy Sources3rd Argentinean and 2nd Latin American Congress in Hydrogen and Sustainable Energy Sources.

[26] D. García-Nieto and V.M. Barragán. A comparative study of the electroosmotic behavior of cation and anion exchange membranes in alcohol-water media. *Electrochimica Acta*, 154:166 – 176, 2015.

[27] T. Yamanaka, T. Takeguchi, H. Takahashi, and W. Ueda. Water transport during ion conduction in anion-exchange and cation-exchange membranes. *Journal of the Electrochemical Society*, 156(7):B831–B835, 2009.

[28] Y.S. Li, T.S. Zhao, and R. Chen. Cathode flooding behaviour in alkaline direct ethanol fuel cells. *Journal of Power Sources*, 196(1):133 – 139, 2011.

[29] Y.S. Li, T.S. Zhao, J.B. Xu, S.Y. Shen, and W.W. Yang. Effect of cathode micro-porous layer on performance of anion-exchange membrane direct ethanol fuel cells. *Journal of Power Sources*, 196(4):1802 – 1807, 2011.

[30] H. Kim, J. Zhou, M. Ünlü, I. Anestis-Richard, K. Joseph, and P.A. Kohl. The effect of hydrophobicity in alkaline electrodes for passive {DMFC}. *Electrochimica Acta*, 56(8):3085 – 3090, 2011.

[31] A. Khalidi, B. Lafage, P. Taxil, and M.J. Clifton. Water transport in the porous electrodes of a hydrogen-oxygen fuel cell. *International Journal of Hydrogen Energy*, 19(3):245–251, 1994.

[32] H. Zhang, H. Ohashi, T. Tamaki, and T. Yamaguchi. Direction and management of water movement in solid-state alkaline fuel cells. *Journal of Physikal Chemistry C,*, 116(14):76507657, 2012.

[33] J.H. Jo and Yi S.C. A computational simulation of an alkaline fuel cell. *Journal of Power Sources*, 84(1):87 – 106, 1999.

[34] M.C. Kimble and R.E. White. A mathematical-model of a hydrogen oxygen alkaline fuel-cell. *Journal of the Electrochemical Society*, 138(11):3370–3382, NOV 1991.

[35] M.C. Kimble and R.E. White. Parameter sensitivity and optimization prediction of a hydrogen oxygen alkaline fuel-cell. *Journal of the Electrochemical Society*, 139(2):478–484, Feb 1992.

[36] L. An, Z.H. Chai, L. Zeng, P. Tan, and Zhao T.S. Mathematical modeling of alkaline direct ethanol fuel cells. *International Journal of Hydrogen Energy*, 38(32):14067 – 14075, 2013.

[37] H. Deng, J. Chen, K. Jiao, and X. Huang. An analytical model for alkaline membrane direct methanol fuel cell. *International Journal of Heat and Mass Transfer*, 74:376 – 390, 2014.

[38] I. Verhaert, S. Verhelst, G. Janssen, G. Mulder, and M. De Paepe. Water management in an alkaline fuel cell. *International Journal of Hydrogen Energy*, 36(17):11011 – 11024, 2011. International Conference on Hydrogen Production (ICH2P)-2010.

[39] K. Jiao, S. Huo, M. Zu, D. Jiao, J. Chen, and Q. Du. An analytical model for hydrogen alkaline anion exchange membrane fuel cell. *International Journal of Hydrogen Energy*, 40(8):3300 – 3312, 2015.

[40] K. Jiao, P. He, Q. Du, and Y. Yin. Three-dimensional multiphase modeling of alkaline anion exchange membrane fuel cell. *International Journal of Hydrogen Energy*, 39(11):5981 – 5995, 2014.

[41] S. Huo, H. Deng, Y. Chang, and K. Jiao. Water management in alkaline anion exchange membrane fuel cell anode. *International Journal of Hydrogen Energy*, 37(23):18389 – 18402, 2012.

[42] H. Deng, D. Jiao, M. Zu, J. Chen, K. Jiao, and X. Huang. Modeling of passive alkaline membrane direct methanol fuel cell. *Electrochimica Acta*, 154:430 – 446, 2015.

[43] C. Weinzierl and U. Krewer. Model-based analysis of water management at anode of alkaline direct methanol fuel cells. *Chemical Engineering Science*, 143:181–193, 2016. cited By 1.

[44] R. Janarthanan, A. Serov, S.K. Pilli, D.A. Gamarra, P. Atanassov, M.R. Hibbs, and A.M. Herring. Direct methanol anion exchange membrane fuel cell with a non-platinum group metal cathode based on iron-aminoantipyrine catalyst. *Electrochimica Acta*, 175:202 – 208, 2015. Polymer Electrolytes Selection of papers from the 14th International Symposium (ISPE-14) 24-29 August 2014, Geelong, VIC, Australia.

[45] C. Coutanceau, L. Demarconnay, C. Lamy, and J.M. Léger. Development of electrocatalysts for solid alkaline fuel cell (safc). *Journal of Power Sources*, 156(1):14 – 19, 2006. Selected papers from the 2nd France-Deutschland Fuel Cell Conference2nd France-Deutschland Fuel Cell Conference.

[46] P.S. Khadke and U. Krewer. Mass-transport characteristics of oxygen at pt/anion exchange ionomer interface. *The Journal of Physical Chemistry C*, 118(21):11215–11223, 2014.

[47] VDI Gesellschaft. *VDI-Wärmeatlas*. Springer, Berlin, 10 edition, 2006. Chapter D.

[48] L. Li and Y. Wang. Quaternized polyethersulfone cardo anion exchange membranes for direct methanol alkaline fuel cells. *Journal of Membrane Science*, 262(12):1 – 4, 2005.

[49] F. Zenith, M. Kraus, and U. Krewer. Model-based analysis of micro-separators for portable direct methanol fuel-cell systems. *Computers & Chemical Engineering*, 38:64 – 73, 2012.

[50] G. Couture, A. Alaaeddine, F. Boschet, and B. Ameduri. Polymeric materials as anion-exchange membranes for alkaline fuel cells. *Progress in Polymer Science*, 36(11):1521 – 1557, 2011. Special Topic: Energy Related Materials.

[51] M. Alesker, M. Page, M. Shviro, Y. Paska, G. Gershinsky, D.R. Dekel, and D. Zitoun. Palladium/nickel bifunctional electrocatalyst for hydrogen oxi-

dation reaction in alkaline membrane fuel cell. *Journal of Power Sources*, 304:332 – 339, 2016.

[52] J.H. Chang, J.H. Park, G.G. Park, C.S. Kim, and O.O. Park. Proton-conducting composite membranes derived from sulfonated hydrocarbon and inorganic materials. *Journal of Power Sources*, 124(1):18 – 25, 2003.

[53] A. Anis, A.K. Banthia, and S. Bandyopadhyay. Synthesis & characterization of pva/sta composite polymer electrolyte membranes for fuel cell application. *Journal of Materials Engineering and Performance*, 17(5):772–779, 2008.

[54] R. O'Hayre, S.W. Cha, W. Colella, and F.B. Prinz. *Fuel Cell Fundamentals*. John Wiley & Sons, Inc, 2016.

[55] W. Lichten. *Skriptum Fehlerrechnung: Eine Einfhrung in die Analyse experimenteller Daten fr Studenten der Naturwissenschaften – Mit Programmen fr alle gngigen Taschenrechner*. Springer Verlag, Berlin-Heidelberg, german edition edition, 1988.

[56] A.B. Littlewood. *Gas Chromatography – Principles, Techniques and Application*. Academic Press, New York – London, 1 edition, 1962.

[57] H. Bahrami and A. Faghri. Multi-layer membrane model for mass transport in a direct ethanol fuel cell using an alkaline anion exchange membrane. *Journal of Power Sources*, 218:286 – 296, 2012.

[58] M. Jischa. *Konvektiver Impuls-, Wärme- und Stoffaustausch*. Vieweg, Braunschweig, 1982.

[59] W. Neubrand. *Modellbildung und Simulation von Elektromembranverfahren*. Logos, Berlin, 1999.

[60] H. D. Baer and K. Stephan. *Heat and Mass Transfer*. Springer Verlag, Berlin-Heidelberg, 3 edition, 2011. Chapter 1, Page 81.

[61] T. Melin and R. Rautenbach. *Membranverfahren – Grundlagen der Modul- und Anlagenauslegung*. Springer Verlag, Berlin-Heidelberg, 3 edition, 2007. Chapter 3, Fig. 3.9.

APPENDIX A

Derivations and Additional Definitions

A.1 Derivation of Equations for Fuel Cell Modelling

Volume flow rates at outlet of anode and cathode are derived as follows: Considering that concentrations depend on the volume they are based on, the amount of a substance in one of the chambers can be defined in two different ways:

$$n_\beta^{\mathrm{loc}} = c_\beta^{\mathrm{loc}} V^{\mathrm{loc}} = c_\beta^{*,\mathrm{loc}} V_\beta^{\mathrm{loc}} \tag{A.1}$$

with the concentration of the pure substance $c_\beta^{*,\mathrm{loc}}$ and the partial volume V_β^{loc} of substance β at location $\mathrm{loc} \in \{\mathrm{A}, \mathrm{C}\}$. Since pressure and temperature in the fuel cell are assumed to be constant, $c_\beta^{*,\mathrm{loc}}$ does not change with time and the component balances can be rearranged to calculate the change of the partial volume of a component:

$$c_\beta^{*,\mathrm{loc}} \frac{dV_\beta^{\mathrm{loc}}}{dt} = c_{\beta,\mathrm{in}}^{*,\mathrm{loc}} F_{\beta,\mathrm{in}}^{\mathrm{loc}} - c_\beta^{*,\mathrm{loc}} F_{\beta,\mathrm{out}}^{\mathrm{loc}} + \dot{n}_\beta^{\mathrm{loc,diff}} + \sigma_\beta^{\mathrm{loc}} \tag{A.2}$$

Neglecting mixing volumes, the sum of the partial volumes of all components is equal to the total volume. Since total volumes of anode and cathode are constant, the sum of Eq. (A.2) for all components can be used to calculate the outlet volume flow rates of anode and cathode chamber:

$$\begin{aligned}
\frac{dV^{\mathrm{loc}}}{dt} &= \sum_\beta \frac{dV_\beta^{\mathrm{loc}}}{dt} = 0 \\
&= \sum_\beta \left(\frac{c_{\beta,\mathrm{in}}^{*,\mathrm{loc}}}{c_\beta^{*,\mathrm{loc}}} F_{\beta,\mathrm{in}}^{\mathrm{loc}} - F_{\beta,\mathrm{out}}^{\mathrm{loc}} + \frac{\dot{n}_\beta^{\mathrm{loc,diff}}}{c_\beta^{*,\mathrm{loc}}} + \frac{\sigma_\beta^{\mathrm{loc}}}{c_\beta^{*,\mathrm{loc}}} \right) \\
&= \sum_\beta \left(\frac{c_{\beta,\mathrm{in}}^{*,\mathrm{loc}}}{c_\beta^{*,\mathrm{loc}}} F_{\beta,\mathrm{in}}^{\mathrm{loc}} + \frac{\dot{n}_\beta^{\mathrm{loc,diff}}}{c_\beta^{*,\mathrm{loc}}} + \frac{\sigma_\beta^{\mathrm{loc}}}{c_\beta^{*,\mathrm{loc}}} \right) - F_{\mathrm{out}}^{\mathrm{loc}}
\end{aligned} \tag{A.3}$$

Considering that $c_\beta^{*,\mathrm{loc}}$ is constant for liquid components and it is equal to total gas concentration for gas components, the volume flows leaving anode and cathode are calculated by:

$$F_{\mathrm{out}}^{\mathrm{A}} = F_{\mathrm{in}}^{\mathrm{A}} + \frac{\dot{n}_{\mathrm{W}}^{\mathrm{A,diff}}}{c_{\mathrm{W}}^{*}} + \frac{\dot{n}_{\mathrm{Me}}^{\mathrm{A,diff}}}{c_{\mathrm{Me}}^{*}} + \sum_{\alpha} \frac{\sigma_\alpha^{\mathrm{A}}}{c_\alpha^{*\mathrm{A}}} \tag{A.4}$$

$$F_{\mathrm{out}}^{\mathrm{C}} = \frac{c_{\mathrm{gas,in}}^{\mathrm{C}}}{c_{\mathrm{gas}}^{\mathrm{C}}} F_{\mathrm{in}}^{\mathrm{C}} + \sum_{\gamma} \frac{\dot{n}_\gamma^{\mathrm{C,diff}} + \sigma_\gamma^{\mathrm{C}}}{c_{\mathrm{gas}}^{\mathrm{C}}} \tag{A.5}$$

A.2 Additional Definitions for Chapter 4

A.2.1 Membrane

The substitutions for the discretised form of mass balances in the membrane Eqs. (4.26) and (4.27) are defined in the following.

For water:

$$I_{\mathrm{W},ijh}^{\mathrm{M,a}} = \frac{f_{i+1jh}^{\mathrm{M}} - f_{ijh}^{\mathrm{M}}}{\left(\Delta z^{\mathrm{M}}\right)^2 \left(2 + f_{i+1jh}^{\mathrm{M}} + f_{ijh}^{\mathrm{M}}\right)} \overset{i=n}{=} \frac{f_{jh}^{\mathrm{Mg}} - f_{njh}^{\mathrm{M}}}{\left(\Delta z^{\mathrm{M}}\right)^2 \left(1 + f_{jh}^{\mathrm{Mg}}\right)} \tag{A.6}$$

$$I_{\mathrm{W},ijh}^{\mathrm{M,b}} = \frac{f_{ijh}^{\mathrm{M}} - f_{i-1jh}^{\mathrm{M}}}{\left(\Delta z^{\mathrm{M}}\right)^2 \left(2 + f_{ijh}^{\mathrm{M}} + f_{i-1jh}^{\mathrm{M}}\right)} \overset{i=1}{=} \frac{f_{1jh}^{\mathrm{M}} - f^{\mathrm{Ml}}}{\left(\Delta z^{\mathrm{M}}\right)^2 \left(1 + f^{\mathrm{Ml}}\right)} \tag{A.7}$$

$$I_{\mathrm{W},ijh}^{\mathrm{M,c}} = \frac{2}{\Delta r} \frac{r_{j+1}}{\left(r_{j+1}^2 - r_j^2\right)} \frac{f_{ij+1h}^{\mathrm{M}} - f_{ijh}^{\mathrm{M}}}{\left(2 + f_{ij+1h}^{\mathrm{M}} + f_{ijh}^{\mathrm{M}}\right)} \overset{j=m}{=} 0 \tag{A.8}$$

$$I_{\mathrm{W},ijh}^{\mathrm{M,d}} = \frac{2}{\Delta r} \frac{r_j}{\left(r_{j+1}^2 - r_j^2\right)} \frac{f_{ijh}^{\mathrm{M}} - f_{ij-1h}^{\mathrm{M}}}{\left(2 + f_{ijh}^{\mathrm{M}} + f_{ij-1h}^{\mathrm{M}}\right)} \overset{j=1}{=} 0 \tag{A.9}$$

$$I_{\mathrm{W},ijh}^{\mathrm{M,e}} = \frac{2}{\Delta \varphi^2} \frac{\ln\left(\frac{r_{j+1}}{r_j}\right)}{\left(r_{j+1}^2 - r_j^2\right)} \frac{f_{ijh+1}^{\mathrm{M}} - f_{ijh}^{\mathrm{M}}}{\left(2 + f_{ijh+1}^{\mathrm{M}} + f_{ijh}^{\mathrm{M}}\right)} \overset{j=1}{=} 0 \tag{A.10}$$

$$\overset{h=a}{=} \frac{2}{\Delta \varphi^2} \frac{\ln\left(\frac{r_{j+1}}{r_j}\right)}{\left(r_{j+1}^2 - r_j^2\right)} \frac{f_{ij1}^{\mathrm{M}} - f_{ija}^{\mathrm{M}}}{\left(2 + f_{ij1}^{\mathrm{M}} + f_{ija}^{\mathrm{M}}\right)}$$

$$I_{\mathrm{W},ijh}^{\mathrm{M,f}} = \frac{2}{\Delta \varphi^2} \frac{\ln\left(\frac{r_{j+1}}{r_j}\right)}{\left(r_{j+1}^2 - r_j^2\right)} \frac{f_{ijh}^{\mathrm{M}} - f_{ijh-1}^{\mathrm{M}}}{\left(2 + f_{ijh}^{\mathrm{M}} + f_{ijh-1}^{\mathrm{M}}\right)} \overset{j=1}{=} 0 \tag{A.11}$$

$$\overset{h=1}{=} I_{\mathrm{W},ija}^{\mathrm{M,e}}$$

For methanol:

$$I^{\mathrm{M,a}}_{\mathrm{Me},\,ijh} = \frac{\left(1+f^{\mathrm{M}}_{ijh}\right)c^{\mathrm{M}}_{\mathrm{Me},\,i+1jh} - \left(1+f^{\mathrm{M}}_{i+1jh}\right)c^{\mathrm{M}}_{\mathrm{Me},\,ijh}}{\left(\rho^{\mathrm{M}}_{i+1jh}+\rho^{\mathrm{M}}_{ijh}\right)\left(\Delta z^{\mathrm{M}}\right)^2} \tag{A.12}$$

$$\overset{i=n}{=} \frac{\left(1+f^{\mathrm{M}}_{njh}\right)c^{\mathrm{Mg}}_{\mathrm{Me},\,jh} - \left(1+f^{\mathrm{Mg}}_{jh}\right)c^{\mathrm{M}}_{\mathrm{Me},\,njh}}{\rho^{\mathrm{Mg}}_{jh}\left(\Delta z^{\mathrm{M}}\right)^2}$$

$$I^{\mathrm{M,b}}_{\mathrm{Me},\,ijh} = \frac{\left(1+f^{\mathrm{M}}_{i-1jh}\right)c^{\mathrm{M}}_{\mathrm{Me},\,ijh} - \left(1+f^{\mathrm{M}}_{ijh}\right)c^{\mathrm{M}}_{\mathrm{Me},\,i-1jh}}{\left(\rho^{\mathrm{M}}_{ijh}+\rho^{\mathrm{M}}_{i-1jh}\right)\left(\Delta z^{\mathrm{M}}\right)^2} \tag{A.13}$$

$$\overset{i=1}{=} \frac{\left(1+f^{\mathrm{Ml}}_{jh}\right)c^{\mathrm{M}}_{\mathrm{Me},\,1jh} - \left(1+f^{\mathrm{M}}_{1jh}\right)c^{\mathrm{Ml}}_{\mathrm{Me},\,jh}}{\rho^{\mathrm{Ml}}_{jh}\left(\Delta z^{\mathrm{M}}\right)^2}$$

$$I^{\mathrm{M,c}}_{\mathrm{Me},\,ijh} = \frac{2\,r_{j+1}}{r^2_{j+1}-r^2_j}\,\frac{\left(1+f^{\mathrm{M}}_{ijh}\right)c^{\mathrm{M}}_{\mathrm{Me},\,ij+1h} - \left(1+f^{\mathrm{M}}_{ij+1h}\right)c^{\mathrm{M}}_{\mathrm{Me},\,ijh}}{\left(\rho^{\mathrm{M}}_{ij+1h}+\rho^{\mathrm{M}}_{ijh}\right)\Delta r} \tag{A.14}$$

$$\overset{j=m}{=} 0$$

$$I^{\mathrm{M,d}}_{\mathrm{Me},\,ijh} = \frac{2\,r_j}{r^2_{j+1}-r^2_j}\,\frac{\left(1+f^{\mathrm{M}}_{ij-1h}\right)c^{\mathrm{M}}_{\mathrm{Me},\,ijh} - \left(1+f^{\mathrm{M}}_{ijh}\right)c^{\mathrm{M}}_{\mathrm{Me},\,ij-1h}}{\left(\rho^{\mathrm{M}}_{ijh}+\rho^{\mathrm{M}}_{ij-1h}\right)\Delta r} \tag{A.15}$$

$$\overset{j=1}{=} 0$$

$$I^{\mathrm{M,e}}_{\mathrm{Me},\,ijh} = \frac{2\ln\frac{r_{j+1}}{r_j}}{r^2_{j+1}-r^2_j}\,\frac{\left(1+f^{\mathrm{M}}_{ijh}\right)c^{\mathrm{M}}_{\mathrm{Me},\,ijh+1} - \left(1+f^{\mathrm{M}}_{ijh+1}\right)c^{\mathrm{M}}_{\mathrm{Me},\,ijh}}{\left(\rho^{\mathrm{M}}_{ijh+1}+\rho^{\mathrm{M}}_{ijh}\right)\Delta\varphi^2} \tag{A.16}$$

$$\overset{h=a}{=} \frac{2\ln\frac{r_{j+1}}{r_j}}{r^2_{j+1}-r^2_j}\,\frac{\left(1+f^{\mathrm{M}}_{ija}\right)c^{\mathrm{M}}_{\mathrm{Me},\,ij1} - \left(1+f^{\mathrm{M}}_{ij1}\right)c^{\mathrm{M}}_{\mathrm{Me},\,ija}}{\left(\rho^{\mathrm{M}}_{ij1}+\rho^{\mathrm{M}}_{ija}\right)\Delta\varphi^2}$$

$$\overset{j=1}{=} 0$$

$$I^{\mathrm{M,f}}_{\mathrm{Me},\,ijh} = \frac{2\ln\frac{r_{j+1}}{r_j}}{r^2_{j+1}-r^2_j}\,\frac{\left(1+f^{\mathrm{M}}_{ijh-1}\right)c^{\mathrm{M}}_{\mathrm{Me},\,ijh} - \left(1+f^{\mathrm{M}}_{ijh}\right)c^{\mathrm{M}}_{\mathrm{Me},\,ijh-1}}{\left(\rho^{\mathrm{M}}_{ijh}+\rho^{\mathrm{M}}_{ijh-1}\right)\Delta\varphi^2} \tag{A.17}$$

$$\overset{h=1}{=} \frac{2\ln\frac{r_{j+1}}{r_j}}{r^2_{j+1}-r^2_j}\,\frac{\left(1+f^{\mathrm{M}}_{ija}\right)c^{\mathrm{M}}_{\mathrm{Me},\,ij1} - \left(1+f^{\mathrm{M}}_{ij1}\right)c^{\mathrm{M}}_{\mathrm{Me},\,ija}}{\left(\rho^{\mathrm{M}}_{ij1}+\rho^{\mathrm{M}}_{ija}\right)\Delta\varphi^2}$$

$$\overset{j=1}{=} 0$$

A.2.2 Diffusion Layer

Substitutions in the diffusion layer are defined as:

$$I^{\mathrm{DL,a}}_{\alpha,ijh} = B^{\mathrm{DL}}_{\beta,i+1}\frac{c^{\mathrm{DL}}_{\alpha,i+1jh}-c^{\mathrm{DL}}_{\alpha,ijh}}{(\Delta z^{\mathrm{DL}}_{jh})^2} - B^{\mathrm{DL}}_{\alpha,i+1}\frac{c^{\mathrm{DL}}_{\beta,i+1jh}-c^{\mathrm{DL}}_{\beta,ijh}}{(\Delta z^{\mathrm{DL}}_{jh})^2} \tag{A.18}$$

$$\overset{i=l}{=} B^{\mathrm{G}}_{\beta}\frac{c^{\mathrm{G}}_{\alpha}-c^{\mathrm{DL}}_{\alpha,ljh}}{\frac{(\Delta z^{\mathrm{DL}}_{jh})^2}{2}} - B^{\mathrm{G}}_{\alpha}\frac{c^{\mathrm{G}}_{\beta}-c^{\mathrm{DL}}_{\beta,ljh}}{\frac{(\Delta z^{\mathrm{DL}}_{jh})^2}{2}} \tag{A.19}$$

$$I^{\mathrm{DL,b}}_{\alpha,ijh} = B^{\mathrm{DL}}_{\beta,i}\frac{c^{\mathrm{DL}}_{\alpha,ijh}-c^{\mathrm{DL}}_{\alpha,i-1jh}}{(\Delta z^{\mathrm{DL}}_{jh})^2} - B^{\mathrm{DL}}_{\alpha,i}\frac{c^{\mathrm{DL}}_{\beta,ijh}-c^{\mathrm{DL}}_{\beta,i-1jh}}{(\Delta z^{\mathrm{DL}}_{jh})^2} \tag{A.20}$$

$$\overset{i=1}{=} B^{\mathrm{PB}}_{\beta}\frac{c^{\mathrm{DL}}_{\alpha,1jh}-c^{\mathrm{PB}}_{\alpha}}{\frac{(\Delta z^{\mathrm{DL}}_{jh})^2}{2}} - B^{\mathrm{PB}}_{\alpha}\frac{c^{\mathrm{DL}}_{\beta,1jh}-c^{\mathrm{PB}}_{\beta}}{\frac{(\Delta z^{\mathrm{DL}}_{jh})^2}{2}} \tag{A.21}$$

$$I^{\mathrm{DL,c}}_{\alpha,ijh} = r_{j+1}\,\Delta z^{\mathrm{DL}}_{h}\big|_{r_{j+1}}\left(B^{\mathrm{DL}}_{\beta,j+1}\left(c^{\mathrm{DL}}_{\alpha,ij+1h}-c^{\mathrm{DL}}_{\alpha,ijh}\right) - B^{\mathrm{DL}}_{\alpha,j+1}\left(c^{\mathrm{DL}}_{\beta,ij+1h}-c^{\mathrm{DL}}_{\beta,ijh}\right)\right) \tag{A.22}$$

$$\overset{j=m}{=} 0$$

$$I^{\mathrm{DL,d}}_{\alpha,ijh} = r_{j}\,\Delta z^{\mathrm{DL}}_{h}\big|_{r_{j}}\left(B^{\mathrm{DL}}_{\beta,j}\left(c^{\mathrm{DL}}_{\alpha,ijh}-c^{\mathrm{DL}}_{\alpha,ij-1h}\right) - B^{\mathrm{DL}}_{\alpha,j}\left(c^{\mathrm{DL}}_{\beta,ijh}-c^{\mathrm{DL}}_{\beta,ij-1h}\right)\right) \tag{A.23}$$

$$\overset{j=1}{=} 0$$

$$\begin{aligned} I^{\mathrm{DL,e}}_{\alpha,ijh} &= \ln\frac{r_{j+1}}{r_{j}}\,\Delta z^{\mathrm{DL}}_{j}\big|_{\varphi_{h+1}}\left(B^{\mathrm{DL}}_{\beta,h+1}\left(c^{\mathrm{DL}}_{\alpha,ijh+1}-c^{\mathrm{DL}}_{\alpha,ijh}\right)\ldots\right. \\ &\qquad \left.\ldots - B^{\mathrm{DL}}_{\alpha,h+1}\left(c^{\mathrm{DL}}_{\beta,ijh+1}-c^{\mathrm{DL}}_{\beta,ijh}\right)\right) \end{aligned} \tag{A.24}$$

$$\overset{j=1}{=} 0$$

$$\overset{h=a}{=} \ln\frac{r_{j+1}}{r_{j}}\,\Delta z^{\mathrm{DL}}_{j}\big|_{\varphi_{1}}\left(B^{\mathrm{DL}}_{\beta,h=1}\left(c^{\mathrm{DL}}_{\alpha,ij1}-c^{\mathrm{DL}}_{\alpha,ija}\right) - B^{\mathrm{DL}}_{\alpha,h=1}\left(c^{\mathrm{DL}}_{\beta,ij1}-c^{\mathrm{DL}}_{\beta,ija}\right)\right)$$

$$I^{\mathrm{DL,f}}_{\alpha,ijh} = \ln\frac{r_{j+1}}{r_{j}}\,\Delta z^{\mathrm{DL}}_{j}\big|_{\varphi_{h}}\left(B^{\mathrm{DL}}_{\beta,h}\left(c^{\mathrm{DL}}_{\alpha,ijh}-c^{\mathrm{DL}}_{\alpha,ijh-1}\right) - B^{\mathrm{DL}}_{\alpha,h}\left(c^{\mathrm{DL}}_{\beta,ijh}-c^{\mathrm{DL}}_{\beta,ijh-1}\right)\right) \tag{A.25}$$

$$\overset{j=1}{=} 0$$

$$\overset{h=1}{=} I^{\mathrm{DL,e}}_{\alpha,ija}$$

with

$$B^{\mathrm{G}}_{\alpha} = \frac{(M_{\beta}-M_{\mathrm{He}})\,y^{\mathrm{G}}_{\alpha}}{M^{\mathrm{G}}_{\mathrm{gas}}} \tag{A.26}$$

$$B^{\mathrm{G}}_{\beta} = \frac{M_{\mathrm{He}}+(M_{\beta}-M_{\mathrm{He}})\,y^{\mathrm{G}}_{\beta}}{M^{\mathrm{G}}_{\mathrm{gas}}} \tag{A.27}$$

$$B^{\mathrm{PB}}_{\alpha} = \frac{(M_{\beta}-M_{\mathrm{He}})\,y^{\mathrm{PB}}_{\alpha,jh}}{M^{\mathrm{PB}}_{\mathrm{gas}}} \tag{A.28}$$

$$B^{\mathrm{PB}}_{\beta} = \frac{M_{\mathrm{He}}+(M_{\beta}-M_{\mathrm{He}})\,y^{\mathrm{PB}}_{\beta,jh}}{M^{\mathrm{PB}}_{\mathrm{gas}}} \tag{A.29}$$

$$B^{\mathrm{DL}}_{\alpha,i} = \frac{\left(M_\beta - M_{\mathrm{He}}\right) y^{\mathrm{DL}}_{\alpha,jh}\Big|_i}{M^{\mathrm{DL}}_{\mathrm{gas}}\Big|_i} \tag{A.30}$$

$$B^{\mathrm{DL}}_{\beta,i} = \frac{M_{\mathrm{He}} + \left(M_\beta - M_{\mathrm{He}}\right) y^{\mathrm{DL}}_{\beta,jh}\Big|_i}{M^{\mathrm{DL}}_{\mathrm{gas}}\Big|_i} \tag{A.31}$$

for $\alpha \neq \beta \in \{\mathrm{W}, \mathrm{Me}\}$. B^{DL}_{α} and B^{DL}_{β} for j and h are defined according to Eqs. (A.30) and (A.31).

A.2.3 Phase Boundary

For methanol, Eq. (4.61) result in a quadratic equation that is solved for $c^{\mathrm{Mg}}_{\mathrm{Me},jh}$:

$$\begin{aligned}
0 = \Bigg[& D^{\mathrm{DL}}_{\mathrm{Me}} M_{\mathrm{Me}} \Bigg(\left(M_{\mathrm{He}} + \left(M_{\mathrm{W}} - M_{\mathrm{He}}\right) y^{\mathrm{PB}}_{\mathrm{W},jh}\right) c^{\mathrm{DL}}_{\mathrm{Me},1jh} \ldots \\
& \ldots - \frac{p^{\mathrm{o}}_{\mathrm{Me}}}{p} \left(M_{\mathrm{He}} c_{\mathrm{gas}} + \left(M_{\mathrm{W}} - M_{\mathrm{He}}\right) c^{\mathrm{DL}}_{\mathrm{W},1jh}\right) \Bigg) - D^{\mathrm{M}}_{\mathrm{Me}} \rho^{\mathrm{M}}_{\mathrm{dry}} \frac{\Delta z^{\mathrm{DL}}_{jh}}{\Delta z^{\mathrm{M}}} \left(1 + f^{\mathrm{M}}_{njh}\right) \ldots \\
& \ldots \cdot \left(\left(M_{\mathrm{Me}} - M_{\mathrm{He}}\right) \frac{p^{\mathrm{o}}_{\mathrm{M}}}{p} + M_{\mathrm{He}} + \left(M_{\mathrm{W}} - M_{\mathrm{He}}\right) y^{\mathrm{PB}}_{\mathrm{W},jh} \right) \Bigg] \left(c^{\mathrm{Mg}}_{\mathrm{Me},jh}\right)^2 \ldots \\
& \ldots + \Bigg[\left(M_{\mathrm{He}} + \left(M_{\mathrm{W}} - M_{\mathrm{He}}\right) y^{\mathrm{PB}}_{\mathrm{W},jh}\right) \left(D^{\mathrm{DL}}_{\mathrm{Me}} c^{\mathrm{DL}}_{\mathrm{Me},1jh} \left(1 + f^{\mathrm{Mg}}_{jh} \left(1 + \frac{M_{\mathrm{Me}}}{M_{\mathrm{W}}}\right)\right) \ldots \right. \\
& \ldots - D^{\mathrm{M}}_{\mathrm{Me}} \frac{\Delta z^{\mathrm{DL}}_{jh}}{\Delta z^{\mathrm{M}}} \left(\frac{\rho^{\mathrm{M}}_{\mathrm{dry}} f^{\mathrm{Mg}}_{jh}}{M_{\mathrm{W}}} \left(1 + f^{\mathrm{M}}_{njh}\right) - \left(1 + f^{\mathrm{Mg}}_{jh}\right) c^{\mathrm{M}}_{\mathrm{Me},njh} \right) \Bigg) \ldots \\
& \ldots - \frac{p^{\mathrm{o}}_{\mathrm{Me}}}{p} \left(1 + f^{\mathrm{Mg}}_{jh}\right) \Bigg(D^{\mathrm{DL}}_{\mathrm{Me}} \left(M_{\mathrm{He}} c_{\mathrm{gas}} + \left(M_{\mathrm{W}} - M_{\mathrm{He}}\right) c^{\mathrm{DL}}_{\mathrm{W},1jh}\right) \ldots \\
& \ldots - D^{\mathrm{M}}_{\mathrm{Me}} \frac{\Delta z^{\mathrm{DL}}_{jh}}{\Delta z^{\mathrm{M}}} \left(M_{\mathrm{Me}} - M_{\mathrm{He}}\right) c^{\mathrm{M}}_{\mathrm{Me},njh} \Bigg) \Bigg] \rho^{\mathrm{M}}_{\mathrm{dry}} c^{\mathrm{Mg}}_{\mathrm{Me},jh} \ldots \\
& \ldots + \left(D^{\mathrm{DL}}_{\mathrm{Me}} c^{\mathrm{DL}}_{\mathrm{Me},1jh} + D^{\mathrm{M}}_{\mathrm{Me}} c^{\mathrm{M}}_{\mathrm{Me},njh} \frac{\Delta z^{\mathrm{DL}}_{jh}}{\Delta z^{\mathrm{M}}} \right) \left(M_{\mathrm{He}} + \left(M_{\mathrm{W}} - M_{\mathrm{He}}\right) y^{\mathrm{PB}}_{\mathrm{W},jh}\right) \ldots \\
& \ldots \frac{\left(\rho^{\mathrm{M}}_{\mathrm{dry}}\right)^2 f^{\mathrm{Mg}}_{jh}}{M_{\mathrm{W}}} \left(1 + f^{\mathrm{Mg}}_{jh}\right)
\end{aligned} \tag{A.32}$$

For water, Eq. (4.62) leads to:

$$
\begin{aligned}
0 =& \frac{\rho^{\mathrm{M}}_{\mathrm{dry}}}{M_{\mathrm{W}}} \Bigg[D^{\mathrm{M}}_{\mathrm{W}} \frac{\rho^{\mathrm{M}}_{\mathrm{dry}}}{M_{\mathrm{W}}} \left(M_{\mathrm{He}} + \left(M_{\mathrm{W}} - M_{\mathrm{He}} \right) y^{\mathrm{PB}}_{\mathrm{W},\,jh} \right) - D^{\mathrm{DL}}_{\mathrm{W}} \frac{\Delta z^{\mathrm{M}}}{\Delta z^{\mathrm{DL}}_{jh}} \ldots \\
& \ldots \left(M_{\mathrm{He}} \left(c^{\mathrm{DL}}_{\mathrm{W},\,1jh} - y^{\mathrm{PB}}_{\mathrm{W},\,jh} c_{\mathrm{gas}} \right) - \left(M_{\mathrm{Me}} - M_{\mathrm{He}} \right) y^{\mathrm{PB}}_{\mathrm{W},\,jh} c^{\mathrm{DL}}_{\mathrm{Me,1jh}} \right) \Bigg] \left(f^{\mathrm{Mg}}_{jh} \right)^2 \ldots \\
& \ldots + \Bigg[D^{\mathrm{M}}_{\mathrm{W}} \frac{\rho^{\mathrm{M}}_{\mathrm{dry}}}{M_{\mathrm{W}}} \Bigg(\left(M_{\mathrm{Me}} - M_{\mathrm{He}} \right) \frac{p^{\mathrm{o}}_{\mathrm{Me}}}{p} c^{\mathrm{Mg}}_{\mathrm{Me},\,jh} + \left(\left(M_{\mathrm{W}} - M_{\mathrm{He}} \right) y^{\mathrm{PB}}_{\mathrm{W},\,jh} + M_{\mathrm{He}} \right) \ldots \\
& \ldots \left(c^{\mathrm{Mg}}_{\mathrm{Me},\,jh} - \frac{\rho^{\mathrm{M}}_{\mathrm{dry}}}{M_{\mathrm{W}}} f^{\mathrm{M}}_{njh} \right) \Bigg) - D^{\mathrm{DL}}_{\mathrm{W}} \frac{\Delta z^{\mathrm{M}}}{\Delta z^{\mathrm{DL}}_{jh}} \Bigg(M_{\mathrm{He}} \left(c^{\mathrm{DL}}_{\mathrm{W},\,1jh} - c^{\mathrm{PB}}_{\mathrm{W},\,jh} \right) \left(\frac{\rho^{\mathrm{M}}_{\mathrm{dry}}}{M_{\mathrm{W}}} + c^{\mathrm{Mg}}_{\mathrm{Me},\,1jh} \right) \ldots \\
& \ldots + \left(M_{\mathrm{Me}} - M_{\mathrm{He}} \right) \left(c^{\mathrm{Mg}}_{\mathrm{Me},\,jh} c^{\mathrm{DL}}_{\mathrm{W},\,1jh} \frac{p^{\mathrm{o}}_{\mathrm{Me}}}{p} - y^{\mathrm{PB}}_{\mathrm{W},\,jh} c^{\mathrm{DL}}_{\mathrm{Me},\,1jh} \left(c^{\mathrm{Mg}}_{\mathrm{Me},\,jh} + \frac{\rho^{\mathrm{M}}_{\mathrm{dry}}}{M_{\mathrm{W}}} \right) \right) \Bigg) \Bigg] f^{\mathrm{Mg}}_{jh} \ldots \\
& \ldots - \Bigg(M_{\mathrm{He}} \left(c^{\mathrm{DL}}_{\mathrm{W},\,1jh} - c^{\mathrm{PB}}_{\mathrm{W},\,jh} \right) c^{\mathrm{Mg}}_{\mathrm{Me},\,jh} + \left(M_{\mathrm{Me}} - M_{\mathrm{He}} \right) \Bigg(c^{\mathrm{Mg}}_{\mathrm{Me},\,jh} c^{\mathrm{DL}}_{\mathrm{W},\,1jh} \frac{p^{\mathrm{o}}_{\mathrm{Me}}}{p} \ldots \\
& \ldots - y^{\mathrm{PB}}_{\mathrm{W},\,jh} c^{\mathrm{DL}}_{\mathrm{Me},\,1jh} c^{\mathrm{Mg}}_{\mathrm{Me},\,jh} \Bigg) \Bigg) \frac{\Delta z^{\mathrm{M}}}{\Delta z^{\mathrm{DL}}_{jh}} D^{\mathrm{DL}}_{\mathrm{W}} - D^{\mathrm{M}}_{\mathrm{W}} \frac{\rho^{\mathrm{M}}_{\mathrm{dry}}}{M_{\mathrm{W}}} \Bigg(\left(M_{\mathrm{Me}} - M_{\mathrm{He}} \right) \frac{p^{\mathrm{o}}_{\mathrm{Me}}}{p} \ldots \\
& \ldots + \left(M_{\mathrm{W}} - M_{\mathrm{He}} \right) y^{\mathrm{PB}}_{\mathrm{W},\,jh} + M_{\mathrm{He}} \Big) c^{\mathrm{Mg}}_{\mathrm{Me},\,jh} f^{\mathrm{M}}_{njh}
\end{aligned}
\tag{A.33}
$$

which is solved for f^{Mg}_{jh}.

A.3 Transformation to Cylindrical Coordinates

Let the transformation of a function $F(\vec{z})$ from Cartesian coordinates $\vec{z} = (z_1, z_2, z_3)^T$ to cylindrical coordinates $\vec{x} = (z, r, \varphi)^T$ be $F(\vec{x})$. The coordinates are transformed as:

$$z_1 = z \tag{A.34}$$

$$z_2 = r \cos \varphi \tag{A.35}$$

$$z_3 = r \sin \varphi \tag{A.36}$$

with the length of the cylinder z, radius of the cylinder r and the angle φ. Adding the square of Eq. (A.35) to the sqare of Eq. (A.36) and dividing Eq. (A.36) by Eq. (A.35) results in:

$$r = \sqrt{z_2^2 + z_3^2} \tag{A.37}$$

$$\varphi = \arctan \left(\frac{z_3}{z_2} \right) \tag{A.38}$$

Therefore, the derivatives of these new coordinates with respect to the original coordinates are:

$$\frac{\partial r}{\partial z_1} = 0 \tag{A.39}$$

$$\frac{\partial r}{\partial z_2} = \frac{0.5}{\sqrt{z_2^2 + z_3^3}} \cdot 2z_2 = \cos\varphi \tag{A.40}$$

$$\frac{\partial r}{\partial z_3} = \frac{0.5}{\sqrt{z_2^2 + z_3^3}} \cdot 2z_3 = \sin\varphi \tag{A.41}$$

$$\frac{\partial \varphi}{\partial z_1} = 0 \tag{A.42}$$

$$\frac{\partial \varphi}{\partial z_2} = \frac{1}{1 + \left(\frac{z_3}{z_2}\right)^2} \cdot \left(-\frac{z_3}{z_2^2}\right) = -\frac{z_3}{z_2^2 + z_3^2} = -\frac{\sin\varphi}{r} \tag{A.43}$$

$$\frac{\partial \varphi}{\partial z_3} = \frac{1}{1 + \left(\frac{z_3}{z_2}\right)^2} \cdot \left(\frac{1}{z_2}\right) = \frac{z_2}{z_2^2 + z_3^2} = \frac{\cos\varphi}{r} \tag{A.44}$$

Hence, transformation of derivatives of function $F(\vec{z})$ results in:

$$\frac{\partial F}{\partial z_1} = \frac{\partial F}{\partial z} = F_z \tag{A.45}$$

$$\begin{aligned}\frac{\partial F}{\partial z_2} &= \frac{\partial r}{\partial z_2}\frac{\partial F}{\partial r} + \frac{\partial \varphi}{\partial z_2}\frac{\partial F}{\partial \varphi} \\ &= \cos\varphi\frac{\partial F}{\partial r} - \frac{\sin\varphi}{r}\frac{\partial F}{\partial \varphi} = \cos\varphi F_r - \frac{\sin\varphi}{r}F_\varphi\end{aligned} \tag{A.46}$$

$$\frac{\partial F}{\partial z_3} = \sin\varphi\frac{\partial F}{\partial r} + \frac{\cos\varphi}{r}\frac{\partial F}{\partial \varphi} = \sin\varphi F_r + \frac{\cos\varphi}{r}F_\varphi \tag{A.47}$$

And the transformation of the second derivatives of $F(\vec{z})$ reads as:

$$\frac{\partial^2 F}{\partial z_1^2} = \frac{\partial^2 F}{\partial z^2} \tag{A.48}$$

$$\begin{aligned}\frac{\partial^2 F}{\partial z_2^2} &= \cos\varphi \frac{\partial}{\partial r}\left(\frac{\partial F}{\partial z_2}\right) - \frac{\sin\varphi}{r}\frac{\partial}{\partial \varphi}\left(\frac{\partial F}{\partial z_2}\right) \\ &= \cos^2\varphi \frac{\partial^2 F}{\partial r^2} - \cos\varphi\sin\varphi \frac{\partial}{\partial r}\left(\frac{1}{r}\frac{\partial F}{\partial \varphi}\right) \; ... \\ &... - \frac{\sin\varphi}{r}\frac{\partial}{\partial \varphi}\left(\cos\varphi \frac{\partial F}{\partial r}\right) + \frac{\sin\varphi}{r^2}\frac{\partial}{\partial \varphi}\left(\sin\varphi \frac{\partial F}{\partial \varphi}\right) \\ &= \cos^2\varphi \frac{\partial^2 F}{\partial r^2} - \cos\varphi\sin\varphi \frac{\partial}{\partial r}\left(\frac{1}{r}\frac{\partial F}{\partial \varphi}\right) + \frac{\sin^2\varphi}{r}\frac{\partial F}{\partial r} \; ... \\ &... - \frac{\sin\varphi\cos\varphi}{r}\frac{\partial^2 F}{\partial \varphi \partial r} + \frac{\sin\varphi\cos\varphi}{r^2}\frac{\partial F}{\partial \varphi} + \frac{\sin^2\varphi}{r^2}\frac{\partial^2 F}{\partial \varphi^2}\end{aligned} \tag{A.49}$$

$$\begin{aligned}\frac{\partial^2 F}{\partial z_3^2} &= \sin\varphi \frac{\partial}{\partial r}\left(\frac{\partial F}{\partial z_3}\right) + \frac{\cos\varphi}{r}\frac{\partial}{\partial \varphi}\left(\frac{\partial F}{\partial z_3}\right) \\ &= \sin^2\varphi \frac{\partial^2 F}{\partial r^2} + \cos\varphi\sin\varphi \frac{\partial}{\partial r}\left(\frac{1}{r}\frac{\partial F}{\partial \varphi}\right) + \frac{\cos^2\varphi}{r}\frac{\partial F}{\partial r} \; ... \\ &... + \frac{\cos\varphi\sin\varphi}{r}\frac{\partial^2 F}{\partial \varphi \partial r} - \frac{\cos\varphi\sin\varphi}{r^2}\frac{\partial F}{\partial \varphi} + \frac{\cos^2\varphi}{r^2}\frac{\partial^2 F}{\partial \varphi^2}\end{aligned} \tag{A.50}$$

Thus, the sum of the second derivatives in cylindrical coordinates simplifies to:

$$\begin{aligned}\frac{\partial^2 F}{\partial z_1^2} + \frac{\partial^2 F}{\partial z_2^2} + \frac{\partial^2 F}{\partial z_3^2} &= \frac{\partial^2 F}{\partial z^2} + \frac{\partial^2 F}{\partial r^2} + \frac{1}{r}\frac{\partial F}{\partial r} + \frac{1}{r^2}\frac{\partial^2 F}{\partial \varphi^2} \\ &= \frac{\partial^2 F}{\partial z^2} + \frac{1}{r}\frac{\partial}{\partial r}\left(r\frac{\partial F}{\partial r}\right) + \frac{1}{r^2}\frac{\partial^2 F}{\partial \varphi^2}\end{aligned} \tag{A.51}$$

A.3.1 Volume Integration in Cylindrical Coordinates

Considering the definition of the volume of a discretisation element $\mathrm{d}V = r\mathrm{d}z\mathrm{d}r\mathrm{d}\varphi$, volume integration in cylindrical coordinates results in:

$$\int_V \mathrm{d}V = \int_\varphi \int_r \int_z r\mathrm{d}z\mathrm{d}r\mathrm{d}\varphi \tag{A.52}$$

Therefore, the volume integral of the sum of the second derivative of the function F is:

$$\int_{z_3}\int_{z_2}\int_{z_1}\left(\frac{\partial^2 F(\vec{z})}{\partial z_1^2}+\frac{\partial^2 F(\vec{z})}{\partial z_2^2}+\frac{\partial^2 F(\vec{z})}{\partial z_3^2}\right)\mathrm{d}z_1\mathrm{d}z_2\mathrm{d}z_3\ ... \tag{A.53}$$
$$... = \int_r\int_\varphi\int_z\left(r\,\frac{\partial^2 F(\vec{x})}{\partial z^2}+\frac{\partial}{\partial r}\left(r\frac{\partial F(\vec{x})}{\partial r}\right)+\frac{1}{r}\frac{\partial^2 F(\vec{x})}{\partial \varphi^2}\right)\mathrm{d}z\mathrm{d}\varphi\mathrm{d}r$$

A.3.2 Surface Integration of Fluxes in Cylindrical Coordinates

For the surface integration it is important to be aware that only the fluxes perpendicular to the surface are accounted for. Therefore, the vector of the fluxes $\vec{\nabla}F(\vec{z}) = (F_{z_1}, F_{z_2}, F_{z_3})$ is multiplied with the norm vector of the surface.

To calculate the integral in cylindrical coordinates, both vector of fluxes and norm vector need to be transformed. The norm vectors $\vec{n}_z$, $\vec{n}_r$ and $\vec{n}_\varphi$ in cylindrical coordinates are calculated by:

$$\vec{n}_z = \frac{\frac{\partial\vec{z}}{\partial z}}{\left|\frac{\partial\vec{z}}{\partial z}\right|} = \begin{pmatrix}1 & 0 & 0\end{pmatrix}^{\mathrm{T}} \tag{A.54}$$

$$\vec{n}_r = \frac{\frac{\partial\vec{z}}{\partial r}}{\left|\frac{\partial\vec{z}}{\partial r}\right|} = \begin{pmatrix}0 & \cos\varphi & \sin\varphi\end{pmatrix}^{\mathrm{T}} \tag{A.55}$$

$$\begin{aligned}\vec{n}_\varphi = \frac{\frac{\partial\vec{z}}{\partial\varphi}}{\left|\frac{\partial\vec{z}}{\partial\varphi}\right|} &= \begin{pmatrix}0 & -r\sin\varphi & r\cos\varphi\end{pmatrix}^{\mathrm{T}}\frac{1}{\sqrt{r^2\sin^2\varphi + r^2\cos^2\varphi}}\\ &= \begin{pmatrix}0 & -\sin\varphi & \cos\varphi\end{pmatrix}^{\mathrm{T}}\end{aligned} \tag{A.56}$$

The vector of fluxes is transformed to:

$$f = \vec{\nabla}F(\vec{x}) = \begin{pmatrix}F_z\\ \cos\varphi F_r - \frac{\sin\varphi}{r}F_\varphi\\ \sin\varphi F_r + \frac{\cos\varphi}{r}F_\varphi\end{pmatrix} \tag{A.57}$$

The resulting surface integrals of fluxes through the surfaces of a volume element are calculated by:

$$I_{x_i} = \int_{A_{x_i}} f^T \cdot \vec{n_{x_i}} dA_{x_i} \tag{A.58}$$

$$\begin{aligned} I_z &= \int_{r_i}^{r_{i+1}} \int_{\varphi_i}^{\varphi_{i+1}} \begin{pmatrix} F_z \\ \cos\varphi F_r - \frac{\sin\varphi}{r} F_\varphi \\ \sin\varphi F_r + \frac{\cos\varphi}{r} F_\varphi \end{pmatrix}^T \begin{pmatrix} 1 \\ 0 \\ 0 \end{pmatrix} r \, \mathrm{d}\varphi \mathrm{d}r \\ &= \int_{r_i}^{r_{i+1}} \int_{\varphi_i}^{\varphi_{i+1}} \frac{\partial F}{\partial z} r \, \mathrm{d}\varphi \mathrm{d}r = \frac{\partial F}{\partial z} \Delta\varphi \frac{1}{2} \left(r_{i+1}^2 - r_i^2 \right) \end{aligned} \tag{A.59}$$

$$\begin{aligned} I_r &= \int_{\varphi_i}^{\varphi_{i+1}} \int_{z_i}^{z_{i+1}} \begin{pmatrix} F_z \\ \cos\varphi F_r - \frac{\sin\varphi}{r} F_\varphi \\ \sin\varphi F_r + \frac{\cos\varphi}{r} F_\varphi \end{pmatrix}^T \begin{pmatrix} 0 \\ \cos\varphi \\ \sin\varphi \end{pmatrix} r \, \mathrm{d}z \, \mathrm{d}\varphi \\ &= \int_{\varphi_i}^{\varphi_{i+1}} \int_{z_i}^{z_{i+1}} r \, F_r \mathrm{d}z \mathrm{d}\varphi = r \frac{\partial F}{\partial r} \Delta z \Delta\varphi \end{aligned} \tag{A.60}$$

$$\begin{aligned} I_\varphi &= \int_{r_i}^{r_{i+1}} \int_{z_i}^{z_{i+1}} \begin{pmatrix} F_z \\ \cos\varphi F_r - \frac{\sin\varphi}{r} F_\varphi \\ \sin\varphi F_r + \frac{\cos\varphi}{r} F_\varphi \end{pmatrix}^T \begin{pmatrix} 0 \\ -\sin\varphi \\ \cos\varphi \end{pmatrix} \mathrm{d}z \mathrm{d}r \\ &= \int_{r_i}^{r_{i+1}} \int_{z_i}^{z_{i+1}} \frac{1}{r} F_\varphi \mathrm{d}z \mathrm{d}r = \frac{\partial F}{\partial \varphi} \Delta z \ln\left(\frac{r_{i+1}}{r_i} \right) \end{aligned} \tag{A.61}$$

These integrals assume that derivation of F with respect to one coordinate is constant with respect to the other coordinates in the volume element.